Dissertation

Cancerogenic action of GIRK1 on mammary epithelial cells

Submitted by

Gebhard Schratter BSc, MSc

for the Academic Degree of

Doctor of Medical Science

(Dr. scient. med.)

at the

Medical University of Graz

Gottfried Schatz Research Center for Signaling, Metabolism and Aging Biophysics

Under the supervision of

Prof. Dr. Wolfgang SCHREIBMAYER

Prof. Dr. Thomas BAUERNHOFER

Prof. Dr. Ruth PRASSL

Dr. Stephan W. JAHN

2019

This thesis is dedicated to my wife Angelika and daughter Anja.

Eidesstattliche Erklärung

Ich erkläre ehrenwörtlich, dass ich die vorliegende Arbeit selbstständig angefertigt und abgefasst, und jene Personen und Institutionen, die am Zustandekommen der Forschungsdaten beteiligt waren, namentlich genannt habe. Andere als die angegebenen Quellen habe ich nicht verwendet und die den benutzten Quellen wörtlich oder inhaltlich entnommenen Stellen habe ich als solche kenntlich gemacht. Die Arbeit an der Dissertation und daraus entstandener Publikationen wurde gemäß den Regeln der „Good Scientific Practice“ durchgeführt.

Gebhard Schratter

Graz, am 21.11.2019

Declaration

I hereby declare that this thesis is my own original work and that I have fully acknowledged by name all of those individuals and organisations that have contributed to the research for this thesis. Due acknowledgement has been made in the text to all other material used. Throughout this thesis and in all related publications I followed the “Standards of Good Scientific Practice and Ombuds Committee at the Medical University of Graz“.

Gebhard Schratter

Graz: 21.11.2019

Disclosures

This thesis has been published in the following original papers:

GIRK1 triggers multiple cancer-related pathways in the benign mammary epithelial cell line MCF10A

Accepted for publication in the Journal "Scientific Reports" by Schratter et al; manuscript in press (21.11.19).

Gebhard SCHRATTER[1,*], Susanne SCHERUEBEL[1,*], Sonja LANGTHALER[2], Katja ESTER[3], Brigitte PELZMANN[1,*], Nassim GHAFFARI TABRIZI-WIZSY[4], Simin REZANIA[1,*], Astrid GORISCHEK[1,*], Dieter PLATZER[1,*], Klaus ZORN-PAULY[1,*], Helmut AHAMMER[1], Andreas PROKESCH[5], Stefanie STANZER[6], Trevor T.J. DeVANEY[1,*], Kurt SCHMIDT[7], Stephan W. JAHN[8], Ruth PRASSL[1,*], Thomas BAUERNHOFER[6,*], Wolfgang SCHREIBMAYER[1,*,+]

[1]: Gottfried Schatz Research Center for Cell Signaling, Metabolism and Aging, Medical University of Graz, Austria.

[2]: Institute for Health Care Engineering with European Testing Center of Medical Devices, Technical University of Graz, Austria

[3]: Laboratory of Experimental Therapy, Division of Molecular Medicine, Ruđer Bošković Institute, Bijenička 54, 10000 Zagreb, Croatia

[4]: Institute of Immunology and Pathophysiology, SFL Chicken CAM Laboratory, Medical University of Graz, Austria

[5]: Cell Biology, Histology and Embryology, Medical University of Graz, Austria

[6]: Division of Oncology, Department of Internal Medicine, Medical University of Graz, Austria

[7]: Institute of Pharmaceutical Sciences, Karl Franzens University of Graz, Austria

[8]: Diagnostic & Research Institute of Pathology, Medical University of Graz, Austria

All co-authors declare that they have no conflicts of interest with the content of this thesis and have explicitly agreed to use their data in the thesis.

I gratefully thank for the financial support by the "Medizinische Forschungsvereinigung" and the Austrian Research Foundation (FWF KLIF-182).

Acknowledgements

First of all, I would like to thank my supervisor **Wolfgang Schreibmayer,** that he brought me into his team in the doctoral school “Translational Molecular and Cellular Biosciences”. We had many interesting discussions and I got feedback all the time during my work and he always had an open door for my questions. I would also like to thank **Thomas Bauernhofer** for being my supervisor, finding time for me and for engaging in interesting and informative discussions. Special thanks to my supervisor **Ruth Prassl**. She is not only a genius in her field, but also a good friend and my mentor. I owe gratitude to **Stephan Jahn** for answering pathology-related questions and for supporting this research. Thank you very much for the assistance!

Special thanks go to **Nassim Ghaffari Tabrizi-Wizsy, Stefanie Stanzer, Brigitte Pelzmann** and **Trevor DeVaney** for all their support, suggestions and help. I thank my fellow team members **Jasmin Maderer; Susanne Scherübel, Patrick Wiedner, Astrid Gorischek, Tony Schmidt, Helmut Ahammer, Klaus Zorn-Pauly, Astrid Grundner, Dieter Platzer, Karin Kornmüller, Andreas Prokesch** and **Johann Krebs** and all the other colleagues at the Institute of Biophysics for helping me with many practical issues and for informative and interesting conversations on my scientific work. I also thank all the other colleagues from the institute, who I did not name by name.

Many thanks also to **Karl Kashofer** of the Diagnostic & Research Institute of Pathology for valuable input and great collaboration. **Andrea Thüringer** of the Diagnostic & Research Institute of Pathology for transcriptome analysis.

Thanks to my family; **Mama** and **Papa** as well as **Ines** and **Elke,** who supported me during this time and beyond. I am deeply grateful for all the support I got from my wife **ANGELIKA** and daughter **ANJA** for cheering me on and standing by me during the ups and downs. It would not have been able to this without you.

Short preface

Es ist nicht genug zu wissen – man muss es auch anwenden.

Es ist nicht genug zu wollen – man muss es auch tun.

Johann Wolfgang von Goethe

Fange nie an aufzuhören und höre nie auf anzufangen!

Marcus Tullius CICERO

Table of Contents

1. List of Abbreviations:

ACh	Acetylcholine
cds	coding sequence
cLSM	confocal Laser Scanning Microscopy
CV	Coefficient of Variation
CT	Cholera Toxin
C-T	Carboxy-Terminus
DAVID	database for annotation, visualization and integrated discovery
DMSO	Dimethylsulfoxid
DNA	DeoxyriboNucleic Acid
E. coli	Escherichia coli
ECL	Enhanced Chemi Luminescence
ECM	Extra Cellular Matrix
EDTA	Ethylenediaminetetraacetic acid
EGF	Epidermal Growth Factor
ER	Estrogen Receptor
ES	Enrichment Scores
FBS	Fetal Bovine Serum
FDR	False Discovery Rate
GEO	Gene Expression Omnibus
GIRK1	G-protein inwardly rectifying potassium channel subtype 1
GO	Gene Ontology
GPCR	G-protein coupled receptor
IP	Immuno Precipitation
IQM	Interactive Quantitative Morphology
KCNJ3	Gene encoding G-protein activated inwardly rectifying
kD	kilo Dalton
KEGG	Kyoto Encyclopedia of Genes and Genomes

kV	kilo Volt
LB	Luria Broth
LSB	Laemmli Sample buffer
MC	cellular Motility Coefficient
MEC	Mammary Epithelial Cell
MCF10A	Michigan Cancer Foundation-10
MCF7	Michigan Cancer Foundation-7
MEBM	Mammary Epithelial Cell Growth Basal Medium
MEM	Minimum Essential Medium Eagle
MM	Master Mix
mRNA	messenger Ribo Nucleic Acid
MVS	Macroscopic Vascularization Score
NEB	New England Bio Labs
NSS	Nystatin Stock Solution
N-T	amino Terminus
PBS	Phosphate-buffered saline
PCR	Polymerase Chain Reaction
Pen/Strep	Penicillin-Streptomycin
PFS	Pipette Filling Solution
PSN	Nystatin containing pipette solution
qPCR	quantitative Polymerase Chain Reaction
RGD	conserved tripeptide Arg-Gly-Asp
RIPA	Radioimmunoprecipitation Assay Buffer
ROI	Region of Interest
RP	Resting Potentials
rpm	revolutions per minute
RT-PCR	Real-Time Polymerase Chain Reaction
SDS	Sodium Dodecyl Sulfate

SOC	Super Optimal broth with Catabolite repression
STAT	Signal Transducers and Activators of Transcription
STR	Short Tandem Repeat
TAE	Tris-Acetate-EDTA
TBST	Tris Buffered Saline with Tween-20
v/v	volume/volume
WB	Western Blot
WT	Wild type
w/v	weight/volume
ZBS	Zeroing Bathing Solution

2 List of Figures

3. List of Tables

4. Zusammenfassung

Verschiedenste Studien haben gezeigt, dass Kaliumkanäle an der Entstehung von Tumoren und Metastasen beteiligt sind. Bei der Untersuchung von ER positiven Patienten-Proben hat man festgestellt, dass bei Brustkrebspatientinnen ein hoher GIRK1-Level an Proteinen und Boten-Ribonukleinsäuren (mRNA) zu finden war. Diese sind auch mit Lymphknotenmetastasen assoziiert und verringern die Überlebens-Chance von Krebs-Patientinnen. GIRK1 ist ein vielversprechendes „Target“ für die Prognose und Therapie von Brustkrebs. Eine höhere Expression von GIRK1-mRNA und -Protein tritt auch in mehreren, aus Brusttumoren kultivierten, Zelllinien auf. Die maligne MCF7-Brustkrebszelllinie exprimiert GIRK1-mRNA bereits in moderaten Mengen. Dies ist einer der Gründe, weshalb diese Zelllinie ein hervorragendes Forschungsmodell für eine erhöhte GIRK1-Expression bei Brusttumoren ist. Dabei hat man festgestellt, dass eine ektopische Hyperexpression von GIRK1 in MCF7-Zelllinien verschiedene Krebsmerkmale verstärkt. Dazu zählen eine erhöhte zelluläre Motilität, Invasivität und Angiogenese, wodurch auch die beobachteten Auswirkungen unter klinischen Bedingungen erklärt werden könnten.

Um festzustellen, ob sich GIRK1 krebsfördernd auswirkt, wurden benigne MCF10A Brustepithel-Zellen, die mit GIRK1 überexprimiert wurden, für Versuche in der Zellkultur herangezogen. Validierung und Charakterisierung von MEC-Zelllinien, die GIRK1 überexprimieren, wurden mithilfe der qPCR- und der Western-Blot-Analyse durchgeführt. Die Membranruhepotentiale wurden mit entsprechenden Kontroll-Zelllinien verglichen. Eine zusätzlich durchgeführte Transkriptom-Analyse hatte ergeben, dass die Überexpression von GIRK1 in gutartigen MECs das Expressionsniveau von rund 1900 Genen beeinflusst bzw. verändert hatte. Man hat festgestellt, dass somit die an mehreren pro-tumorgenen „Pathways“ beteiligt waren. Durchgeführte DAVID Pathway-Analysen haben ergeben, dass viele dieser Transkripte in Richtung spezifischer Zellfunktionen und pro-tumorgener Wirkung reguliert waren. „Heatmaps“ zeigen den quantitativen Effekt auf ausgewählte Gencluster und unterstreichen das Ausmaß der zellulären Regulation, die durch die Überexpression von GIRK1 ausgeübt wurden. Bei der Überexpression von GIRK1 in MCF10A-Kontrolllinien war die Beweglichkeit und die Zellgeschwindigkeiten wesentlich erhöht. Dies ist darauf zurück zu führen, dass die Veränderung des Transkripts auch mit einer Veränderung der Beweglichkeit (auf Zellebene) in einem direktem Zusammenhang steht.

Der am stärksten regulierte funktionelle Gen-Cluster ist hochreguliert und umfasst nachgeschaltete Elemente, die durch das Cytokin Interferon-γ (IF-γ) ausgelöst wurden. In der vorliegenden Studie löste die Überexpression von GIRK1 in der MCF10A-Zelllinie

mehrere IF- γ-Signalelemente aus. Von diesen ist bekannt ist, dass sie in Brust-Epithelzelllinien pro-tumorgen wirken. Wir habe tiefgreifende Veränderungen des zellulären Phänotyps bei Überexpression von GIRK1 in gutartigem MCF10A beobachtet. Bei der vorliegenden Untersuchung wurde festgestellt, dass die Überexpression nur EINER einzelnen K^+ -Kanal-Untereinheit, die für eine Zelle sehr wichtig ist, die Vitalparameter einer gutartigen MEC-Linie in Richtung Krebs verschoben werden kann. Zusammenfassend lässt sich sagen, dass eine Störung von Kaliumkanälen möglicherweise eine neue therapeutische Möglichkeit einer Therapie, für diese Art des Subtyps des Estrogenrezeptor-positiven Brustkrebses, ergibt. Dies ermöglicht Ärzten eine verbesserte Therapieplanung und ermöglicht Ihnen individuell auf den Patienten und dessen Krankheit einzugehen.

5. Abstract

Cancerogenic action of GIRK1 on mammary epithelial cells

Several studies have shown that potassium channels are involved in the development of tumor and metastasis formation. Excessive protein and messenger ribonucleic acid (mRNA) levels of GIRK1 have been found in estrogen receptor positive (ER^+) breast cancer samples. They are associated with lymph node metastasis and reduced the probability of survival of patients. GIRK1 poses a promising target for the prognosis and therapy of breast cancer. Substantial expression of GIRK1 mRNA and protein also occurs in several cell lines cultured from breast tumors. The malignant MCF7 breast cancer cell line expresses GIRK1 mRNA already at moderate levels. Therefore, this cell line provides an excellent model for increased GIRK1 expression in breast tumors. Ectopic hyperexpression of GIRK1 in MCF7 cell lines has shown to aggravate several cancer hallmarks, including increased cellular motility, invasiveness and angiogenesis and is, thereby providing an explanation for the observed impact under clinical conditions.

In order to investigate whether GIRK1 also act cancerogenic on benign MCF10A mammary epithelial cells, overexpressing GIRK1 have been engineered. Validation and characterization of mammary epithelial cell (MEC) lines overexpressing GIRK1, examined by qPCR and Western Blot analysis. Membrane resting potentials (RPs) were compared to controls. Transcriptome analysis reverted that the overexpression of GIRK1 in benign MECs affects expression levels of about 1900 genes involved in several cellular pro-tumorigenic pathways. Visualization and Integrated Discovery (DAVID) Pathway Analysis revealed that many of these transcripts are regulated towards specific cellular functions and pro-tumorigenic actions. Heat maps display the quantitative effect on selected gene clusters and underscore the amount of cellular regulation exerted by GIRK1 overexpression. Upon GIRK1 overexpression, motility and cellular velocities of the benign MCF10A control lines were substantially increased and associated with transcriptional changes of genes that are linked to motility at the cellular level.

The most prominently regulated functional cluster is upregulated and comprises downstream elements which are triggered by the cytokine interferon-γ (IF-γ). In the present study, overexpression of GIRK1 in MCF10A cell line triggered several downstream IF-γ signaling elements known to act pro-tumorigenic in MEC lines. We observe profound changes in cellular phenotype upon GIRK1 overexpression in benign MCF10A. In this examination, it was found that the overexpression of only one single K^+-channel subunit, which is of high importance to a cell and, can shift the vital parameters of a benign MEC-line towards cancer hallmarks. Research has shown that disturbance with potassium

channels potentially offers a new therapeutic window for the subtype of ER^+ breast cancer treatment. This enables physicians to carry out improved therapy planning.

6. Introduction

The breasts of female mammals consist of lobes, ducts, blood- and lymphatic vessels. Each lobe is divided into smaller segments called lobules ending in dozens of tiny bulbs. These lobules and bulbs are linked by thin tubes called ducts (Figure 1). The human breast houses the mammary gland which produces and delivers milk through developing a broad tree like network of branched ducts. In adulthood an extensive remodelling occurs regularly during the menstrual cycle, a factor that enhances its fragility to carcinogenesis (Javed and Lteif, 2013). The onset of breast cancer is first locally restricted to the breast. Subsequently, the breast cancer can metastasize to the lymph nodes and distant organs. Prognostic markers are used for the initial diagnosis and allows to judge the transition to a systemic disease has presumably occurred.

There are several ways that can lead to malignancy. Traditionally, breast cancer is classified into three different subtypes. They are based on the presence and absence of three receptors, which are found on breast cancer cells. Hormone receptor (HR) positive breast cancers express estrogen and/or progesterone receptors (ER/PR), human epidermal growth factor receptor 2 (HER-2) positive breast cancers overexpress HER-2. The triple negative breast cancer is negative for ER,PR and HER-2 (Tinoco et al., 2013). ER/PR positive carcinoma is associated with particular somatic mutations affecting numerous genes involved in signal transduction, including ion channels (Woolston, 2015).

Ion channels play an important role in a variety of physiological processes such as formation and transmission of excitation in nerves, the heart or skeletal muscle is based on electrical processes at the cell membrane. Ions, such as K^+, Na^+ and Ca^{2+} are unsymmetrically distributed across the plasma membrane, and these result in an electrochemical gradient, which is maintained through active transport (Pardo and Stuhmer, 2014). The basis of these electrical processes is the flow of small ions, for instance potassium, sodium or calcium through a special class of membrane proteins, called ion channels. Ion channels are integral membrane proteins that form a pore in the cell membrane, allowing the passage of specific ions through the lipid bilayer of the membrane. Variations in ionic gradients across cellular membranes play an important role in almost all cellular events, including electrical conductance, proliferation, secretion, motility, cell death, and transcriptional regulation. Molecular genetic studies have shown, that changes in the expression of multiple ion channels have been implicated in malignancy of healthy tissue in mammals, including breast cancer (Prevarskaya et al., 2018). Changes in the activity of ion channel proteins can potentially contribute to several of the hallmarks of cancer and therefore to malignant

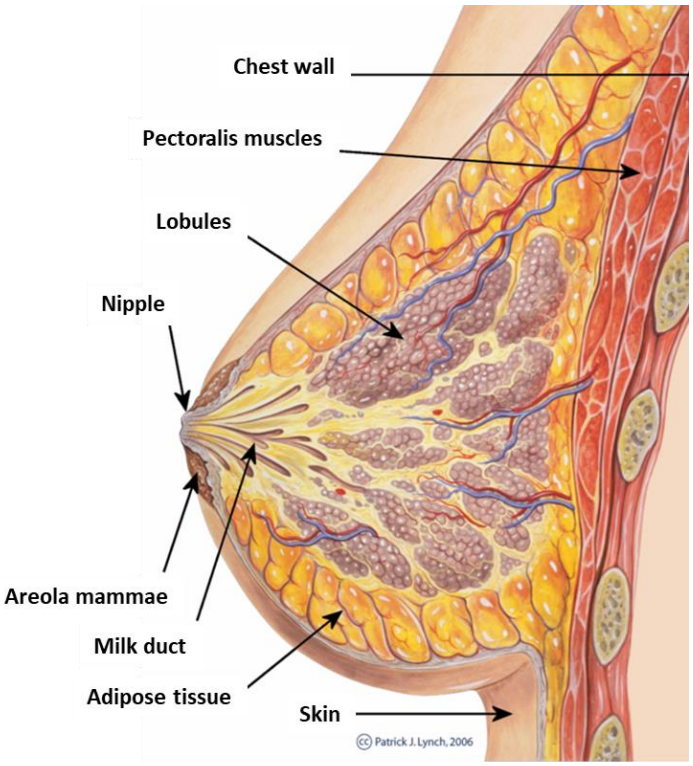

https://en.wikipedia.org/wiki/Lactiferous_duct#/media/File:Breast_anatomy_normal_scheme.png

Figure 1: Human Breast Anatomy Sectional View. The breast, or mammary gland, consists of chest wall, pectoralis muscles, lobules, nipple, areola mammae, milk duct, adipose tissue and skin. Modified according to https://commons.wikimedia.org/wiki/File:Breast_anatomy_normal_scheme.png. This file is licensed under the Creative Commons Attribution 3.0 Unported license.

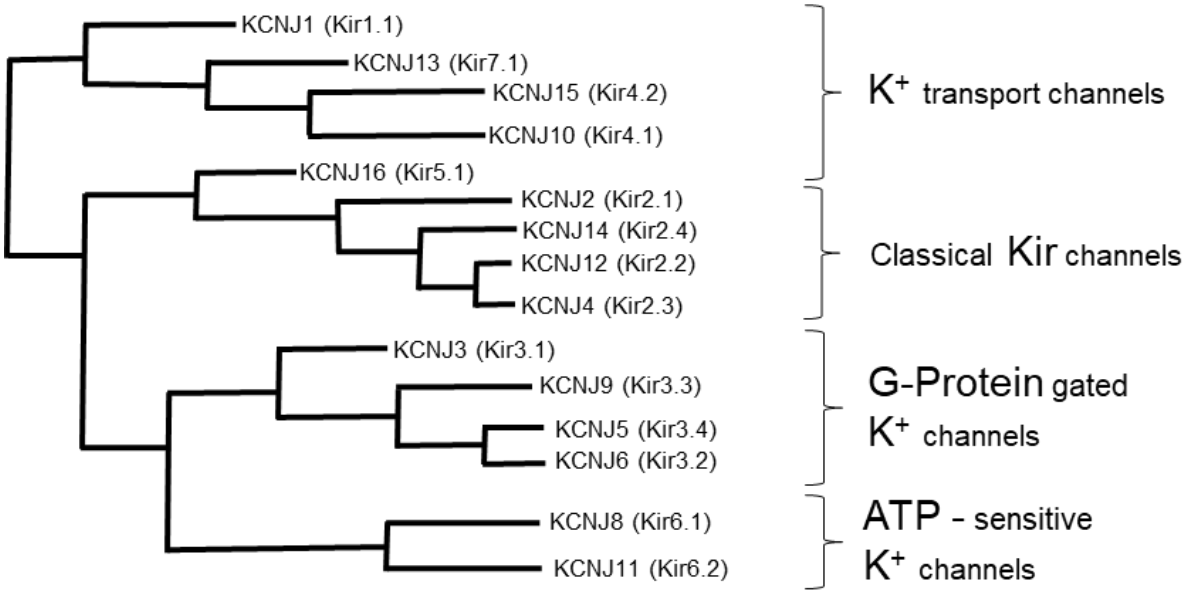

Figure 2: Phylogenetic tree of Kir channels. Amino acid sequence alignment and phylogenetic analysis of the 15 known subunits of human potassium channels. These subunits can be classified into four functional groups: K+ transport channels, classical Kir channels, G-protein gated K+ channels and ATP-sensitive K channels.

transformation of breast cells (Jonathan et al., 2017). Seven Kir channel subfamilies (Kir 1 - Kir 7) are known and can be classified into four functional groups: K^+ transport

channels, classical Kir channels, G-protein gated K^+ channels (GIRKs), shown in figure 2, and ATP-sensitive K^+ channels (Hibino et al., 2010).

G-Protein-activated Inwardly Rectifying Potassium Channels (GIRK) belong to the family of inwardly rectifying K^+ channels (Kir1–Kir7). GIRKs play important roles in the nervous system, heart, pancreas, blood platelets and in the regulation of lipid metabolism in fat cells (Dascal, 1997, Dascal, 2001, Iwanir and Reuveny, 2008, Smith et al., 2001, Shankar et al., 2006, Shankar et al., 2004, Perry et al., 2008). These channels link the presence of extracellular signaling molecules to the hyperpolarization of the membrane potential. GIRK channels are activated followed by the binding of ligands (e.g. neurotransmitters such as acetylcholine (ACH), dopamine, opioids, serotonin, adenosine, Gamma-AminoButyric Acid (GABA) or hormones) to their related G protein-coupled receptors (GPCRs), which become activated (see figure 3).

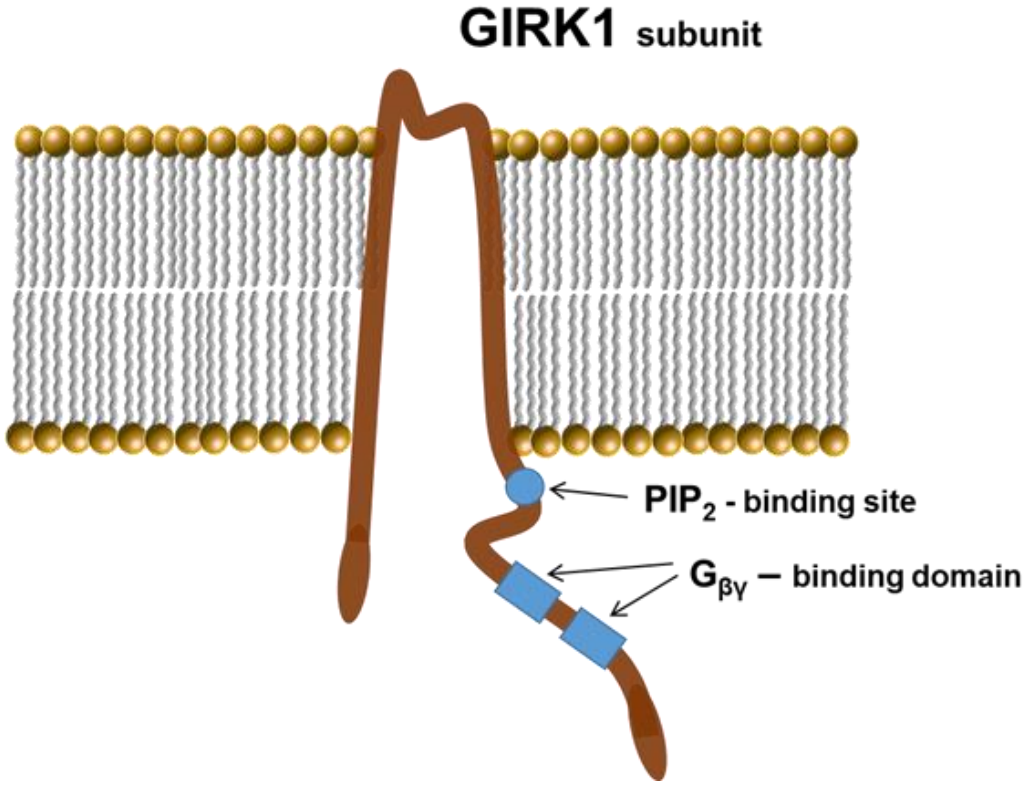

Figure 3: Basic structure of the GIRK (Kir) channel. Schematic representation of the positions of identified domains of GIRK1 which are responsible for interaction of GIRK1 and G protein subunits or phosphatidylinositol 4,5-bisphosphate (PIP2) and positions of two identified G protein βγ-binding regions. Domains and hydrophobic core region of GIRK1 are also shown.

Ligand binding triggers receptor activation that couples to and activates heterotrimeric G proteins. The ligand binding triggers the dissociation of the βγ subunits of pertussis toxin-sensitive G proteins, which bind to the GIRK channel and in return activate the K^+ channel

(see Figure 4). This allows the movement of K^+ out of the cell causing a more negative resting membrane potential (Walsh, 2011).

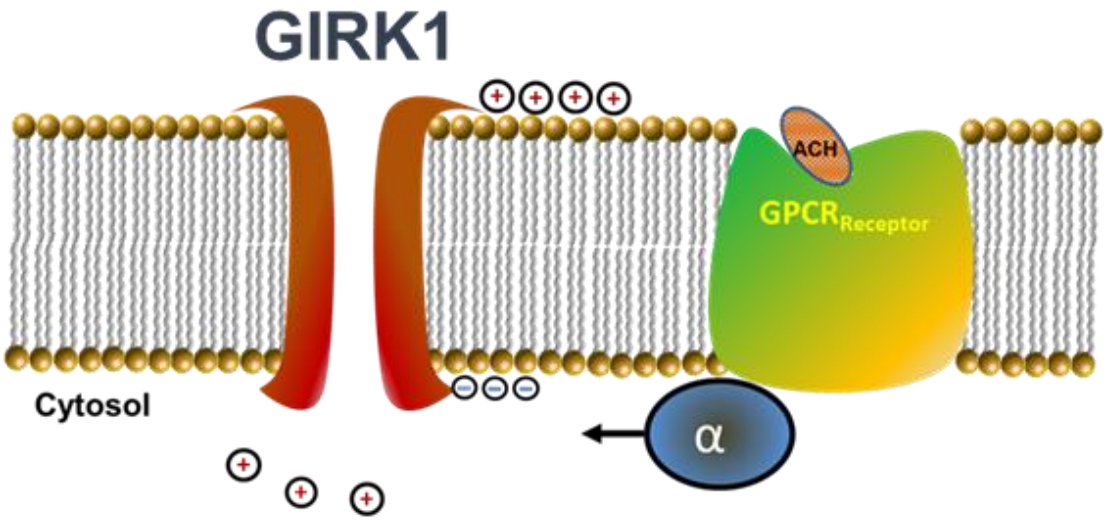

Figure 4: Regulation of GIRK channels. Neurotransmitter Acetylcholine (ACH) binds to a receptor protein (GPCR receptor) which is coupled to an inhibitory G protein. GIRK channels are activated by migration and direct binding of Gβγ subunits from GPCR receptor to GIRK.

Four different genes exist in the human genome, encoding GIRK1 (Kir3.1), GIRK2 (Kir3.2), GIRK3 (Kir3.3) and GIRK4 (Kir3.4) subunits that form heterotetrameric and/or homotetrameric channels in the plasma membrane as seen in Figure 5 (Lüscher and Slesinger, 2010). Among other things, the different isoforms vary in their cytoplasmic N- and C-terminal domains. Connections between inherited and/or somatic mutations in genes encoding GIRKs with neuronal, endocrine and cardiac disorders have been established, underlining the important role of this inhibitory G-protein pathway for normal as well as the pathophysiological function of human organs (Luscher and Slesinger, 2010, Mulatero et al., 2013, Nolte et al., 2017). GIRK1, also known as KCNJ3 (Kir3.1), which is mapped in chromosome 2 (Cytogenetic location: 2q24.1). The overexpression of GIRK1 has been reported in tumors of the breast, which is the most diagnosed cancer in women worldwide (Stringer et al., 2001, Jemal et al., 2010). Excessive protein and messenger ribonucleic acid (mRNA) levels of GIRK1 were found to be associated with lymph node metastasis and reduced probability of survival of breast cancer patients (Brevet et al., 2008, Stringer et al., 2001, Kammerer et al., 2016, Wagner et al., 2010). Overexpression of GIRK1 mRNA and protein also occurs in numerous cell lines cultivated from breast tumors (Plummer et al., 2004, Dhar and Plummer, 2006, Kammerer et al., 2016).

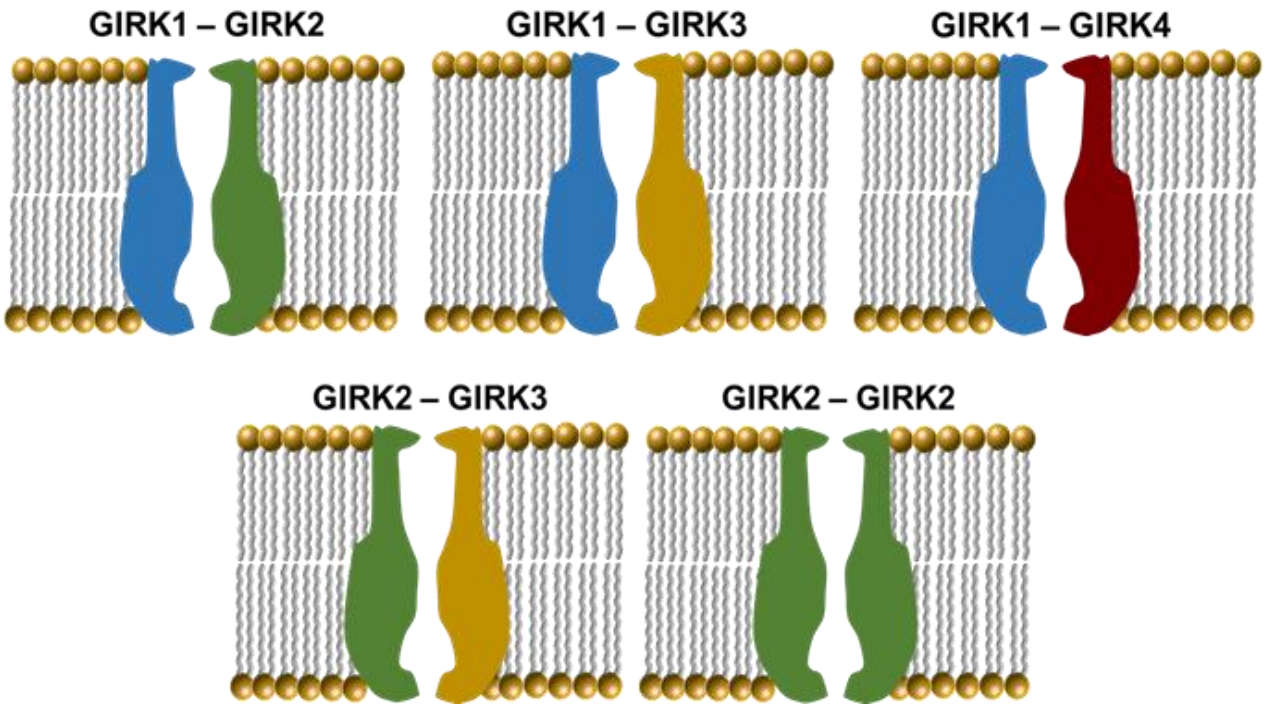

Figure 5: Possible formations of GIRK channel subunits. GIRK subunits form functional heterotetramers like: (GIRK1-GIRK2, GIRK1-GIRK3, and GIRK1-GIRK4) and also homotetramers (GIRK2-GIRK2).

In order to answer the question whether GIRK1 not only promotes progression of the disease, but also acts cancerogenic in healthy tissue, we studied the biological effects of GIRK1 overexpression on a benign MCF10A mammary epithelial cell (MEC) line. Successful overexpression was validated through qPCR and Western Blot analysis. We could verify that the $MCF10A^{GIRK1}$ and $MCF7^{GIRK1}$ tansfected cell lines exhibit relevant overexpression of GIRK1 mRNA and protein compared to the respective WT lines. In addition, GIRK1 mRNA and protein levels are substantial in the malign estrogen receptor positive $MCF7^{WT}$ line compared to the benign $MCF10A^{WT}$ MEC line. Therefore, the set of cell lines generated pose a plausible model to study functional effects of elevated GIRK1 levels in benign and malignant MECs. The malignant $MCF7^{WT}$ breast cancer cell line already expresses GIRK1 mRNA at moderate levels.

In order to identify cellular pathways altered by GIRK1 overexpression, we investigated the transcriptome wide expression changes of MCF10A cells induced by stable GIRK1 overexpression. This transcriptomic profiles of MCF10A were investigated using the next-Generation RNA sequencing. This analysis enables the fast profiling and deep investigation of the whole transcriptome of the MCF10A cell lines. Two software tools were used to identify biological functions and pathways. Data was analyzed by database for annotation,

visualization and integrated discovery (DAVID)-Analyzes and gene by set enrichment analysis (GSEA) (Huang da et al., 2009).

Membrane resting potentials (RPs) were measured and compared to control samples. RPs demonstrate that functional GIRK channels form upon overexpression of GIRK1 in the malignant MCF7 and in the benign MCF10A MEC lines.

Neoplasia associated with vital parameters such as motility, velocity, invasion, adhesion, wound healing, proliferation and angiogenesis was evaluated. Different vital assays were performed on the benign MCF10A and malign MCF7 cell lines and compared to GIRK1 overexpressing MECs. The results were correlated to GIRK1 mRNA expression levels. Some vital assays indicate that divergent biological properties can be correlated with differentially expressed pathways derived from transcriptome analysis. This will allow to identify a possible influence of GIRK1 overexpression on the progression of the human disease.

Our data provide strong evidence that GIRK1 potassium channels not only promote progression of cancer in already malign MECs, but also act cancerogenic in healthy MECs overexpressing GIRK1. An abnormal expression of potassium channels is a common observation in tumors, and can alter tumor behavior in many different ways.

7. Aim of the Study

Based on previously described findings (Stringer et al., 2001, Brevet et al., 2008, Wagner et al., 2010, Rezania et al., 2016, Kammerer et al., 2016), it seemed promising to study the effect of GIRK1 overexpression on benign MCF10A cells and compared the results to malign MCF7 cell lines.

Verification of GIRK1 overexpression:

- Quantification of qPCR for different cell lines to compare GIRK1 expression levels
- Comparison of GIRK1 overexpressions in Western Blots (WB) and Immunoprecipitations (IP)

To assess the effects of GIRK1 the following steps were taken to achieve this goal:

- Effect of GIRK1 overexpression on the resting membrane potential of MEC cells with native GIRK1 protein (electrophysiological recordings and analysis).
- Transcriptome analysis of different MCF10A cell lines by using the next-Generation RNA sequencing. Two software tools (DAVID and GSEA). were used to identify biological functions and pathways.
- Biological validation of vital parameters
    - Chick Chorioallantoic Membrane (CAM) Assay
    - Cell adhesion assay (Extracellular Matrix Interaction Assay)
    - EdU proliferation Assay
    - In vitro Motility Assay
    - Invasion Assay
    - Wound healing Assay
    - Colony Formation Assay
    - Mammosphere Forming Assay

8. Materials and Methods

8.1 Cell lines and culture conditions

MCF7 cell line:

Organism: Homo sapiens, human

Tissue: mammary gland, breast; derived from metastatic site: pleural effusion

Disease: adenocarcinoma

Cell Type: epithelial

Morphology: epithelial

Growth Properties: adherent

Progesterone- and Estrogen receptor positive

MCF7 cells were cultured in a complete growth medium: MEM (Minimum Essential Medium Eagle) from Merck, M2279-500ML, FBS (Fetal Bovine Serum) from Merck F7524-500ML Lot No 025M3355 at a final concentration of 10%, Sodium Pyruvate 100 mM (ThermoFisher 11360039) at a final concentration of 1%, L-Glutamine solution 200 mM (Merck G7513-100ML) final concentration of 1% and (100 U/mL and 100 ng/mL) Penicillin-Streptomycin (Pen/Strep) (Merck, P0781-100ML)

Minimal medium: Minimum Essential Medium Eagle (Merck, M2279-500ML), Sodium Pyruvate 100 mM (ThermoFisher 11360039) in a final concentration of 1%, L-Glutamine solution 200 mM (Merck G7513-100ML) final concentration of 1% and also Pen/Strep with a final concentration of 1%.

Freeze medium: Complete growth medium supplemented with 5% (v/v) DMSO (Dimethylsulfoxide) from VWR 23486.297.

Proliferation: The cells were thawed out of the liquid nitrogen and seeded for multiplication in a TC-Flask T25, stand. vent. cap (Sarstedt, 83.3910.002). The old medium was changed every 2 days until the TC-Flask reached 90% cell density. Now they are ready for splitting. The old medium was aspirated and washed twice with phosphate-buffered saline (PBS). They can be splitted by using TrypLE™ Express Enzyme (ThermoFisher, 12604013). The cells were incubated with TrypLE™ for 5 to 10 minutes. Following this treatment, the cells dissolved from the cell culture dish bottom. The trypE action in the cell suspension was stopped with 200 µl FBS. After centrifugation, the cells were resuspended with 1 mL of medium and filled in new dishes. The total amount of cells can be divided and seeded 1:4 into several cell culture dishes.

All MCF7 cell lines were free of mycoplasma contamination, as tested routinely (Core Facilities Alternative Biomodels & Preclinical Imaging, Medical University of Graz, Austria). The integrity of the cell lines was verified by short tandem repeat (STR) analysis (see appendix). MCF7 Cell line was kindly provided by Prof. Bauernhofer (Division of Oncology, Department of Internal Medicine, Medical University of Graz, Austria).

MCF10A cell line:

Organism: Homo sapiens, human
Tissue: mammary gland; breast
Disease: fibrocystic disease
Cell Type: epithelial
Morphology: epithelial
Growth Properties: adherent

MCF10A cells were cultured in a complete growth medium No 1: MEBM (Lonza, Mammary Epithelial Cell Growth Basal Medium) from Lonza, CC-3151, including single components also from Lonza, CC-4136 and 0,004% CT (Cholera Toxin) from Merck, C8052-.5MG.

Complete growth medium No 2: DMEM/F-12, GlutaMAX™ Supplement (ThermoFisher, 31331028), Bovine Pituitary Extract (ThermoFisher, 13028014) at a concentration of 50µg/mL, EGF (Epidermal Growth Factor) from Merck, E4127-.1MG at a final concentration of 20 ng/mL, Hydrocortisone (Merck, H0396-100MG) at a final concentration of 0,5 µg/mL, Insulin human (Merck, I2643-25MG) at a final concentration of 10 µg/mL and CT (Merck, C8052) 0,02µL/mL.

Freeze medium: Complete growth medium supplemented with 5% DMSO (VWR, 23486.297).

Minimal medium: MEBM (Lonza, Mammary Epithelial Cell Growth Basal Medium) from Lonza, CC-3151, GA-1000 0.50 mL (Lonza, CC-4081) and 0,004% CT from Merck.

The cells were kept in a cell culture incubator (Memmert ICO) at 37°C and 5% CO_2. The culture medium was refreshed every two to three days and cells were splitted at 80% to 90% confluence using TrypLE™.

To achieve optimum cell growth, the used medium was sucked off from the cell culture dish with a syringe and sterile filtered. This is referred to a conditioned medium. The old “used” medium and the new medium, 50% of each were mixed together and added to the cell in each dish because cell-to-cell contact can promote cellular growth.

Stable transfections of MCF7 GIRK1a variants and vector controls were performed by Astrid Gorischek. Stable transfection of MCF10A overexpression was also performed by Astrid Gorischek (from Gottfried Schatz Research Center for Cell Signaling, Metabolism and Aging, Medical University of Graz).

All MCF10A cell lines were free of mycoplasma contamination, as tested routinely by Core Facilities Alternative Biomodels & Preclinical Imaging, Medical University of Graz, Austria. The integrity of the cell lines was verified by short tandem repeat (STR) analysis (see appendix). MCF10A Cell line was kindly provided by Prof. Bauernhofer (Division of Oncology, Department of Internal Medicine, Medical University of Graz, Austria).

8.2 Preparation of pIRES2eGFP vector control

To carry out the experiments, an empty pIRES2eGFP (PIRES2eGFP Clontech, 6029-1) was used to see in figure 6. This vector was linearized with MfeI (R0589S, NewEnglandBiolabs) and SacI (R0156S, NewEnglandBiolabs) and both restriction enzymes were unique cutters. For the restrictions analysis, a 1% agarose gel and a 1 kb deoxyribonucleic acid (DNA) ladder (NEB, N0469S; Promega, G5711) were used. The vector was sequenced by Eurofins Genomics.

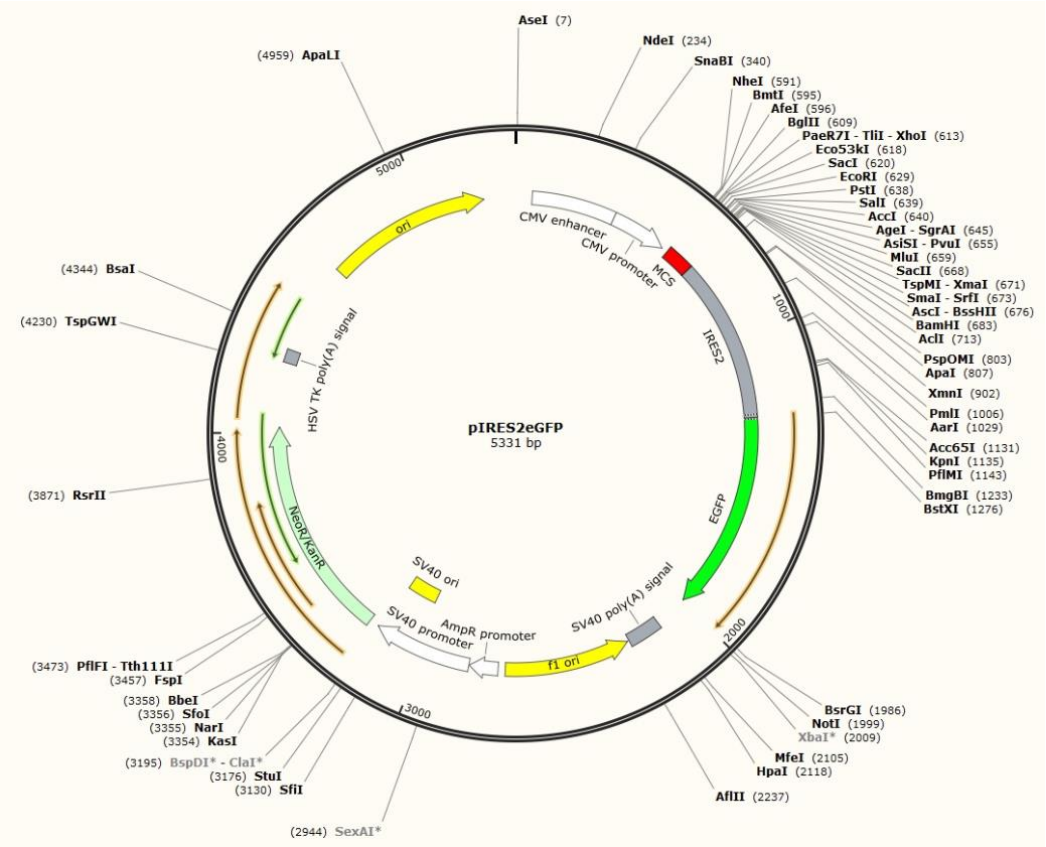

Figure 6: Empty pIRES2eGFP vector. (Created by SnapGene software (from GSL Biotech; available at snapgene.com).

To determine the best annealing temperature for PCR a temperature interval of 10°C was used for gradient PCR to obtain sufficient inset DNA. The PCR products were cut off the analytic Agarose gel and cleaned by Wizard® SV Gel and PCR Clean-Up System (Promega, A9281). For the linearization of the DNA vector, the restriction enzyme AseI (R0526S, NewEnglandBiolabs) was used.

In addition, we subcloned the insert encoding human GIRK1a in the pIRES2eGFP vector. The insert construct is the gene of hG1a (GRIK1). GIRK1a: Homo sapiens potassium channel, inwardly rectifying subfamily J, member 3 (KCNJ3), transcript variant 1, also known as GIRK1a. NCBI Reference Sequence: NM_002239.3 (from NCBI data base) https://www.ncbi.nlm.nih.gov/nuccore/386781835/ mRNA: CDS: 196.1701 .

The bicistronic pIRES2eGFP-GIRK1 vector was developed by inserting GIRK1. Restriction enzymes for inserting GIRK1-DNA were BamHI and NheI.

8.2.1 Duplication of pIRES2eGFP vector

Electrocompetent XL1-Blue *E. Coli* bacteria (*Escherichia coli*) (Stratagene, #200228) were transferred from the -80°C freezer to a Styrofoam box filled with ice, where the cells were thawed slowly. The electroporation cuvettes were precooled on ice and parallel to that of a sterile SOC (Super Optimal Broth with Catabolite Repression) medium (ThermoFisher, 15544034) preheated to 37 ° C. A value of 2.00 kV was set on the Bio-Rad electroporator. After mixing the prepared cell suspension, an aliquot of 80µL was pipetted into the cold cuvette. 1 µg DNA was added to the cells under gentle mixing. An electrical pulse from the electroporator was submitted to the samples. 5 mL SOC Medium (held at 37°C) was added to the cells and resuspended. The mixed solution was transferred to a sterile 15 mL tube (SARSTEDT 62.554.002). The tube was incubated at 37°C for 1 hour with shaking at 250 revolutions per minute (rpm). 200 µL of this transformation mixtures was plated on Luria broth (LB) agar plate containing kanamycin (10µg/mL) (Merck, K0254-20ML) and 17 hours incubated at 37°C.

8.2.2 Colony counting and multiply clones

After counting colonies on LB agar plates, two of them were taken for bacterial culture. Each clone was transferred in a sterile 15 mL tube including 5 mL LB medium with kanamycin (10 µg/mL). The bacteria cells were incubated for 5 hours in an incubator (ThermoScientific, MaxQ 4000) at 37°C shaking at 250 rpm. The cloudy bacteria solution was transferred in 90 mL LB medium with kanamycin (10 µg/mL) and incubated overnight under the same conditions. After several centrifugations, the bacteria were separated from the nutrient solution and thus a cell pellet could be harvested for a midiprep.

8.2.3 Midiprep for isolation of plasmid DNA and restriction analysis

After 18 hours in LB medium, tubes were taken from the incubator and midipreps were done according to manufacturer's protocol (QIAGEN, 12143). To check the vector, a restriction analysis was carried out by digesting the PCR products.

Protocol for restriction analysis:

Aqua dest.	14.5	µL
DNA (1µg/µL)	3,0	µL
CutSmart (NEB, B7204S)	2.0	µL
SacI	0.5	µL
MfeI	0.5	µL

The components were mixed in a 1.5 mL reaction tube (Greiner, 616201). Thereafter, the sample was briefly centrifuged and placed in a thermocycler mixing block (Biozym, MB-102) at 37 ° C for 3 hours. To check the size of the digested plasmid, two restrictions-enzymes SacI, from NEB (NewEnglandBioLabs R0156S) and MfeI (NEB, R0589S) were used. A 1.0% agarose gel (Roth, 2267.1) including 2 µL GelRed (VWR, 41003) in 1x Tris-Acetate-EDTA (TAE) buffer and DNA Ladder 0,1–10 kb (NEB, N0469S; Promega, G5711) was prepared. All samples were applied to the gel. As a control uncut plasmid was additionally applied to the agarose gel. The gel was placed into a tank (Embi Tec, RunOne Electrophoresis cell) and covered with 1x TAE buffer. The voltage on the Power Supplies was set to 50V and the gel ran for 60 minutes. After running the gel, it was transferred onto the tray and the gel was scanned with BioRad GelDoc EZ Imager.

8.2.4 Primer for sequencing

Specific primers were used for sequencing the DNA (Eurofins Genomics, Austria)

eGFP N -Term rev, reverse primer:	5´ -CAGCTTGCCGTAGGTG-3´
CMV fw, forward primer:	5´ -CGGTGGGAGGTCTATATAAGC-3´

8.2.5 Linearization of plasmid DNA for transfection

For stable transfection of MCF10A cell line, the circular pIRES2eGFP plasmid was linearized with a unique cutter AseI, (NEB, #R0526S).

Master mix (MM) for cutting the DNA was as following:

pIRES2eGFP solution (0,48µg/µL)	50	µL
3.1 Buffer (NEB, B7203S)	20	µL
AseI	6	µL
RNAse free water	124	µL

The probe was gently mixed in 1.5 mL reaction tubes and then briefly centrifuged. The sample was incubated for 24 hours at 37°C. A 1,5% agarose gel was used to evaluate the samples. 1 µl 6 x loading dye purple (NEB, B7025S) with 2 µl linearized DNA diluted with water to 10 µL were mixed and loaded in the 1.5% agarose gel. The size of the DNA-lines was checked with the DNA ladder (NEB, N0469S). Before transfecting the cells, DNAs were cleaned up by Wizard SV Gel and PCR clean-up System (Promega, A9281) according to manufactures protocols.

8.3 Transfecting MCF10A cells

The cells were thawed out of the liquid nitrogen and seeded in a TC-Flask T25. To ascertain similar conditions for the experiments, the cells were splitted after thawing from the liquid nitrogen at least 2 times before the transfection. After the MCF10A cells are in exponential growth they can be further processed. Cells were harvested by trypsinization using TrypLE Express (ThermoFisher, 12604-013) and replicated in 6-well tissue culture dishes (Merck, Corning Costar TC-Treated Multiple Well Plates, CLS3516-50EA) in a final concentration of 20 000 cells per well. 2 mL growth medium was added to each well and incubated for 24 hours. After the cells had reached a confluence of 70% to 80%, transfecting was performed. For each 6 well plate, 3 µg of plasmid DNA, 10 µl of Lipofectamine 2000 (ThermoFisher, 11668027) and 242 µL of Opti-MEM Reduced Serum Medium (ThermoFisher, 11058021) were mixed in 1,5 mL reaction tubes and incubated for 15 minutes at room temperature. Before the mixture was added, the old medium of each well was sucked off and replaced by 1 mL fresh medium. The transfection solution was added drop wise to each well. The cells were incubated for 18 hours in 37°C and 5% CO_2. After the cells have been exposed to the DNA for appropriate time, they were checked using a laser scanning microscope (Leica DMIRE2) for a GFP signal. The cells were incubated for 48 hours in complete medium, trypsinized and replated in the selective medium with appropriate selective antibiotic G418 disulfate salt (Merck, A1720-1G) according to kill curve (done by Astrid Gorischek). The selection MEBM medium had a antobiotic-concentration of 16µg/mL. The medium was changed every day for the first 3 days than every 2 days for the next 2 weeks. This is the best way to remove the debris of dead cells from the cell culture dishes. After having more than 80% confluence, the transfected MCF10A cells were trypsinized and washed twice with PBS (ThermoFisher, 10010-023) and resuspended in 2 mL PBS. $10x10^4$ cells were seeded in 10 cm dishes TC Dishes 100 (Sarstedt, 83.3902). After reaching 30% - 40% confluence 1 - 4 clones were selected by hand under a cLSM microscope based on the fluorescence intensity. Using the cloning cylinder (Merck, TR-1004). One side of the sterile cloning cylinders was greased to allow the cylinder to seal the TC shell 100 (Sarstedt, 83.3902) after it had been placed on the plastic tray at the correct position. A curved forceps

was used for pressing the cylinder on a center of a small cluster of transfected cells. The cylinder was gently pressed to create a seal between cylinder and the plate. Only the cells inside of the cloning cylinder were washed with PBS and dissociated with TrypLE. MCF10A cells were removed from TC dish 100 and washed with PBS. The cells were transferred in TC-Plate 96 well (Sarstedt, 83.3924.005) and filled with 200 µL MEBM growth medium. After the cells reached to 80% of confluence, they were trypsinized and put in a 12-well plate and later on in a 10 cm dish. After the cells reached 90% of confluence, they were trypsinized and prepared for sorting. The fluorescent cells were sorted by cell sorting machine (FACS Aria, BD Biosciences). Every cell with a positive eGFP-signal was sorted in a 96 well plate filled with 100 µL growth medium with appropriate selective antibiotic G418. The medium was changed 2-3 times per week. After the cells reached to 90% of confluence, they were trypsinized and put in a 12-well plate and later on in T-25 flask Aliquots of MCF10A and MCF7 cells were stored in liquid nitrogen.

8.3.1 Confocal laser scanning microscopy

The stable cell lines were checked regularly after stable growing and splitting. Cells were cultured on 6 x 6 mm #1 glass plates (Menzel-Gläser 244087) and scanned by using a Leica inverted microscope with a laser-scanning module attached (DMIRE2 and TCS SL2; Leica Microsystems, Heidelberg, Germany). Cells were observed by the 10x and 20x objectives and 12-bit resolution. eGFP can be excited by the 488 nm laser line and is optimally detected at 509 nm.

8.4 Western blot

Western blotting is using specific antibodies to identify proteins that have been separated based on size by SDS gel-electrophoresis. For preparation of protein lysate from cell lines, two TC Dishes 35 (Sarstedt, 83.3900) of 90% confluence were used. Cells were washed twice with ice-cold PBS, lysed in 200 µL Frackelton buffer (10 mM Tris, 50 mM NaCl, 30 mM $Na_4P_2O_7$, 50 mM NaF, 200 mg/L Triton X-100, pH 7) including cOmplete Mini Protease Inhibitor Cocktail tablet (Merck, 11836170001), and sonicated using an ultrasound device (ECONO-Clean TVEN) for 30 minutes followed by centrifugation at 13200 rpm (4°C; 15 min). After that, the cell suspension was centrifuged off and 4x Laemmli sample buffer (BioRad, 1610747) was added to supernatant. The samples were denatured for 5 minutes at 95°C. Protein concentration in the supernatant was determined (Bradford, 1976). A SDS-gel electrophoresis (Laemmli, 1970). (SDS-PAGE 12%) including a protein marker (ThermoFisher, Spectra™ Multicolor Broad Range Protein Ladder 26634) was carried out. The SDS gel was run at 80 V for 20 minutes and then at 120 V until the end. After electro transfer (150mA, on ice) on Immobilon-P PVDF Membrane (Merck, IPVH07850) the membranes were stained with 0,5% Ponceau S solution (Merck, P7170) according to the

manufactures protocol to check the protein transfer (washed in aqua dest). Membranes were blocked in 3% Difco TM Skim Milk (BD Biosciences, 232100) solved in TBST for 30 minutes at room temperature on a shaker. The membranes were incubated overnight with the primary antibody diluted in 5 % BSA (Roth 3854.2) in TBST at 4 °C on a shaker. The membranes were washed 3 times with 3% Difco TM Skim Milk followed by incubation with the secondary antibody for 1 hour at room temperature on an IKA KS260 shaker. After 3x washing with 3 % Difco TM Skim Milk in TBST (10 minutes) and additional washing in TBST buffer (5 minutes), followed by incubation with ECL-Select (GE-Healthcare) antibody–protein complexes the membranes were analyzed by ChemiDoc Imagers (BioRad, ChemiDoc MP). Table 1 summarizes the antibodies that were tested to determine the product with the highest specificity and the dilutions used are mentioned. For Western blots, GIRK1 (Alomone) 1-st Ab GIRK1 (C-T Alomone, rabbit polyclonal) (dilution 1:800 in 5 % [w/v] BSA), 2-nd Ab Peroxidase Goat Anti-Rabbit (1:10000 in 3 % [w/v] skim milk), were used. For Wbs after IP an Ab (against N-T) of Girk1 were used. 1-st Ab is MK4 polyclonal rabbit (homemade) (1:250 in 5 % [w/v] BSA), 2-nd Ab Clean Blot IP detection reagent (1:5000 in 3 % [w/v] skim milk). In order to detect the GIRK1 channel both at the C-terminal and at the N-terminal further Ab's were used. GIRK 1 (Abcam 119246) mouse monoclonal (dilution 1:500 in 5 % [w/v] BSA) and, as second antibody Clean Blot IP detection reagent (1:5000 in 3 % [w/v] skim milk).

Table 1: Primary anti-GIRK1 antibodies for Western Blots

Product	Supplier	Source	Clonality	Dilution
GIRK MK4 N-T	**Kurt Schmidt**	**rabbit**	**polyclonal**	**1:250**
GIRK1 APC-005 C-T	**Alomone Labs**	**rabbit**	**polyclonal**	**1:800**
Clean Blot IP detection reagent 21230	**ThermoFisher**	**horseradish peroxidase conjugate**		**1:5000**
Peroxidase Goat Anti-Rabbit IgG 111-035-144	**Jackson Immuno Research**	**goat**	**polyclonal**	**1:10000**
GIRK 1 119246	**Abcam**	**mouse**	**monoclonal**	**1:500**

8.5 Immunoprecipitation

MCF7 cell of 90% confluence were lysed in a TC Flask T75 (Sarstedt, 83.3911.002). The cells were gently broken by lysis to make the protein accessible to the antibody. Cells were washed twice with ice-cold PBS and lysed in 500 µL Frackelton buffer. The cells released from the surface of the dishes were transferred to an 1,5 mL reaction tube and placed on

ice. Subsequently, the cell lysate was placed in an ultrasound device for 30 minutes, filled with ice. After that, the cell suspension was centrifuged. In the clear supernatant 150 µL Pierce™ Protein A Agarose (ThermoFisher, 20333) were added. The reaction tube was constantly rotated for one hour at a temperature of 4 °C. Thereafter, the sample was centrifuged (Eppendorf 5415R) for 3 minutes, 4°C and 4000 rpm. The supernatant was transferred in a new reaction tube. 15 µL GIRK1 antibody (Alomone Labs, APC-005) were added. The reaction tube was constantly rotated at 4°C over night. 225 µL Pierce™ Protein A Agarose were added and incubated for 2 hours under rotation. The probe was centrifuged for 3 minutes, 4°C and 4000 rpm. The supernatant of the sample was discarded and the pellet was washed 3 times with 500 µl of Frackelton buffer. 30 µL 4x Laemmli buffer (BioRad, 1610747) was added to the sample before incubation at (95°C, 5 minutes, 4000rpm RT). Bound protein was analyzed by Western-blot from Astrid Gorischek.

8.6 Quantitative PCR

To quantify gene expression, a real-time polymerase chain reaction (RT-PCR) and a quantitative polymerase chain reaction (qPCR) were performed.

8.6.1 Harvesting of cell pellets and RNA isolation

Cells were cultured in TC-Flask (T25) with complete growth medium. After reaching 70 - 80% confluency, cells were trypsinized and washed twice with PBS (the exact procedure can be found under point 8.1 “proliferation”). The RNA was isolated from the freshly prepared cell-pellet. For purification of the total RNA from the cell-pellet, the QIA shredder spin column (Qiagen, 79645) and RNeasy Mini Kit (Qiagen, 74104) were used. The RNA was extracted according to manufacturer’s protocol. The concentration of the total RNA was measured by Nanodrop 2000c (Peqlab) and 1µg of RNA were used for converting to cDNA. The remaining amount of the RNA was shock frozen in liquid nitrogen. The RNA was stored at -80°C for further experiments. For converting to cDNA, QuantiTect Rev. Transcription kit (Qiagen, 205311) was used and 1µg of RNA was converted to cDNA according to manufacturer’s protocol. The obtained cDNA was diluted 1:25 in RNase-free water and used for the qPCR analysis. The samples were analyzed by qPCR QuantiFast SYBR Green PCR Kit (Qiagen, 204054).

8.6.2 Primers for qPCR

Real time RT-PCR protocol run by using LightCycler 480 system (Roche Diagnostics, Austria) and Thermal Cycler C1000 Touch (BioRad).

The following primers were used:

YWHAZ-f, primer forward:	5´-ACTTTTGGTACATGTGGCTTCAA-3´
YWHAZ-rev: primer reverse:	5´-CCGCCAGGACAAACCAGTAT-3´
GAPDH, primer forward:	5′-ATGGGGAAGGTGAAGGTCG-3′
GAPDH, primer reverse:	5′-GGGGTCATTGATGGCAACAATA-3′
GIRK1a , primer forward:	5′-GTGGAAACAACTGGGATGAC-3′
GIRK1a , primer reverse:	5′-GTTGCATGGAACTGGGAGTA-3′
qPCR-LAMB3B, primer forward:	5´-CTTTGACCCCGCTGTGTTTG-3´
qPCR-LAMB3B, primer reverse:	5´-CTGACACCGCTCACAGTTCT-3´
qPCR-COL6A2, primer forward:	5´-GCAGAGCTGTCCTTCGTGT-3`
qPCR-COL6A2, primer reverse:	5´-TGGGTACCACGTTCTCGTT-3´
qPCR-IL1B, primer forward:	5´-TGAGCTCGCCAGTGAAATGA-3`
qPCR-IL1B, primer reverse:	5´-AGATTCGTAGCTGGATGCCG-3`
qPCR-SERPINE1, primer forward:	5´-GCCAGTGGAAGACTCCCTTC-3´
qPCR-SERPINE1, primer reverse:	5´-GTGCTGCCGTCTGATTTGTG-3´
qPCR-CCBE1, primer forward:	5´-GGACACACGTGGACCTACAG-3´
qPCR-CCBE1, primer reverse:	5´-GTCGTCGCGATTTTGCTCTC-3´
qPCR-IFI6, primer forward:	5´-GGTGAGAATGCGGGTAAGGAT-3´
qPCR-IFI6, primer reverse:	5´-AGGTCAGGGCCTTCCAGAAC-3´
qPCR-OAS2, primer forward:	5´-CGTTGGTGTTGGCATCTTCTG-3´
qPCR-OAS2, primer reverse:	5´-TGCATTGTCGGCACTTTCCA-3´

Total RNA from the MCF10A samples was also obtained by using the RNeasy Mini Kit. The RNA was extracted according to manufacturer's protocol. The converted cDNA was 1:25 diluted and used for the qPCR. The specific primers are oligonucleotides and specific for each gene. The following primers were used:

Kit hTP53_pb2_F, primer forward:	5'-GAGGTTGGCTCTGACTGTACC3′
hTP53_pb2_R, primer reverse:	5'-TCCGTCCCAGTAGATTACCAC3′
hCDKN1A_F primer forward:	5′-GGCAGACCAGCATGACAGATT-3′
hCDKN1A_R primer reverse:	5'-GCGGATTAGGGCTTCCTCTT-3′

hGADD45a_F, primer forward: 5'-GAGAGCAGAAGACCGAAAGGA-3′

hGADD45a_R, primer reverse: 5'-CACAACACCACGTTATCGGG-3′

hMDM2_pb1_F; primer forward: 5'-GAATCATCGGACTCAGGTACATC-3′

hMDM2_pb1_R, primer reverse: 5'-TCTGTCTCACTAATTGCTCTCCT-3′

The primers (hTP53, hCDKN1A, hGADD45a and hMDM2) were kindly provided by Andreas Prokesch (Gottfried Schatz Research Center, Department of Histology; Medical University of Graz, Austria).

MM for qPCR:

QuantiFast CYBR green	5	µL
Forward primer 10pmol/mL	1	µL
Reverse primer 10pmol/mL	1	µL
Specific cDNA 1/25 diluted	3	µL

PCR reactions were carried out on a LightCycler 480 system or Thermal Cycler C1000. For the Light Cycler 480 the Multiwell plates 96 white (Roche, 04 729 692 001) were used. The above ingredients were mixed together as MM. This also applies to Thermal Cycler C1000 Touch with Hard Shell 480 PCR plates 96-well (BioRad). Subsequently, the plates were sealed with plate sealer and shortly centrifuged (900 rpm/2 min). All samples were measured in triplicates. The PCR is of 40 cycles. The relative mRNA expression levels of GIRK1 gene compared to the housekeeping genes YWHAZ and GAPDH were calculated using $2^{\Delta\ \Delta Ct}$ (Livak and Schmittgen, 2001). For calculating the gene expression data from quantitative real-time PCR experiments the REST 2009 software from QIAGEN was used. REST 2009 Software (Pfaffl et al., 2002) were also used.

8.7 Transcriptome analysis

The relationship between genotype and phenotype plays a central role in developmental biology. Transcriptome analyzes of cell lines are good strategies to connect genotype to phenotype. Essentially all cells within an individual organism have a virtually identical genotype, but the individual transcriptomes reflect expression of a subset of genes, which is defined by their epigenetic state. Individual cell lines (different clones) show a unique transcriptome, which can be used to evaluate gene regulation, physiological functions, behavior and phenotype during development. To evaluate gene regulation, behavior and phenotype during development an additional transcriptome analysis of different MCF10A cell lines was carried out (Tang et al., 2011). The RNA was isolated from the freshly prepared cell-pellet. For purification of the total RNA from the cell-pellet, the QIA shredder spin column (Qiagen, 79645) and RNeasy Mini Kit (Qiagen, 74104) were used. The RNA

was extracted according to manufacturer's protocol. The concentration of the total RNA was measured by Nanodrop 2000c (Peqlab). The RNA was kept in -80°C freezer (Eppendorf). 10ng of the isolated RNA was heat inactivated for 10 min at 80 °C followed by cDNA Synthesis using the SuperScript® VILO™ cDNA Synthesis Kit (Thermo Fisher, 11754050).

Figure 7: Transcriptome Sequencing by Ion Torrent Next-Generation Sequencing. Automated production of Ion AmpliSeq transcriptome libraries using the Ion S5 XL and Ion PIv3 Chip containing 8 barcoded chips for sample tracking.

DNA library was generated using the Ion AmpliSeq™Transcriptome (ThermoFisher, A26325) together with Ion PI™ Chip Kit (ThermoFisher, A26771). Human Gene Expression Kit (Thermo Fisher) according to the manufacturer's instructions. The transcriptome analysis was done by Andrea Thüringer (Diagnostic & Research Institute of Pathology; Medical University of Graz). The Ion S5 XL (ThermoFisher Scientific) was used (sown in Figure 7). Sequencing was performed on an Ion S5 XL benchtop sequencer (Thermo Fisher Scientific) to a length of 200 base pairs. On average 8 million reads were sequenced per sample. Data analysis was performed using the Ampliseq RNA Transcriptome Workflow of the Ion Torrent Suite. Briefly, amplicons were mapped to a human transcriptome reference (AmpliSeq_Transcriptome_21K.v1) and mapping reads were counted for each transcript and exported to a tabular file. It is a high throughput sequencing application and enables to get a DNA library. Data were analyzed by Torrent Server. For simultaneous measurements of the expression levels of 20,000 human Reference Sequence (RefSeq) genes in a single

assay the Ion AmpliSeq™ Transcriptome Human Gene Expression Kit (ThermoFisher, A26325) together with Ion PI™ Chip Kit (ThermoFisher, A26771) were used.

For analyzing the data, Database for Annotation, Visualization and Integrated Discovery (DAVID version v6.7), was used. This tool provides a comprehensive set of functional annotation to understand biological meaning behind large list of genes. For annotation a fuzzy clustering concept as functional classification by measuring relationships among the annotation terms based on the degree of their co-association with genes in order to cluster somewhat heterogeneous, yet highly similar annotation into functional annotation groups was used (Huang da et al., 2009). This analysis was done by Andreas Prokesch (Cell Biology, Histology and Embryology; Medical University of Graz). Two DAVID functional clusters with top 50 2x up and 4 with 2x down regulated genes were analyzed. Heatmaps of genes comprising the gene ontology (GO) term “wound healing, extra cellular matrix, cell division, motility and IF-γ response” that is enriched in a DAVID functional annotation analysis focused on GO biological processes were created. Data were taken from two independent experiments, using different MCF10A cell passages.

8.8 Vital parameters

8.8.1 Chick Chorioallantoic Membrane (CAM) Assay

To study angiogenesis the CAM Assay was taken. Fertilized leghorn chicken eggs were obtained from a local hatchery (Schropper GmbH, Gloggnitz, Austria) and the eggs were incubated at 37°C and 60% humidity. The egg shells were cracked on day 3 of embryonic development and the embryos were incubated in a sterile dish for additonal applications. For further incubation of 7 days, the chicken embryos were placed into a sterilized plastic dish and placed in a MultiQuip Incubator at 37 °C with 50% humidity. Briefly, the cells were diluted to a concentration of 1×10^6 cells/15 µL, counted with Luna II (BioZym) cell counter and cell counting slides (BioZym, 872010). Cells were applied as shown in table 2. MCF10A cells (WT, vector control and overexpressors) were applied in volumes of 20 µL in a 1:1 mixture with Matrigel (BD Biosciences, 356237) (10^6 cells/onplant) within 5 mm silicone rings applied on vascular branches of the CAM (Ribatti et al., 2006b). After 4 days of incubation progression of tumor growth was monitored by photo documentation (Olympus SZX16). The intensity of angiogenesis and the formed tumor size were analyzed and measured as tumor area [mm^2]. This is a special program IQM (Interactive Quantitative Morphology) (Kainz et al., 2015).

Table 2: Overview of cell lines that were used for CAM Assay. $1x10^6$ cells were placed on each 5 mm silicon ring. MCF10A wilde type, vector control and mutants were used.

3 eggs per cell linie	cells/egg 1	cells/egg 2	cells/egg 3	Silicon-ring/Eggs	cells/silicon-ring
MCF10A WT	3 mio cells	3 mio cells	3 mio cells	3 pcs	1 mio
MCF10A pIRES2eGFP #1	3 mio cells	3 mio cells	3 mio cells	3 pcs	1 mio
MCF10A pIRES2eGFP #2	3 mio cells	3 mio cells	3 mio cells	3 pcs	1 mio
MCF10A pIRES2hG1a #1	3 mio cells	3 mio cells	3 mio cells	3 pcs	1 mio
MCF10A pIRES2hG1a #3	3 mio cells	3 mio cells	3 mio cells	3 pcs	1 mio

8.8.2 Proliferation assay (EdU Assay)

For the direct measurement of cells in the S-phase, 5-ethynyl-2′-deoxyuridine (EdU) a nucleoside analog of thymidine, was used. Cells grown in the presence of EdU incorporate the link at thymidine during the S-phase. The fluorophore-labeled chemical component reacts with the incorporated EdU enabling a detection by flow cytometry (Buck et al., 2008). Briefly, MCF10A cells ($2x10^5$) were seeded in 6 well plates and incubated in cell culture incubator with complete growth medium. After reaching 70% - 80% confluency a 10 mM solution of the EdU (ThermoFisher, Click-iT™ EdU Pacific Blue™ Flow Cytometry Assay Kit C10418) was added to each well. After 3 hours incubation time, cells were harvested and washed with 3 mL 1% BSA (Bovine serum albumin) (Roth, 3854.2) and finally solved in PBS. The Click-iT assay was used for preparation of the cells according to the manufacturer's protocol. Cells without staining and treatment were integrated as controls in all experiments. To define cell cycle (G1/G0; S; G2/M), a fluorescent DNA binding dye 7-AAD Viability Staining Solution Peridinin Chlorophyll Protein Complex (PerCP-A) were used. Samples were acquired on a LSRII (BD Bioscience, Vienna, Austria), and data were analyzed with the DIVA software (BD Bioscience).

8.8.3 In vitro motility assay

This assay can be used to determine quantitatively if cells are capable, depending on the mutation, to move (Turnbull and Whitchurch, 2014). By using time-lapsed cell tracking, individual movements of each cell can be analyzed. The recorded migration route provides information about the movement length and direction at a given time point (Kramer et al., 2013). MCF10A and MCF7 (WT, vector controls and overexpressors) were used. In each 24 well tissue culture plate (FALCON, 353847) $2x10^4$ MCF10A cells and $5x10^4$ MCF7 cells were seeded into each well and were allowed to grow. Cell monolayers were grown to 20% confluency in complete growth medium. On the day of the experiment, the liquid medium was totally sucked off and replaced with 800 µL fresh medium. Single cell motility properties were studied with the cell observer (Zeiss, Axiovert 200M) by following cell migration. Frames were taken at different positions every 20 min over a period of 72 h. From each well of the 24 well plate, five representative sections were taken for analysis. Cells were tracked

with ImageJ open-source software (1.51j8; Wayne Rasband, NIH, http:// imageJ.NIH.gov/) using the manual tracking plugin. For analyzing the data the VBA_v25 macro, which was written by Wolfgang Schreibmayer, was used. The used time interval for the subsequent analysis was 20 minutes. xy-calibration was 1µm.

8.8.4 ECM Cell adhesion assay

The extracellular matrix (ECM) is recognized as a dynamical and complex environment. It is involved in multiple cell-pathological processes (Hellewell et al., 2017). The colorimetric CHEMICON® ECM Cell Adhesion Array Kit (Merck, ECM540), for characterization of cell

Table 3: Characterization of cell adhesion. The different ECM components were shown in the table. Wells were coated with Collagen I, Collagen II, Collagen IV, Fibronectin, Laminin, Tenascin and Vitronectin, abbreviated as Col I, Col II, Col IV, FN, LN, TN and VN, respectively (triplicates were made for each experiment).

MCF10A WT			hG1a#3			eGFP#1			hG1a#1		
Col I	Col I	Col I	Col I	Col I	Col I	Col I	Col I	Col I	Col I	Col I	Col I
Col II	Col II	Col II	Col II	Col II	Col II	Col II	Col II	Col II	Col II	Col II	Col II
Col IV	Col IV	Col IV	Col IV	Col IV	Col IV	Col IV	Col IV	Col IV	Col IV	Col IV	Col IV
FN	FN	FN	FN	FN	FN	FN	FN	FN	FN	FN	FN
LN	LN	LN	LN	LN	LN	LN	LN	LN	LN	LN	LN
TN	TN	TN	TN	TN	TN	TN	TN	TN	TN	TN	TN
VN	VN	VN	VN	VN	VN	VN	VN	VN	VN	VN	VN
Neg	Neg	Neg	Neg	Neg	Neg	Neg	Neg	Neg	Neg	Neg	Neg

adhesion and quantitative comparison of multiple samples/cell lines, used. The ECM components are: human Collagen Type I (Col I), human Collagen Type II (Col II), human Collagen Type IV (Col IV), human Fibronectin (FN), human Laminin (LN), human Tenascin-C (TN) and human Vitronectin (VN). Three independent experiments for each cell line were performed in triplicates. The ECM components were rehydrated with 200 µL PBS for each well and incubated for 10 minutes, while the cells in TC-Flask (T25) were trypsinized. Before the suspension was used, cells were regenerated in assay buffer for 10 minutes. The final cell suspension had a concentration of 1.0 - 2.0x10^6 cells/well and was applied in cell culture dishes containing MEBM medium.

100 µL of cell suspension with different cells (MCF10A WT, vector control and overexpressors) was added in each well as shown in table 3. The incubation time was two hours at 37°C in a CO_2 incubator. The unattached cells were sucked off and the attached cells were treated with cell stain solution. Finally, the plastic dishes were washed with distilled water. The plate was air-dried for 5 minutes. 100µL of Extraction Buffer were added to each well and incubated by gently rotating for 10 minutes on a shaker at room

temperature. The absorbance at 540-570 nm was determined on a plate reader (CLARIOstar, BMG LABTECH Inc., Cary, NC, USA).

8.8.5 Invasion assay

Migration is a key property of live cells. One useful method to examine cell migration is cell invasion (Justus et al., 2014). As FBS (Fetal Bovine Serum) is not suitable as chemoattractant for MCF10A, Therefore, a growth medium was tested to find a functioning chemoattractant. Appropriate culture conditions for MCF10A cells (self-made minimal medium) are described in chapter 8.1. For MCF7 cells the minimal medium without FBS was used.

A Corning® BioCoat™ Matrigel® Invasion Chambers (Corning, 354480) was taken from -20°C storage and equilibrated to room temperature. The chamber was placed under the laminar flow hood. For rehydration, 500 µL minimal culture medium were added to the interior of the inserts. 500 µL PBS were also added to the bottom of the wells. The 24 well plate was rehydrated for 2 hours in a humidified tissue culture incubator. After rehydration, the medium was carefully removed without disturbing the layer. An MCF10A cell suspension, containing minimal medium inclusive $5x10^4$ cells/mL, was made. Complete growth medium including chemoattractant was added to the wells of the Falcon TC Companion Plate. Sterile forceps to transfer the control inserts to the wells containing the chemoattractant were used. Care was taken to avoid bubble formation on the underside of the membrane. 1×10^4 MCF10A cells and $2,5 \times 10^4$ MCF7 cells were added to each 24 well chamber. Cells were incubated for 22 hours in a humidified tissue culture incubator at 37°C and 5% CO_2 atmosphere. The non-invading cells were removed from the upper surface of the membrane by gently scrubbing with a cotton swab. Before staining, 1 mL -20°C cold methanol (Roth, 0082.1) was added to the chamber. After removing the methanol, the chamber was air-dried for 5 minutes. The cells on the lower surface of the membrane were stained with 0,5% crystal violet stain solution (Merck, C0775). All samples were air-dried and photographed. (With the friendly support of Rudi Schmid Cell Biology, Histology and Embryology). The ZEISS Axio Zoom V16 microscope was used for the documentation. Three independent experiments for each cell line were performed in triplicates.

8.8.6 Wound healing assay

A wound healing assay, also known as scratch assay, was carried out to check cell migration. A ‘‘scratch’’ was made in a cell monolayer, capturing the images at the beginning and at defined intervals during cell migration closing the scratch (Liang et al., 2007). MCF10A and MCF7 (WT, vector control and overexpressors) were plated into 24 well plates (BD, 353847). $1,5 \times 10^5$ cells were seeded per dish. After growing to 90% confluency a

scratch was made across the center of the cell monolayer with a yellow pipette tip (Sarstedt, 70.760.012), resulting in a scratch width of approximately 1mm. Detached and damaged cells were removed by carefully aspirating off the medium and rinsing with PBS before addition of 700µL fresh complete growth medium. The plate was put in a cell observer (Zeiss Axiovert 200M) and monitored for 72 hours with 20 minutes' interval for MCF10A and 30 minutes' interval for MCF7 cells. Three independent experiments for each cell line were

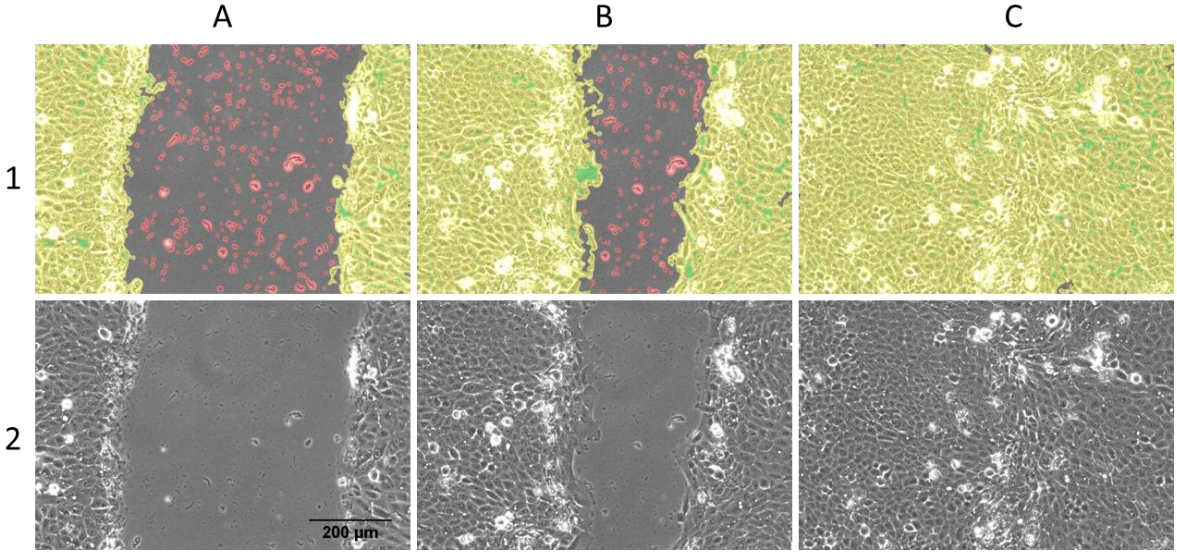

Figure 8: Image processing and analysis of the wound healing assay. Both rows show the wound healing progress over a period of 72 hours. Row 2 shows the images before analysis. Row 1 demonstrates the analysis algorithm used (see supp. material) and the coloration of the detected (red and yellow) and measured areas (yellow) enabling a fine tuning of the parameters for each analysis series and application Vertical A is start point, vertical B is time point after 24 hours and vertical C is end point. The green patches are areas which have been included using the fill holes feature of imageJ.

performed in triplicates. For analyzing the data, ImageJ software (1.51j8) (Schneider et al., 2012) and ALGov9 macro which was written by Trevor DeVaney were used. After median correction and image stabilization a fourier bandpass filter was used. A low pass FFT (Fast Fourier Transform) filter was used to remove the pixel noise and other disadvantageous effects. A high pass FFT filter was used to remove low frequency changes in the illumination of the image resulting in a constant background level for further processing (figure 8). The image was then analyzed using a variance filter and a median filter and subsequently a threshold was set. The binary images were used to show the detected areas and superimposed on the original image as a control measure. The parameters for each step were set using a dialog window. The image sequence is then processed using the accepted parameters and the results saved as a table of results and a composite image. The wound healing images in a time series were analyzed for gap area over time.

8.8.7 Colony Formation Assay (Clonogenic Assay)

The clonogenic assay or colony formation assay is an *in vitro* cell survival assay of a single cell to grow into a colony. The assay tests cells in the population for its ability to undergo an unlimited division (Franken et al., 2006). A representative micrographs of 35 mm microplate slots per experimental group were made and the stained colonies were visible as dark spots. Statistical analysis of MCF10A cell lines were made and three independent experiments for each cell line were performed in triplicates. MCF10A and MCF7 cells were cultured according to the requirement (chapter 8.1). For each 6 well plate 100 pcs MCF10A single cells were seeded in 1000 µL medium. For MCF7, 200 single cells were seeded and cultured in 1000 µL medium. Both are plated in 6 well plates. On day 8 the cells were fixed and stained. The 6 well plates were washed with PBS solution and fixed for 5 minutes, with fixing solution (85% methanol 15% acetic acid). 100% acetic acid (Merck, 1000632500) was used to prepare the fixing solution. After washing with distilled water, cells were incubated for 2 hours with 1000 µL 0,5% crystal violet stain solution. Samples were washed with distilled water and air dried at room temperature. All the prepared 6 well plates were scaned with CanonScan 4400F. The evaluation was carried out by means of ImageJ software (1.51j8). Three independent experiments for each cell line were performed in triplicates.

8.8.8 Electrophysiological Recordings and Analysis

MCF10A and MCF7 cells were seeded on 6 x 6 mm coverslips in 24 well plates, cultured as described for more than 24 h before electrophysiological experiments were started. For recording, the coverslips were transferred to a bathing chamber in bathing solution (NaBS) mounted to the stage of an inverted microscope (IM35, Zeiss, Germany). Using whole cell patch clamp method and nystatin perforation as previously described (Mullner et al., 2000), resting membrane potentials were recorded at RT not longer than 20 minutes after the cells were removed from the incubator. Briefly, nystatin stock solution (NSS) was prepared by dissolving nystatin (N6261, Merck, Darmstadt, Germany) in DMSO (analytical grade, Merck, Darmstadt, Germany) at a concentration of 50mg/mL, aliquoted and stored at -20 ^{o}C until use. Nystatin containing pipette solution (PSN) was prepared by pipetting 200 µL NSS into 10 mL pipette filling solution (PFS; in 15 mL Falcon tube) under sonication using ultrasonic cleaning bath (Emmi-H22, EMAG AG, Mörfelden-Walldorf, Germany). After nystatin addition, PSN was sonicated for one additional minute, stored on ice and filtered (Wahtman Rotrand 0,2 µm, FP30/0,2-CA-510462200, Fisher Scientific) immediately before use. Patch clamp pipettes were pulled from borosilicate glass capillaries (Assistent Mikro-Haematokrit capillary tubes, Hecht, Fisher Scientific; final resistance was 1–2.5 MΩ). After Gigaseal formation, perforation was monitored by capacitance measurements. After successful perforation, as judged by capacitance > 25 pF, resting membrane potential was low pass

filtered at 50 Hz and recorded for 20 seconds using Axopatch-200A amplifier (Molecular Devices, USA). Traces were digitized at 1 kHz using the Digidata 1322A interface (Molecular Devices, USA) using Clampex 9.2 software (Molecular Devices, USA). Membrane resting potential was measured by averaging the entire trace using the Clampfit 10.3 software (Molecular Devices, USA). The composition of solutions used was as follows (concentrations given in parenthesis in mmol/L): NaBS: KCl (2), NaCl (148), $MgCl_2$ (4), $CaCl_2$ (1) and HEPES (10), buffered with NaOH to pH:7.4. PFS: KCl (20), K^+/aspartate$^-$ (120), NaCl (10), $MgCl_2$ (4), $EGTA^-/K^+$ (1) and HEPES, buffered with KOH to pH: 7.4.

8.8.9 Mammosphere Forming Assay

Mammosphere Forming is a standard tool in breast cancer research. The ability to form several generations of non-adherent cells is related to the self-renewal ability of the stem cells (Manuel Iglesias et al., 2013, Schwarzenbacher et al., 2019). The adherent growing MEC cell line MCF10A was dissociated into single cells using trypsin/ Ethylenediaminetetraacetic acid (EDTA) solution (Merck, T4174-100mL) and 2000 single cells per well were seeded in ultra-low attachment 6-well plates (Corning, NY, USA) using serum-free MEBM (Lonza, CC-3151) medium (SFM). SFM was supplemented with 1 x B27 supplement (ThermoFisher, 17504044), 20 ng/ mL human epidermal growth factor EGF (Peprotech, Hamburg, Germany), 10 ng/mL human basic fibroblast growth factor FGF (Peprotech), 20 IU/mL Heparin (Baxter, Vienna, Austria) and 1% antibiotic/antimycotic solution (Thermo Fisher Scientific, containing 10,000 units/mL of penicillin, 10,000 µg/mL of streptomycin, and 25 µg/mL of Gibco Amphotericin B. Three independent experiments for each cell line were performed in triplicates. Mammospheres were observed and counted under a microscope 10 days later. Three replicates were done per cell line.

8.9 Statistical analysis

Statistical analysis of data was performed using SPSS embedded in Sigmaplot (SPW 14.0, Systat Software Inc.). In short, datasets consisting of more than two experimental groups were tested for normal distribution and one way or rank based ANOVA was performed as appropriate. Subsequent pairwise comparisons were performed using appropriate algorithms. For the comparison of two experimental groups, student's t-test was used. Statistics for cell migration was computed with public domain software R, version 3.5.3 and RStudio software version 1.1.463 (RStudio Team (2016), R Core Team 2019). In case of MCF10A cells, means of data were analysed with a bootstrap-t method based ANOVA using the R function t1waybt (Wilcox 2017), followed by post hoc tests using the R function linconbt (Wilcox, 2017) allowing also a robust comparion of all pairs of groups. In case of MCF7 cells, due to pronounced skewness, medians were analysed with a percentile bootstrap method using the R function Qanova (Wilcox, 2017) followed by pairwise median

comparisons using a percentile bootstrap method implemented in the R function medpb (Wilcox, 2017). Holm method was used for adjustment of p-values due to multiple comparisons. To compare deciles the R function, qcomhfMC (Wilcox, 2017) was used combining a percentile booststap method with a quantile estimator allowing tied values.

9. Results

The following sections are dedicated to describe the results of this thesis and discuss them. These data were also largely published in (Schratter et al., in press)

9.1 Analysis of GIRK1 levels in benign and malign MEC cell lines

To prove the common origin of the MEC cell lines MCF10A und MCF7, STR profiling of the parental cell line was performed. All analyzed samples showed the short tandem repeat (STR) profile at the markers CSF1PO, D5S818, D13S317, D7S820, D16S539, vWA, TH01, TPOX, and Amelogenin (to find in 11.2 STR-Analyzis). We found no cross contamination in the MEC cell lines.

First, we determined the mRNA levels of GIRK1 in MCF10A and MCF7 cells lines. To catalog molecular variations, we profiled the gene expression levels by qPCR. Second, we traced the protein expression of GIRK1 by Western blot (WB) analysis in benign MCF10A cell lines and malignant MCF7 whole-cell lysates probed with different GIRK1 Antibodies. Third, the effect of GIRK1 overexpression on resting membrane potential of MCF10A cells and MCF7 cells was measured.

9.1.1 Characterization of pIRES2eGFP vector

To successfully detect the presence of the vector in MCF10A control cell lines, the green fluorescent protein (eGFP) gene was inserted into the MCF10A cells via the pIRES2eGFP vector. The 5308 bp empty pIRES2eGFP vector was checked by using the restriction enzymes MfeI and SacI for cutting the circular vector. After restriction digest of the empty vector, DNA fragments were analyzed using agarose gel electrophoresis. The result of the analysis can be seen in figure 9.

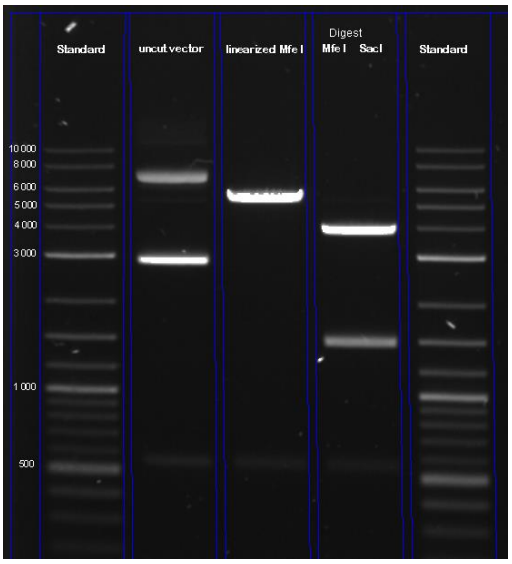

Figure 9: Empty pIRES2eGFP vector. Circular vector was linearized with MfeI and SacI. Both restriction enzymes are unique cutters. DNA bands of pIRESeGFP after digesting with restriction enzymes. Line 1: Standard, Line 2: Uncut empty vector, Line 3: pIRES2eGFP cut with MfeI, Line 4: DNA cut with MfeI and SacI; Line5: Standard

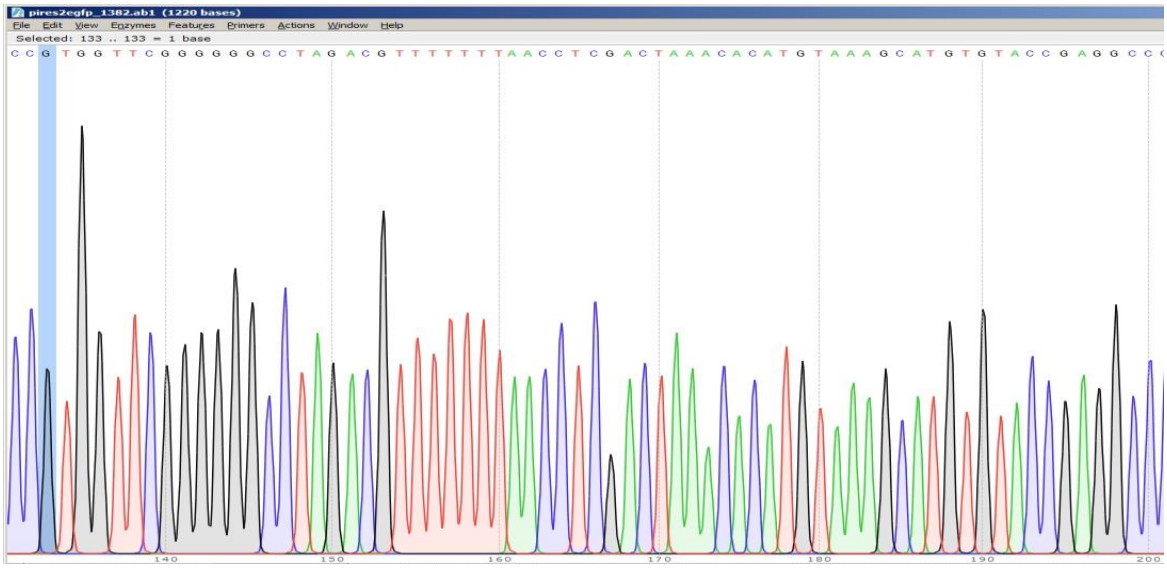

Figure 10: Shows a part of the DNA results of the pIRES-vector sequencing. The figure show an example of a Sanger sequencing read. The four bases, Adenin (A), Guanin (G), Cytosin (C) und Thymin (T), are detected using different fluorescent labels. These are detected and represented as peak of four different colours. They can be interpreted to determine the DNA sequence.

The empty vector was transformed in *E. coli* XL-1 to get sufficient DNA for stable transfection in MCF10A cell lines. After purification, the DNA of the empty pIRES2eGFP vector was totally sequenced. A part of the results can be seen in figure 10.

9.1.2 Overexpression of single fusion proteins

The 6777 bp pIRES2eGFP-GIRK1 vector was created by inserting GIRK1 coding sequence (cds). Restriction enzymes for inserting GIRK1-DNA were BamHI and NheI. The bicistronic pIRES2eGFP vector digested with BamHI and NheI was ligated to DNA segment GIRK1. Transformation was done with *E. coli* XL-1 bacteria. When pIRES2eGFP-GIRK1 digested with HindIII and PciI, a band of 5239 bp for the cloning vector and a band of 1538 bp for the GIRK1 were observed (Figure 11). For stable transfection in MCF10A and MCF7 cells, the vector DNA was linearized by using AseI. After transfection in MEC cells the positive clones were checked by confocal laser scanning microscopy (cLSM). The 6777 bp vector was checked by using the restriction enzymes HindIII and PciI for cutting the circular vector. After restriction digest of the vector, DNA fragments were analyzed using agarose gel electrophoresis. The result of the analysis can be seen in figure 12.

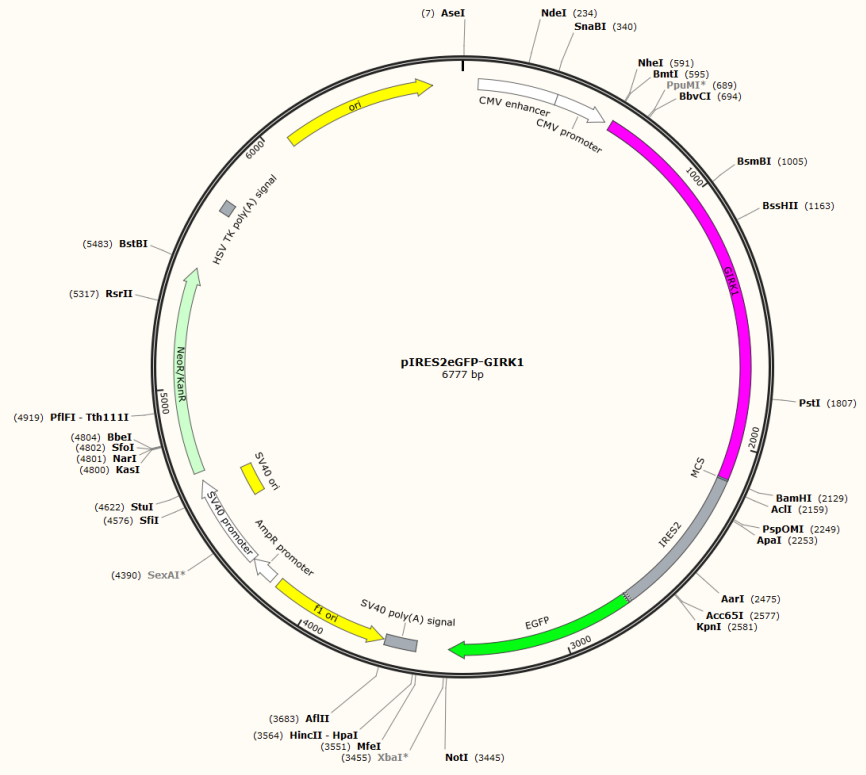

Figure 11: DNA construct including GIRK1. Map of pIRES2eGFP with the GIRK1 insert is shown and highlighted in purple. Created by SnapGene software (from GSL Biotech; available at snapgene.com).

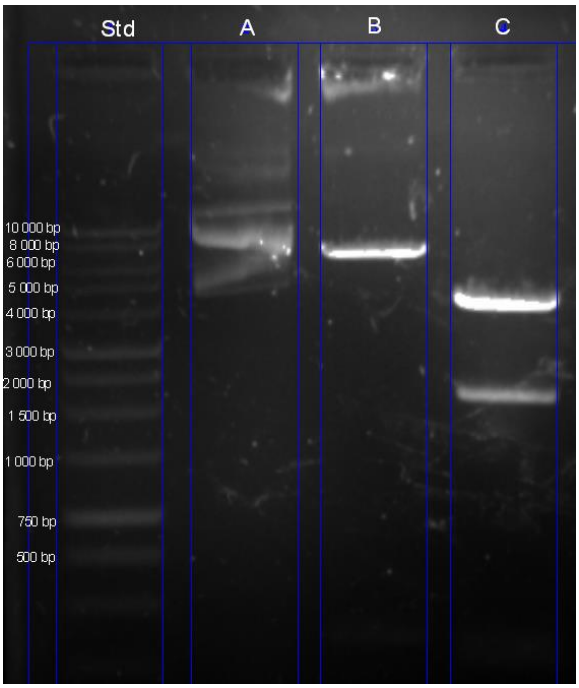

Figure 12: The pIRES2eGFP-GIRK1 vector. Circular vector was linearized with HindIII and PciI. Both restriction enzymes are unique cutters. DNA bands of GIRK1 vector after digesting with restriction enzymes. First line: Standard, Line A: Uncut empty vector, Line B: Vector cut with HindIII, Line C: DNA cut with HindIII and PciI

9.1.3 Manufacturing of stable cell lines

Kill curve test of G418 for MCF10A cells was performed by Astrid Gorischek. The best G418 antibiotic concentration level for MCF10A clones was 16µg/mL. 1 - 4 clones were selected by cLSM based on the fluorescent intensity by using the cloning cylinder (seen in figure 13). Transfected cells with eGFP signal were isolated and picked from a 10 cm dish containing many clones. Confocal image overlays of MCF10A cells were made (figure 14).

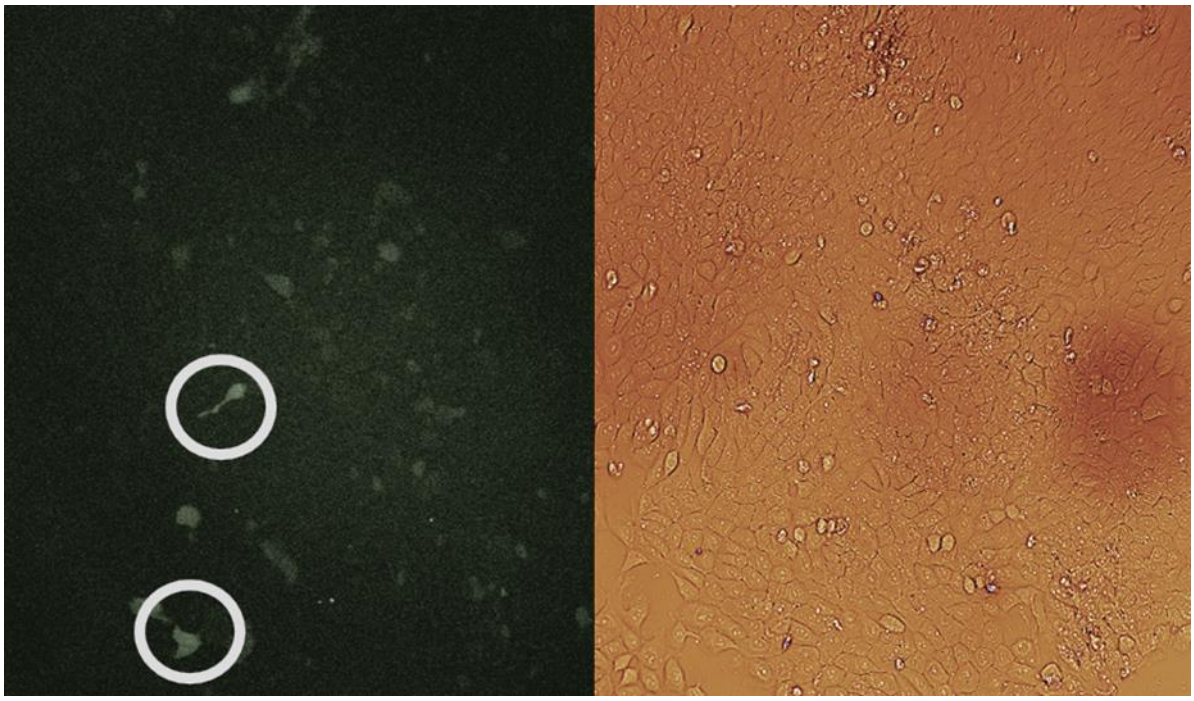

Figure 13: MCF10A clones of stable transfected cells. Left: Strongly florescent clones are selected by cLSM based on the fluorescent intensity by using a cloning cylinder (to be seen as a white circle). Right: Picture show phase contrast light microscopy of cells grown on tissue culture dish.

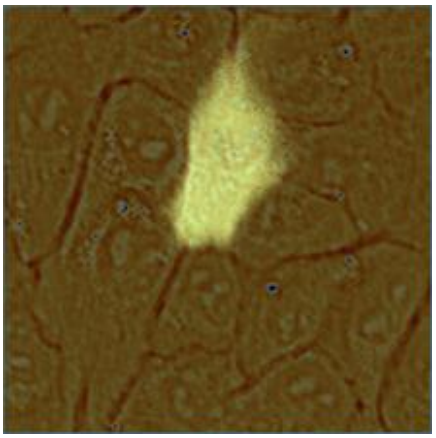

Figure 14: Overlay Image of MCF10A cells. Strongly florescent cells were selected by cLSM. Picture show an overlay of phase contrast and fluorescence microscopy.

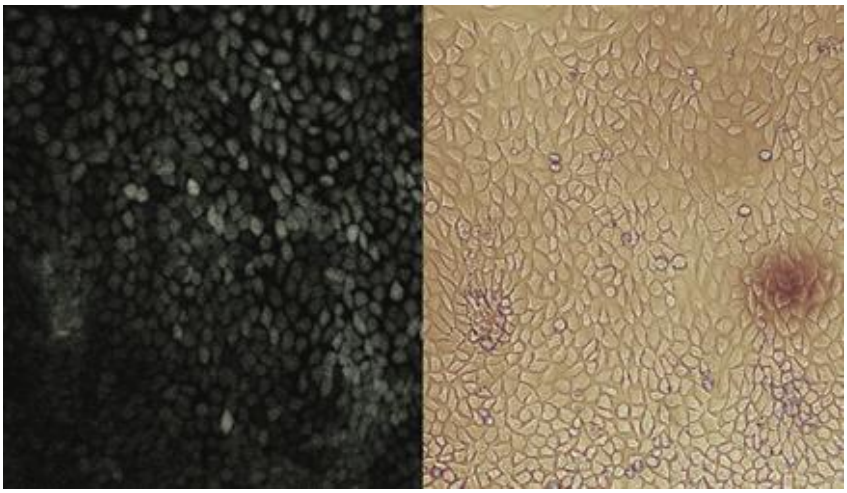

Figure 15: Transfected MCF10A clones for single cell sorting. Left: Cells with a strong eGFP signal detected by cLSM. Right: Phase contrast light microscopy of cells grown on tissue culture dish.

After growing, around 100 clones, in selection medium the MCF10A cells were placed in 6-well tissue culture dishes. The fluorescence was checked regularly every 4 – 5 days. All sorted cells showed an eGFP signal under the microscope (figure 15). Only transfected cells with a strong eGFP signal were taken for further experiments. Cell sorting was performed using 0,9 x 10^6 cells. After sorting on LSRII, the cells were placed in 96 well plates. Between 1 and 4 cells were seeded automaticaly in each well by single cell sorting as seen in figure 16. After 80% of confluence, the cells were trypsinized and placed in 12-well plates. Aliquots were stored (passage P8 - P12) in liquid nitrogen.

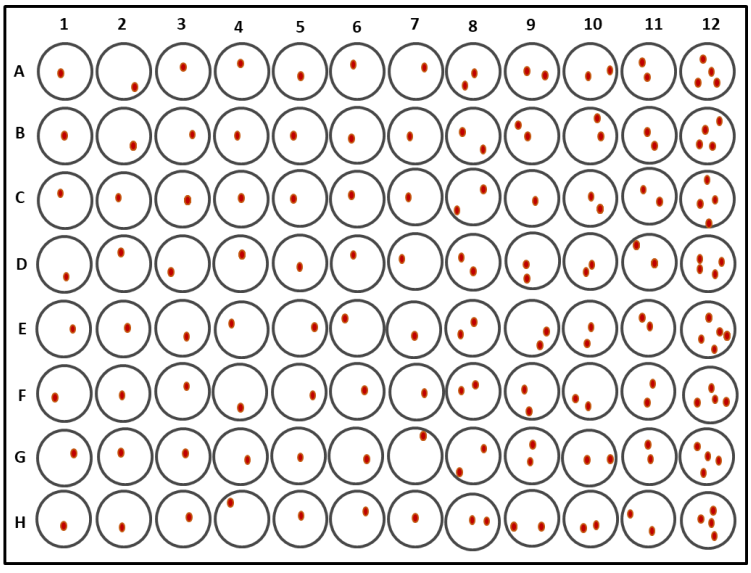

Figure 16: A sketch of 96-well plate including single MCF10A cells after cell sorting. Lane 1 - 7 are single cells sorted, Lane 8 – 11 are two cells seeded in each well and in Lane 12 were 4 cells are seeded per well.

9.1.4 Validation and characterization of the cell lines via qPCR and WB

In order to check successful overexpression of GIRK1 in the produced cell lines, the mRNA levels were assessed. MCF10A^{WT} mRNA expression values were taken as a normalization factor. Expression of mRNA encoding GIRK1 was increased more than four orders of magnitude in MCF10A^{GIRK1} cells when compared to MCF10A^{WT}, where GIRK1 mRNA was barely detectable (observed CT value as measured by qPCR was 35.26 ± 1.32 (mean ± SEM); N=6). In comparison GIRK1 mRNA levels were more than two orders of magnitude higher in the malign MCF7^{WT} vs. the benign MCF10A^{WT} ($p<0.001$). Overexpression of GIRK1 caused a further increase of mRNA levels by two orders of magnitude in MCF7^{GIRK1} when compared to MCF7^{WT}. mRNA expression levels of control cell lines (MCF10A^{eGFP} and MCF7^{eGFP}) resembled the respective wild type lines. Figures 17 and 18 show the different concentrations of GIRK1 mRNA of the MCF10A and MCF7 cell lines. Expression of mRNA encoding GIRK1 was increased four orders of magnitude in MCF10A^{GIRK1} cells, when compared to MCF10A^{WT}. Compared to the benign MCF10A^{WT} cell line, the malign estrogen receptor positive MCF7^{WT} cells exerted increased GIRK1 mRNA concentrations by about two orders of magnitude higher than found in MCF10A^{WT}. Additionally, the overexpression of GIRK1 caused mRNA levels to increase approximately 2-3 orders of magnitude in MCF7^{GIRK1} when compared to MCF7^{WT}.

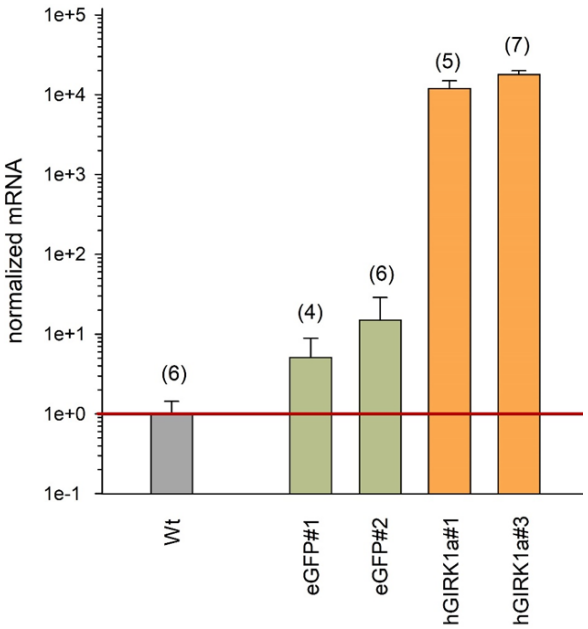

Figure 17: GIRK1 mRNA expression levels in MCF10A cells. mRNA expression values were taken as normalization factor for MCF10A and MCF7 cell lines. The red line represents the normalization of MCF10^{WT} to 1. Number of experiments is given in parenthesis above each bar.

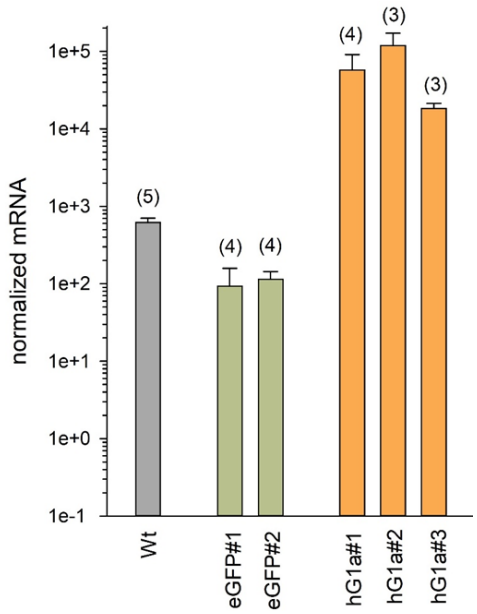

Figure 18: GIRK1 mRNA expression levels in MCF7 cells. mRNA expression values taken from MCF10A^{WT} were taken as normalization factor for MCF7 cell lines. Number of experiments is given in parenthesis above each bar.

The mRNA expression levels of both cell lines, manipulated to express the empty vector did not differ significantly from respective wild types (WTs). Taken together, the mRNA expression levels of both cell lines is displayed in figure 19.

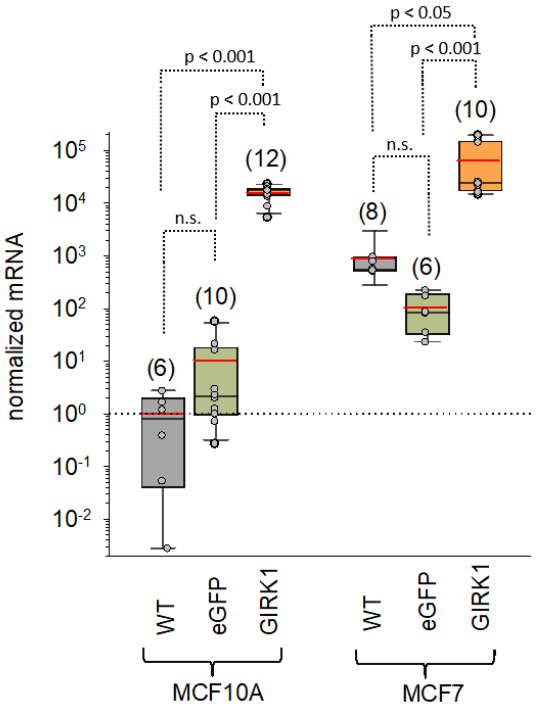

Figure 19: Overexpression of GIRK1 mRNA in transfected MCF10A and MCF7 cells. GIRK1 mRNA levels normalized to MCF10A^{WT}. WT, eGFP and GIRK1 denote wildtype, eGFP (control) and GIRK1 overexpressors, respectively. Number of experiments is given in parenthesis above each bar. P-values for statistically significant differences are indicated above brackets (n.s.: statistically not significant). Reprinted from (Schratter et al.) in press.

WB analyses were performed to detect the protein levels of GIRK1 in overexpressed benign MEC (MCF10A) and malign MCF7 breast cell lines. The protein band detected for the size of GIRK1 is 57 Kilodalton (kD). While not detectable in WT and control lines, GIRK1 protein was clearly detectable upon overexpression, both in MCF10A and MCF7 lines. Although mRNA encoding GIRK1 in MCF7^{WT} is clearly detectable, protein amounts are minute and could not be reliably detected via WB (figure 20 and 21). Sometimes but not always a scarcely reproducible weak bands of GIRK1 was visible in MCF^{WT}. The cause for the missing band could be the low limit of detection in WBs. Therefore, to check for the presents of GIRK1 protein in MCF7 cell lines, immunoprecipitation (IP) was done.

Figure 20: WB analysis of cell lysates. MCF10A cell lysates (3µg protein per slot was applied) probed with GIRK1^{CT}. Ab. #1: MCF10A^{WT} , #2: MCF10A^{eGFP} and #3: MCF10A^{GIRK1}. Reprinted from (Schratter et al.) in press.

Figure 21: WB analysis of cell lysates. MCF7 cell lysates (3µg protein per slot was applied) probed with GIRK1^{CT}. Ab. #1: MCF7^{WT}, #2: MCF7^{eGFP} and #3: MCF7^{GIRK1}. Reprinted from (Schratter et al.) in press.

In order to reliably verify whether GIRK1 does get indeed synthesized from mRNA transcripts in MCF7WT, immunoprecipitation (IP) was performed using specific antibody (Ab) directed against GIRK1 C-terminus (C-T). GIRK1 protein was found in the precipitate. This results are shown in figure 22. Taken together, the results clearly confirm the successful generation of GIRK1 overexpressing cell lines, both MCF10A as well as MCF7. In addition, the small but clearly increased mRNA levels in MCF7WT when compared to MCF10AWT, indicate that the MCF7WT cell line represents a plausible model to study functional effects of elevated GIRK1 levels in malignant breast tumors.

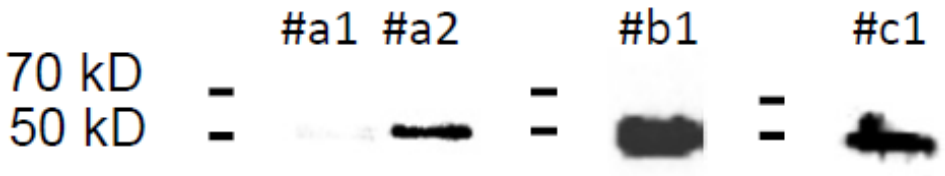

Figure 22: Immunoprecipitation of GIRK1 in different cell lines. WB analysis of immunoprecipitates derived using GIRK1^{CT} Ab on MCF7^{WT} cell lysates. *Left*: membrane probed with using GIRK1^{CT} Ab. #a1: lysate (30 µL), #a2: IP (30 µL). Middle: #b1: IP (30 µL) membrane probed with using GIRK1^{NT} Ab (N-terminal) Ab. Right: #c1: IP (30 µL). Membrane probed with using monoclonal GIRK1 Ab. Reprinted from (Schratter et al.) in press.

9.1.5 Validation of p53 in overexpressed MCF10A cells using qPCR

Many different types of cancer show a high incidence of p53 mutations, which are amongst the most studied tumor suppressor proteins (Muller and Vousden, 2014). We also used RT-PCR to quantitatively analyze the expression of exogenous p53 and p53-targeted genes, such as p21, MDM2, and GADD35A. The REST 2009 Software tool was used for calculating the gene expression data to a relative expression (tables 4-7). We found no significant difference between the p53, p21, hMDM2 and GADD45α indicating that GIRK1 overexpression dose not exert effects on p53, p21, MDM2, and GADD35A expression.

Table 4: Relative expression report of p53 calculated with the REST 2009 Software tool. Expression level of p53 is not increased in overexpressed cell lines compared to control cell lines.

Results — P53 from MCF10A^{Wt} against MCF10A$^{GFP\#1}$

Gene	Type	Reaction Efficiency	Expression	Std. Error	95% C.I.	P(H1)
GAPDH	REF	1	1,128			
YWHAZ	REF	1	0,887			
p53	TRG	1	0,47	0.461 - 0.496	0.455 - 0.500	0,038

Results — P53 from MCF10A^{Wt} against MCF10A$^{GFP\#2}$

Gene	Type	Reaction Efficiency	Expression	Std. Error	95% C.I.	P(H1)
GAPDH	REF	1	0,895			
YWHAZ	REF	1	1,117			
p53	TRG	1	0,93	0.869 - 0.973	0.844 - 1.020	0,153

Results — P53 from MCF10A^{Wt} against MCF10A$^{GIRK1a\#1}$

Gene	Type	Reaction Efficiency	Expression	Std. Error	95% C.I.	P(H1)
GAPDH	REF	1	0,684			
YWHAZ	REF	1	1,462			
p53	TRG	1	0,81	0.770 - 0.860	0.745 - 0.880	0,063

Results — P53 from MCF10A^{Wt} against MCF10A$^{GIRK1a\#3}$

Gene	Type	Reaction Efficiency	Expression	Std. Error	95% C.I.	P(H1)
GAPDH	REF	1	0,694			
YWHAZ	REF	1	1,441			
p53	TRG	1	0,88	0.849 - 0.919	0.833 - 0.945	0

Table 5: Relative expression report of p21 calculated with the REST 2009 Software tool. Expression level of p21 was not increased in overexpressed cell lines compared to control cell lines.

Results — p21 from MCF10A^{Wt} against MCF10A$^{GFP\#1}$

Gene	Type	Reaction Efficiency	Expression	Std. Error	95% C.I.	P(H1)
GAPDH	REF	1	1,244			
YWHAZ	REF	1	0,804			
p21	TRG	1	0,82	0.644 - 1.275	0.636 - 1.290	0,317

Results — p21 from MCF10A^{Wt} against MCF10A$^{GFP\#2}$

Gene	Type	Reaction Efficiency	Expression	Std. Error	95% C.I.	P(H1)
GAPDH	REF	1	1,002			
YWHAZ	REF	1	0,998			
p21	TRG	1	1,43	1.113 - 2.202	1.103 - 2.324	0,084

Results — p21 from MCF10A^{Wt} against MCF10A$^{GIRK1a\#1}$

Gene	Type	Reaction Efficiency	Expression	Std. Error	95% C.I.	P(H1)
GAPDH	REF	1	0,794			
YWHAZ	REF	1	1,26			
p21	TRG	1	1,08	0.810 - 1.686	0.767 - 1.801	1

Results — p21 from MCF10A^{Wt} against MCF10A$^{GIRK1a\#3}$

Gene	Type	Reaction Efficiency	Expression	Std. Error	95% C.I.	P(H1)
GAPDH	REF	1	0,78			
YWHAZ	REF	1	1,282			
p21	TRG	1	1,60	1.235 - 2.443	1.223 - 2.630	0,058

Table 6: Relative expression report of GADD45α calculated with the REST 2009 Software tool. Expression level of GADD45α is not increased in overexpressed cell lines compared to control cell lines.

Results GADD45α from MCF10A^{Wt} against MCF10A$^{GFP\#1}$

Gene	Type	Reaction Efficiency	Expression	Std. Error	95% C.I.	P(H1)
GAPDH	REF	1	1,158			
YWHAZ	REF	1	0,864			
45alpha	TRG	1	0,50	0.448 - 0.537	0.430 - 0.585	0

Results GADD45α from MCF10A^{Wt} against MCF10A$^{GFP\#2}$

Gene	Type	Reaction Efficiency	Expression	Std. Error	95% C.I.	P(H1)
GAPDH	REF	1	0,92			
YWHAZ	REF	1	1,087			
45alpha	TRG	1	1,07	0.994 - 1.128	0.974 - 1.215	0,392

Results GADD45α from MCF10A^{Wt} against MCF10A$^{GIRK1a\#1}$

Gene	Type	Reaction Efficiency	Expression	Std. Error	95% C.I.	P(H1)
GAPDH	REF	1	0,694			
YWHAZ	REF	1	1,441			
45alpha	TRG	1	1,06	0.987 - 1.118	0.975 - 1.199	0,413

Results GADD45α from MCF10A^{Wt} against MCF10A$^{GIRK1a\#3}$

Gene	Type	Reaction Efficiency	Expression	Std. Error	95% C.I.	P(H1)
GAPDH	REF	1	0,741			
YWHAZ	REF	1	1,349			
45alpha	TRG	1	1,24	1.144 - 1.343	1.100 - 1.419	0,063

Table 7: Relative expression report of hMDM2. Expression level of hMDM2 is not increased in overexpressed cell lines compared to control cell lines.

Results hMDM2 from MCF10A^{Wt} against MCF10A$^{GFP\#1}$

Gene	Type	Reaction Efficiency	Expression	Std. Error	95% C.I.	P(H1)
GAPDH	REF	1	1,103			
YWHAZ	REF	1	0,906			
hMDM2	TRG	1	0,53	0.449 - 0.633	0.430 - 0.667	0,082

Results hMDM2 from MCF10A^{Wt} against MCF10A$^{GFP\#2}$

Gene	Type	Reaction Efficiency	Expression	Std. Error	95% C.I.	P(H1)
GAPDH	REF	1	0,873			
YWHAZ	REF	1	1,146			
hMDM2	TRG	1	0,94	0.785 - 1.133	0.690 - 1.314	0,652

Results hMDM2 from MCF10A^{Wt} against MCF10A$^{GIRK1a\#1}$

Gene	Type	Reaction Efficiency	Expression	Std. Error	95% C.I.	P(H1)
GAPDH	REF	1	0,713			
YWHAZ	REF	1	1,403			
hMDM2	TRG	1	1,33	1.101 - 1.622	0.959 - 1.859	0,102

Results hMDM2 from MCF10A^{Wt} against MCF10A$^{GIRK1a\#3}$

Gene	Type	Reaction Efficiency	Expression	Std. Error	95% C.I.	P(H1)
GAPDH	REF	1	0,699			
YWHAZ	REF	1	1,431			
hMDM2	TRG	1	1,80	1.416 - 2.203	1.306 - 2.703	0

9.2 Vital Parameters

Cell culture models are substantial for the fundamental study of cellular pathways and for the discovery of critical genes involved in cancer. In order to monitor potential effects of stable GIRK1 overexpression, different vital parameters were recorded. All vital assays were performed using MCF10A and MCF7 wild type cell lines and the associated clones. Individual clones of GIRK1 overexpressing or eGFP controls were pooled and analyzed collectively.

9.2.1 GIRK1 Wound Healing Assay for MCF10A and MCF7 cells

Collective cell migration in adulthood takes place during tissue repair but also in the course of malignant processes. The 2D wound healing assay is hence regarded to be an excellent tool for monitoring cancer hallmarks of cells in culture (Ilina and Friedl, 2009). Wound healing rates of MCF10A^{GIRK1} cells were substantially reduced when compared to MCF10A^{WT} or MCF10A^{eGFP} controls (Figure 23). In contrast, overexpression of GIRK1 in MCF7 cells resulted in an increase of the wound healing rate, although only marginally and statistically not significant (Figure 24). Notably, overexpression of GIRK1 affects wound healing of MCF10A and MCF7 cells in different manner.

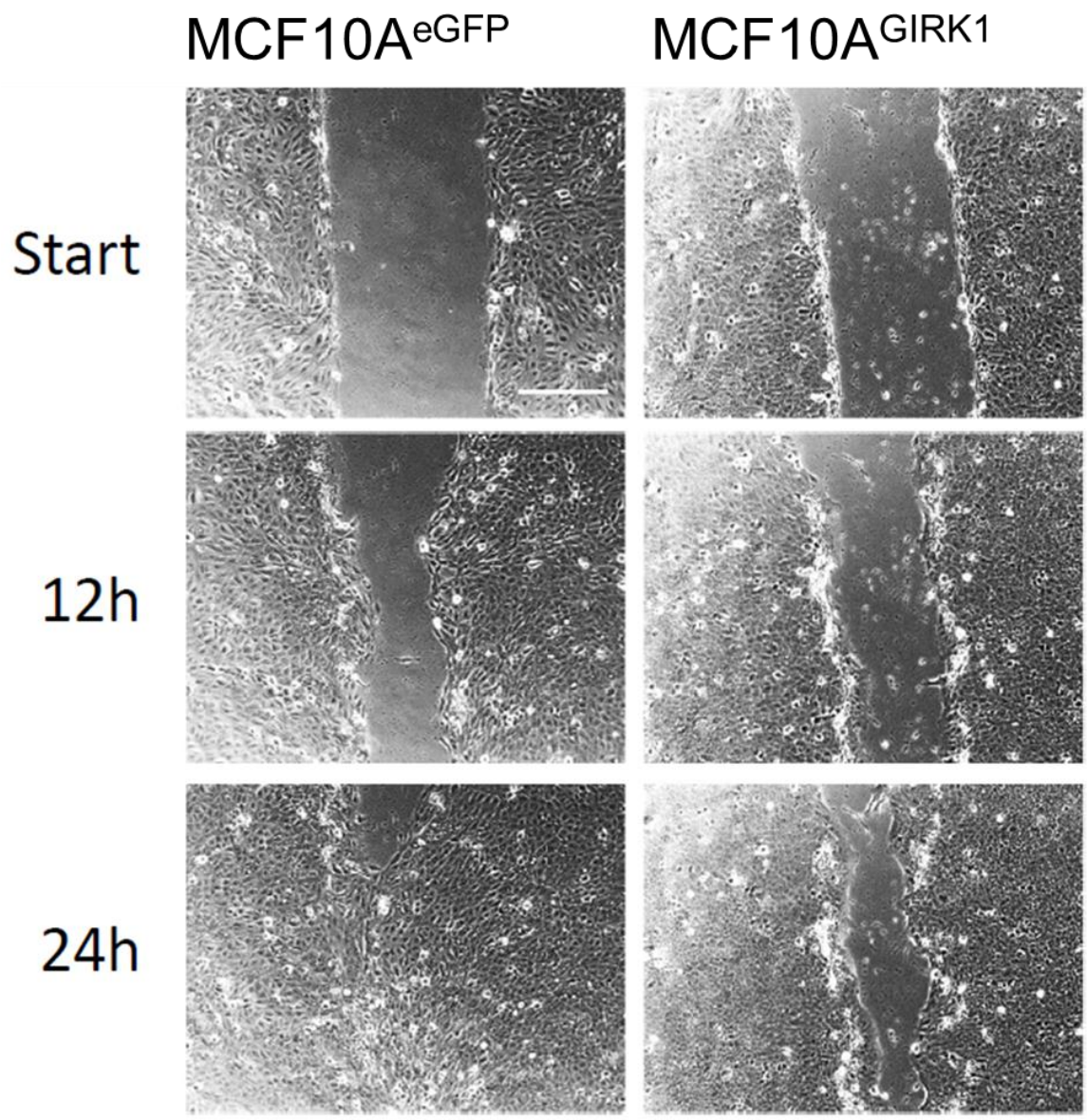

Figure 23: Wound healing assay. Representative images of the wound healing process of MCF10A cells. Representative frames recorded at different time points during the wound healing process. Comparison between vector control (left) to overexpressors (right). Scale bar correspond to 200 µm. Reprinted from (Schratter et al.) in press.

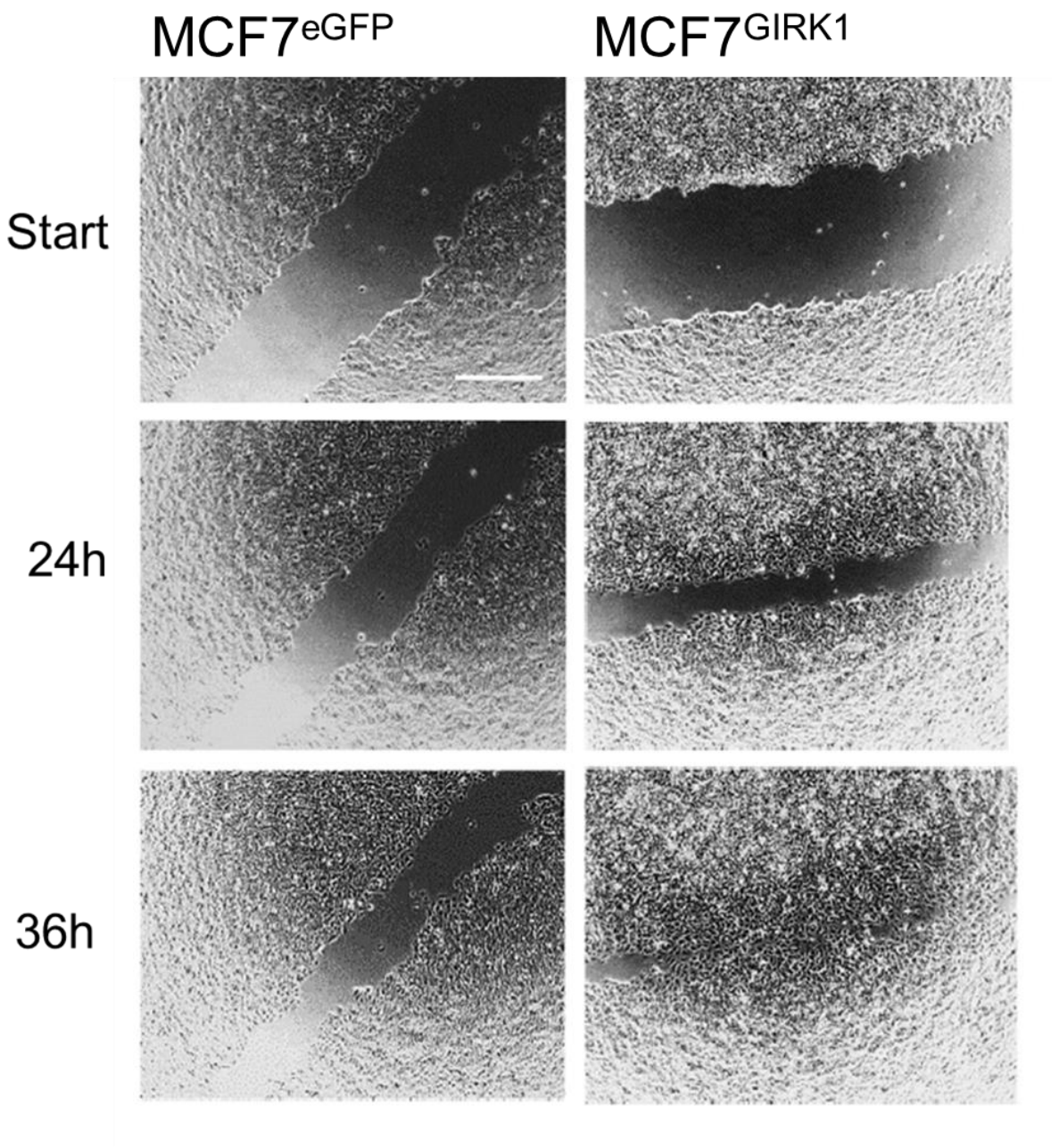

Figure 24: Wound healing assay. Representative images of the wound healing process of MCF7 cells. Representative frames recorded at different time points during the wound healing process. Comparison between vector control (left) to overexpressors (right). Scale bar correspond to 200 µm. Reprinted from (Schratter et al.) in press.

Wound healing rates of MEC cell lines were calculated in % per hour. Number of experiments for MCF10A and MCF7 cell lines are given in parenthesis above each box plot. Wound healing rates of MCF10A^{GIRK1} cells were reduced when compared to MCF10A^{WT} or MCF10A^{eGFP} controls (Figure 25). Differences for MCF7 were not significant at the statistical level (Figure 26).

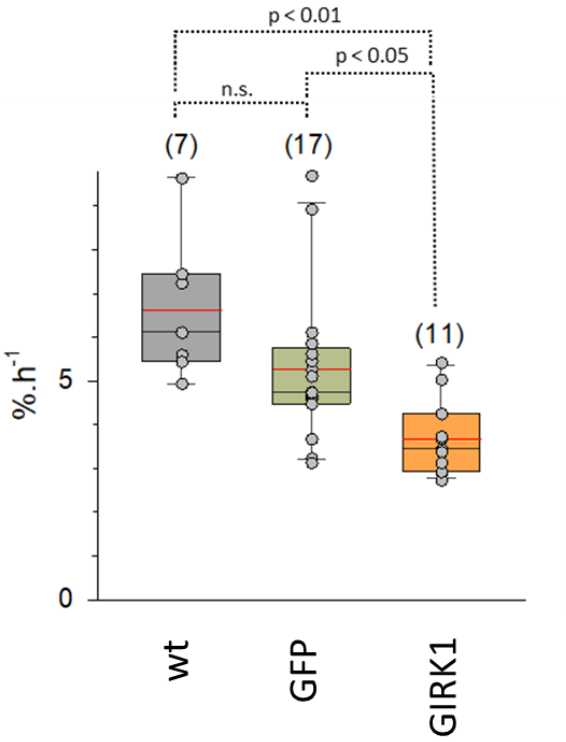

Figure 25: Wound healing rates of MCF10A cells. Statistical anlaysis of wound healing rates of MCF10A cells. WT: MCF10AWT, eGFP: MCF10AeGFP and GIRK1: MCF10AGIRK1. The median value is represented by the black line within the box, box margins represent 75% and 25% percentiles, whiskers indicate 90% and 10% percentiles. The red line represents the mean value. Individual values are shown as grey circles. The number of individual cells is given in parenthesis above each box. Statistical significant differences between groups are indicated above brackets (n.s.: statistically not significant). Reprinted from (Schratter et al.) in press.

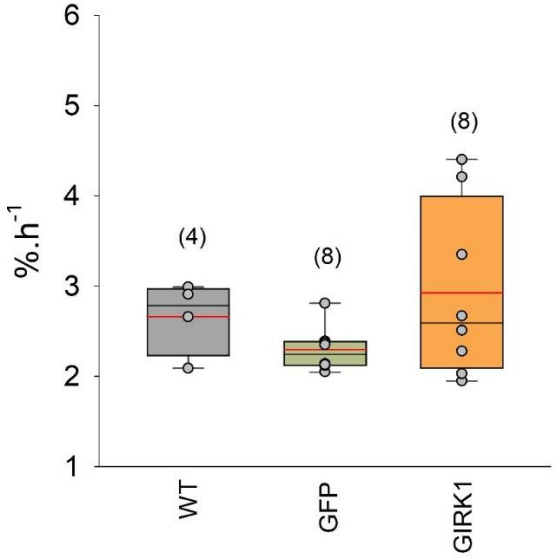

Figure 26: Wound healing rates of MCF7 cells. Statistical anlaysis of wound healing rates of MCF7 cells. WT: $MCF7^{WT}$, eGFP: $MCF7^{eGFP}$ and GIRK1: $MCF7^{GIRK1}$. The median value is represented by the black line within the box, box margins represent 75% and 25% percentiles, whiskers indicate 90% and 10% percentiles. The red line represents the mean value. Individual values are shown as grey circles. The number of individual cells is given in parenthesis above each box. Reprinted from (Schratter et al.) in press.

9.2.2 Neovascularization and proliferation of MCF10A assessed via CAM assay.

The chick chorioallantoic membrane assay (CAM) angiogenesis system allows the macroscopic semi quantitative evaluation of the vasoproliferative response by analyzing the branching of blood vessels observed under a stereomicroscope (Ribatti et al., 2006a). The tumorgenicity of the MCF10A^{WT} cells, vector control and GIRK1 overexpressing cells were tested by the CAM assay using MCF10A cells developed to a micro-tumor on top of a chick embryo grown ex ovo. Figure 27 and 28 shows an exemplary sample for the positioning of a silicone ring on a chick embryo. In each of these silicone rings, the same amount of MEC cells was applied.

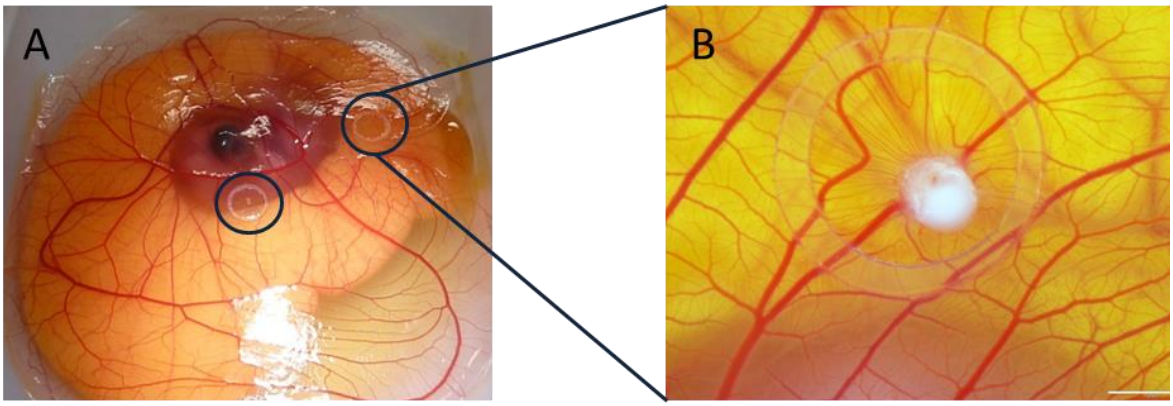

Figure 27: CAM Assay. Image A shows exemplarily the position of the silicon rings. Image B is one sample image used in the analysis of the CAM assay. The white scale bar represents a length of 2mm.

On each chick embryo 1 x 10^6 single cells per onplant were placed on top of the CAM. After 4 days of incubation, the MCF10A cells formed a compact round-shaped structure at the surface of the chicken membrane.

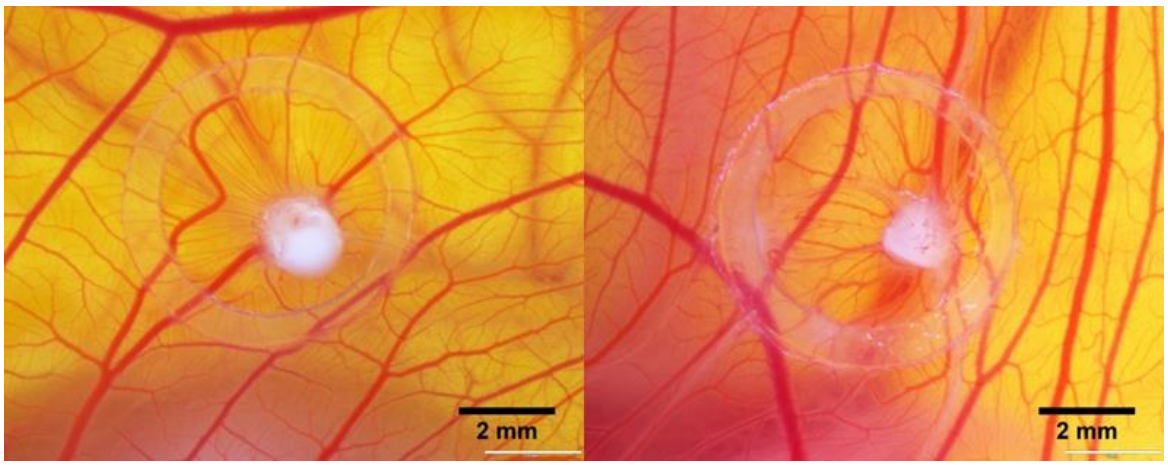

Figure 28: Vascularization and growth of MCF10A xenoplants planted on CAM assay. Representative image of an onplant taken on day 4 after beginning. Left: Onplant consisting of MCF10A^{eGFP} cells. Right: Onplant consisting of MCF10A^{GIRK1} cells. The black bar represents a length of 2mm. Reprinted from (Schratter et al.) in press.

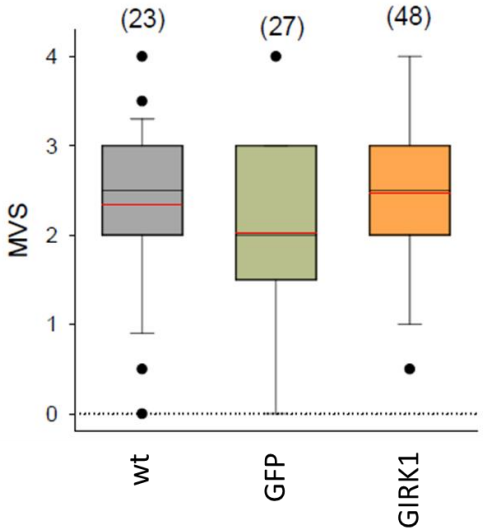

Figure 29: Macroscopic vascularization scores (MVS). Grey: MCF10A^{WT}, green: MCF10A^{eGFP} vector control and overexpressed orange: MCF10A^{GIRK1}. Box plots represent median value, 25% and 75% percentiles, respectively. Mean values are indicated by red line. Whiskers denote 10% and 90% percentiles; black circles denote single values outside the 10% and 90% percentiles. Number of individual onplants is given in parenthesis above each box. Differences were not significant at the statistical level. A Kruskal-Wallis One Way Analysis of Variance on Ranks was used for analysis. Reprinted from (Schratter et al.) in press.

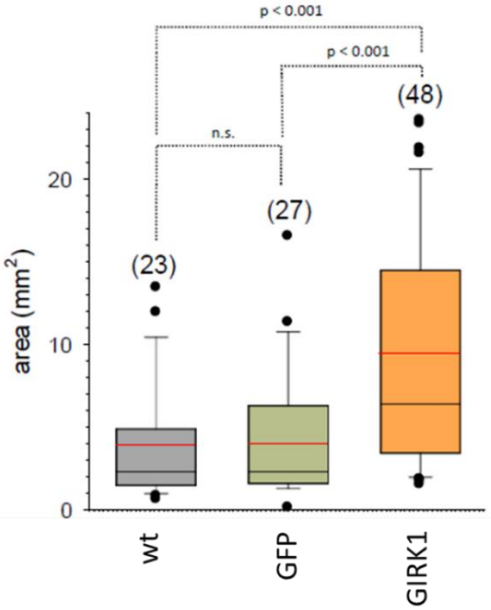

Figure 30: Onplant area measured in after 4 days of growth. Grey: MCF10A^{WT}, green: MCF10A^{eGFP} vector control and overexpressed orange: MCF10A^{GIRK1}. Box plots represent median value, 25% and 75% percentiles, respectively. Mean values are indicated by red line. Whiskers denote 10% and 90% percentiles; black circles denote single values outside the 10% and 90% percentiles. Number of individual onplants is given in parenthesis above each box. P-values for statistically significant differences are indicated above brackets (n.s.: statistically not significant). A Kruskal-Wallis One Way Analysis of Variance on Ranks was used for analysis. Reprinted from (Schratter et al.) in press.

Overexpression of GIRK1 did not affect angiogenesis of MCF10A cells, when scored using a scale ranging from zero to five. There was no apparent difference in the macroscopic vascularization scores (MVS) among $MCF10^{WT}$, vector control and GIRK1 overexpressors (Figure 29). A similar behavior was observed for MCF7 cells and $MCF7^{GIRK1}$ (Rezania et al., 2016). Apart from that, the growth rate as assessed via the onplant areas (Kainz et al., 2015), were largely enhanced by GIRK1 overexpression. The size of the tumor formation differed at macroscopic level. There is no clear difference in MVS MCF7 GIRK1 overexpressors when compared to control in the work of Rezania et al. (Rezania et al., 2016). GIRK1 overexpression in $MCF10A^{GIRK1}$ induced a massive increase in onplant growth rate, when compared to controls (figure 30).

9.2.3 Cell proliferation assay (EdU Assay) and detection by flow cytometry

The detection of EdU label is very sensitive and can be accomplished in less than one hour. The small size of the fluorescent azides reacts with the incorporated EdU to allow detection by flow cytometry (Salic and Mitchison, 2008). For all vital parameters, the cells were photographed (10x magnification) under the microscope (Nikon Eclipse Ts2) to check the cell condition before and after treatment to see in figure 31 (Motic Images Plus 3.0 software).

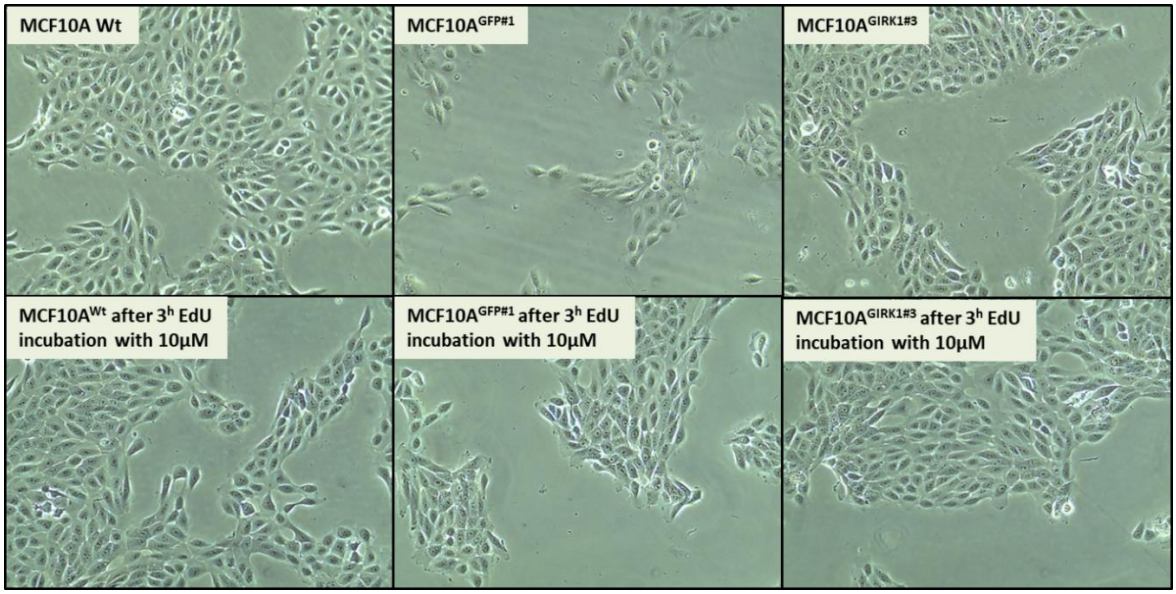

Figure 31: Vital parameter before and after treatment with EdU. This picture shows a representative example. Cell vitality was assessed before starting any other assay (10x magnification; Nikon Eclipse Ts2).

When monitoring cell cycle and proliferation via gated cell sorting, it became evident that the parameters tested in both cell lines were unaffected in GRIK1 overexpressed cells

(Figures 32-33). It can be concluded that the GIRK1 overexpression in proliferative signaling remained practically unchanged in MCF10A and MCF7. For MCF7 cells Rezania et al. (Rezania et al., 2016) observed a similar behavior. In this study the authors could show that also cell adhesion remained unaffected by GRIK1 overexpression.

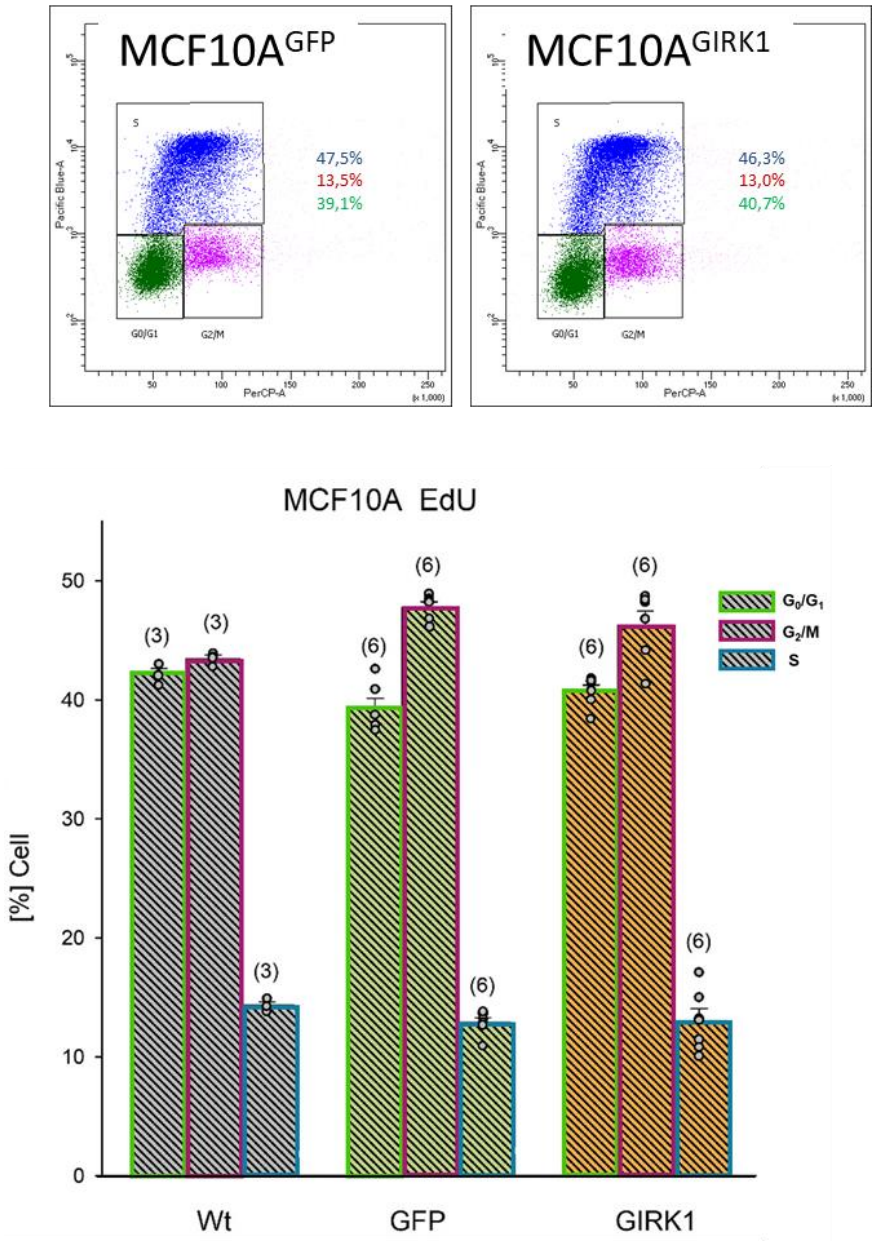

Figure 32: Proliferation of MCF10A cell lines in cell culture. Upper picture. Results from the assessment of cell cycle using gated cell sorting according to fluorescence intensities (% of cells) for PerCP-A (x-axis) and PacificBlue-A (y-axis) Figures show vector control (upper left) and GIRK1 overexpressed MCF10A cell lines (upper right). Individual cells represented as dots, a particular phase of the cell cycle are surrounded by colored lines (green line: G0/G1 phase; purple line: G2/M phase and blue line: S phase). Lower picture. Statistics for the percentage of time spent at different stages of the cell cycle. The differences between WT, eGFP and GIRK1 do not differ statistically significant for MCF10A.

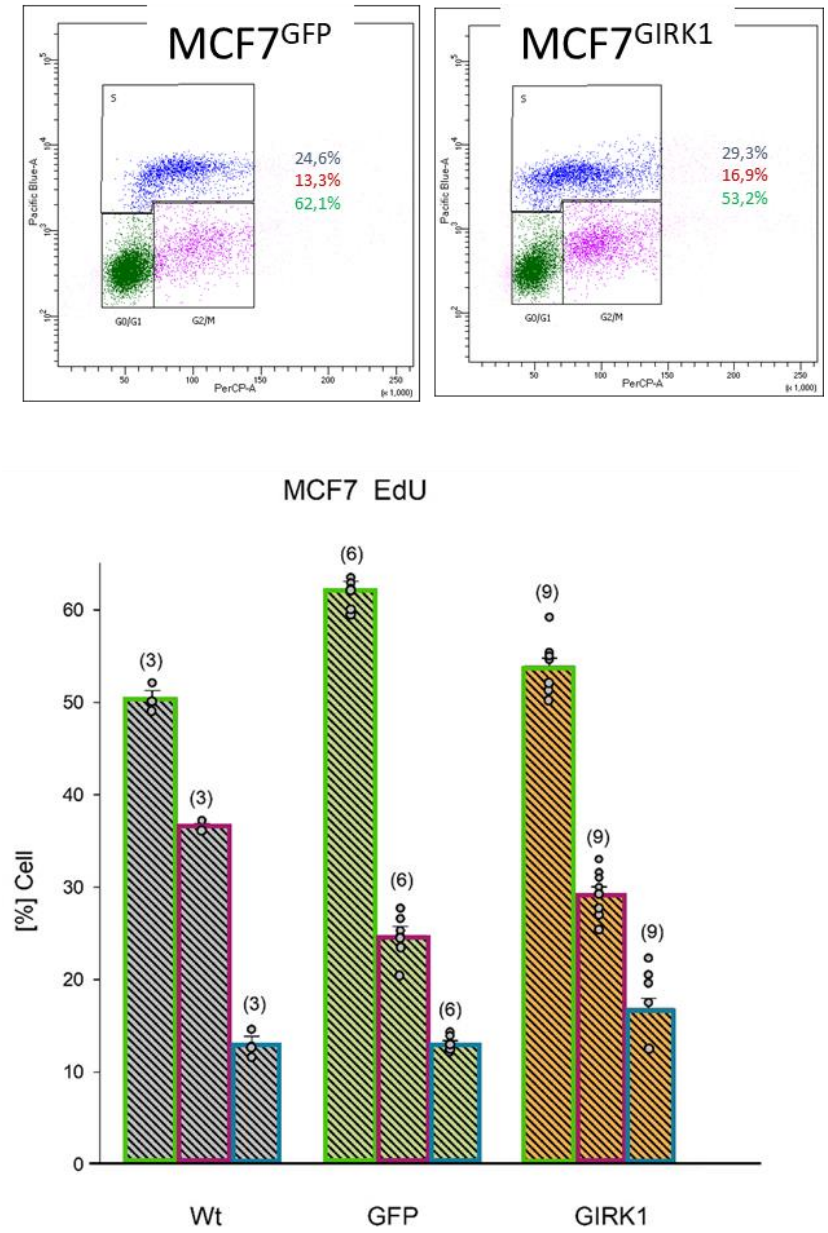

Figure 33: In vitro cell proliferation studies of GIRK1 overexpression in MCF7 cells. Upper picture. Results from the assessment of cell cycle using gated cell sorting according to fluorescence intensities (% of cells) for PerCP-A (x-axis) and PacificBlue-A (y-axis) Figures show vector control (left) and GIRK1 overexpressed MCF7 cell lines (right). Individual cells represented as dots, a particular phase of the cell cycle are surrounded by colored line (green line: G0/G1 phase; purple line: G2/M phase and blue line: S phase). Lower picture. Statistics for the percentage of time spent at different stages of the cell cycle. The differences between WT, eGFP and GIRK1 do not differ statistically significant for MCF7.

9.2.4 Electrophysiological Recordings and Analysis

In a previous study, single channel recording revealed the existence of single functional GIRK1 channels in MCF7$^{GIRK1/YFP}$ cells, but at very low density (Rezania et al., 2016). Hence, we used the membrane potential, that reacts very sensitive to the presence of few functional channel proteins.

In MCF10A^{GIRK1} ,membrane resting potentials (RPs) were -52.8 ± 4.5 mV (mean value ± SEM) and hyperpolarized when compared to controls that ranged around -24 mV (MCF10A^{WT}: -24.3 ± 3.2 mV, MCF10A^{eGFP}: -24.5 ± 3.6 mV; to see in figure 34). In the presence of 200 nmol/l tertiapin-Q, a specific blocker of GIRK1 containing GIRK channels (Drici et al., 2000, Kitamura et al., 2000), RPs approached end exceeded control values (19.0 ± 2.3 mV), indicating that overexpressed GIRK1 protein produces functional K^+ channels in MCF10A. RPs in the MCF7 based lines were also assessed (Figure 35). Additional MCF7 based cell lines, stably overexpressing chimeric GIRK1/eYFP protein that had been characterized previously (Rezania et al., 2016), were also included into the analysis. Both MCF7^{GIRK1} and MCF7$^{GIRK1/eYFP}$ exerted hyperpolarized RPs when compared to respective controls, albeit the differences in RPs between overexpressors and control groups were less pronounced in comparison to benign MCF10A lines. Moreover, when GIRK channels were blocked by tertiapin-Q in MCF7^{GIRK1}, RPs with -17.0 ± 4.3 mV were the most depolarized among MCF7 based lines and considerably higher when compared to MCF7^{WT} (-27.2 ± 3.1 mV). This fact indicates not only that functional GIRK channels form upon overexpression of GIRK1 also in the malignant MCF7 MEC lines, but minute amounts of functional GIRK channel complexes already preexist in MCF7^{WT}.

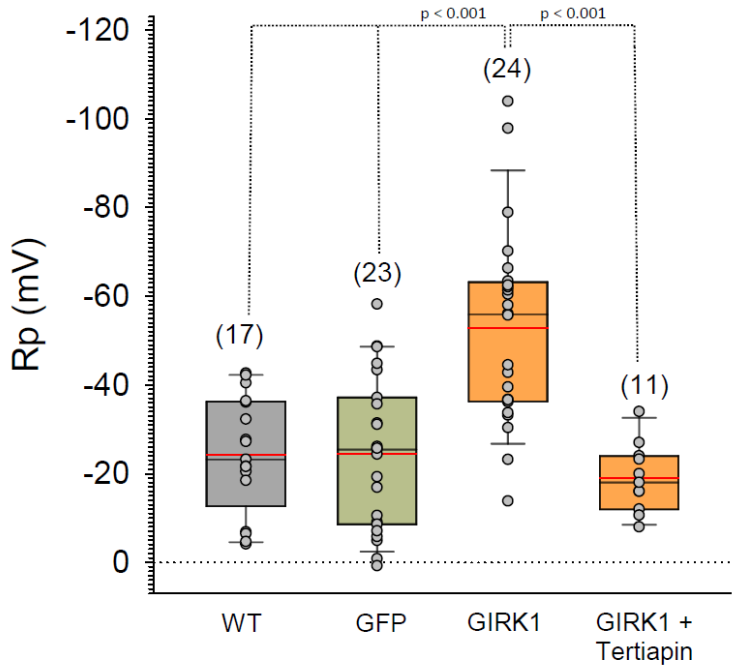

Figure 34: Effect of GIRK1 overexpression on resting potential of MCF10A cells. Blocking of GIRK1 channels by Tertiapin depolarizes membrane to wild type values. Grey: MCF10A^{WT}, green: MCF10A^{eGFP} vector control and overexpressed orange: MCF10A^{GIRK1}. Box plots represent median value, 25% and 75% percentiles, respectively. Mean values are indicated by red line. Whiskers denote 10% and 90% percentiles; grey circles denote single cells. Number of individual cells is given in parenthesis above each box. P-values for statistically significant differences are indicated above brackets. Reprinted from (Schratter et al.) in press.

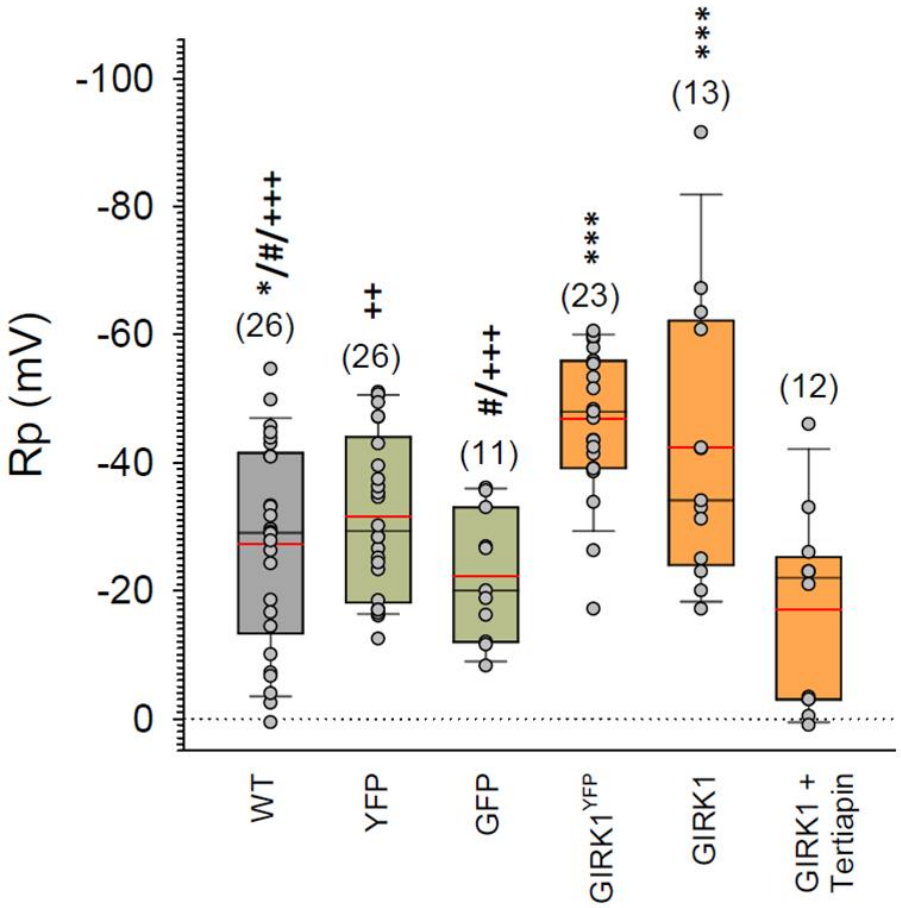

Figure 35: Effect of GIRK1 overexpression on resting potential of MCF7 cells. Grey: $MCF7^{WT}$, green: $MCF7^{eGFP}$/$MCF7^{YFP}$ vector control and overexpressed as orange: $MCF7^{GIRK1}$/$MCF7^{GIRK/YFP}$. Box plots represent median value, 25% and 75% percentiles, respectively. Mean values are indicated by red line. Whiskers denote 10% and 90% percentiles; grey circles denote single cells. Number of individual cells is given in parenthesis above each box. P-values for statistically significant differences are indicated above brackets (n.s.: statistically not significant). Reprinted from (Schratter et al.) in press.

9.2.5 Effect of GIRK1 overexpression on MCF10A single cell motility and velocity

The motility of eukaryotic cells is essential for many biological functions, as well in cell developing. Motility dysfunctions are involved in several life-threatening pathologies such as cancer and metastasis (Ziebert and Aranson, 2016). Differences in the in vitro single cell motility tests observed between wild type, vector control and GIRK1 overexpressing cells are reflected in the differential rate of motion.

Flower plots in figure 36 show the effect of GIRK1 variant overexpression on MCF10A single cell motility (cellular trajectories). Time-lapse microscopy revealed that $MCF10A^{GIRK1}$ overexpressed cells exhibited massively elevated agility when compared to control cell lines. This effect of GIRK1 overexpression is also shown in Figure 37.

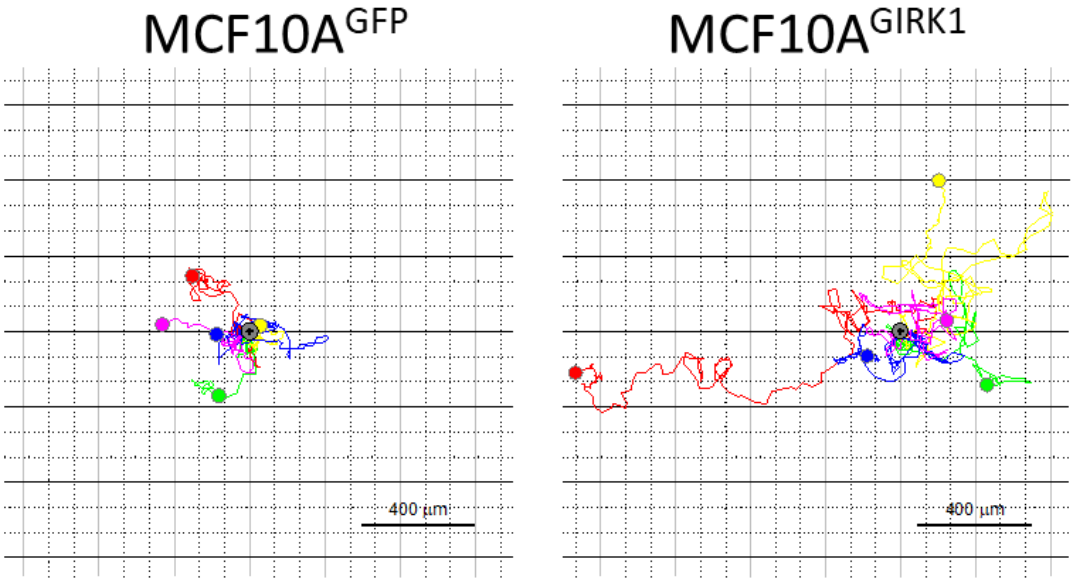

Figure 36: Effect of GIRK1 overexpression on MCF10A single cell motility. (Left) Migration of five selected MCF10A^{eGFP} cells over the entire observation interval. Flower plots showing cellular trajectories for the entire observation interval of 72 h (colored line). Starting position of each individual cell was set to zero coordinates (grey circle). Colored circles indicate the positon of an individual cell after 72 h. (Right) same as left but MCF10A^{GIRK1} . Reprinted from (Schratter et al.) in press.

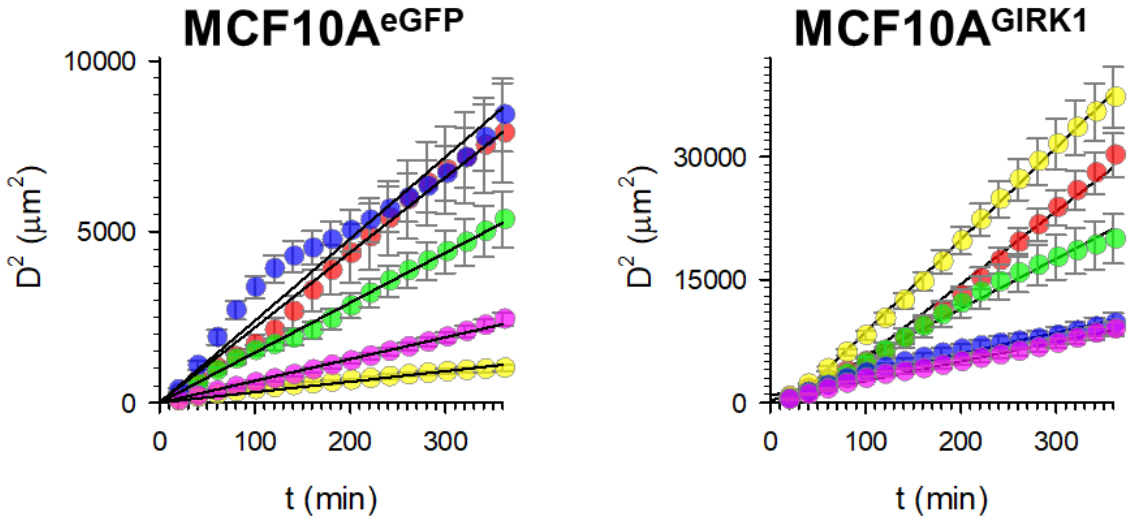

Figure 37: Effect of GIRK1 variant overexpression on MCF10A single cell motility. Squared distance as a function of time for the five cells is shown (circles; bars indicate standard error). Lines represent a linear fits through the data. Left: MCF10A^{eGFP}; Right: MCF10A^{GIRK1}. Reprinted from (Schratter et al.) in press.

The present results were obtained for cellular migration, as displayed by cellular motility coefficient (MCs). Through the observed transcriptional regulation, GIRK1 overexpression greatly enhanced migration of MCF10A as assessed via cellular MC. Statistical analysis of

MC derived from the different experimental groups (WT: MCF10A^{WT}; eGFP: MCF10A^{eGFP}; GIRK1: MCF10A^{GIRK1}) are shown in (Figure 38).

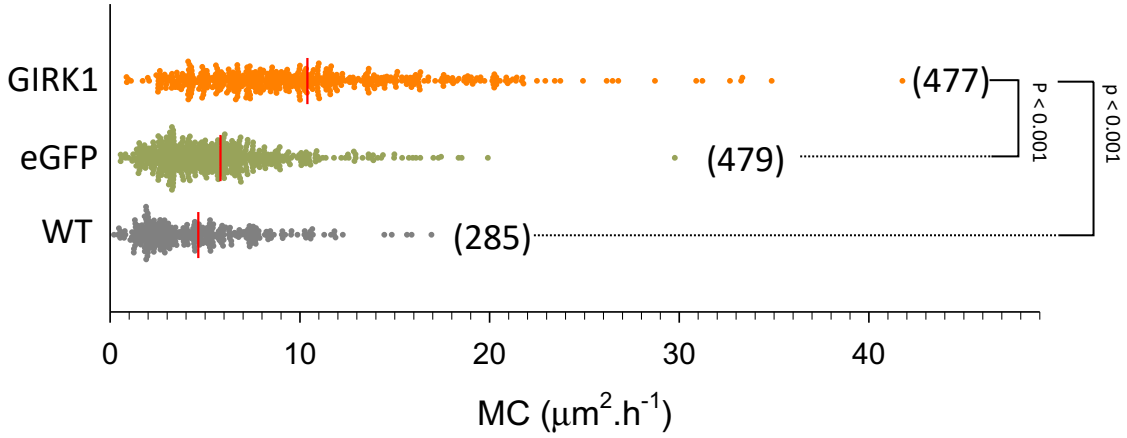

Figure 38: Graphical and statistical representation of cellular motility coefficients for different experimental groups. Statistical analysis of motility coefficients derived from the different experimental groups. WT: MCF10A^{WT}, eGFP: MCF10A^{eGFP} and GIRK1: MCF10A^{GIRK1}. The median value is represented by the black line within the box, box margins represent 75% and 25% percentiles, whiskers indicate 90% and 10% percentiles. The red line represents the mean value. Individual values are shown as dots. The number of individual cells is given in parenthesis besides each box. Statistical significant differences between groups are indicated by brackets. Reprinted from (Schratter et al.) in press.

When cellular velocities were directly quantified, it became evident that average velocities of MCF10A cell were greatly augmented upon overexpression of GIRK1. Our findings indicate that there is an increase of velocity in MCF10A^{GIRK1} cells compared to the control groups during the entire observation interval of 50 h (Figure 39).

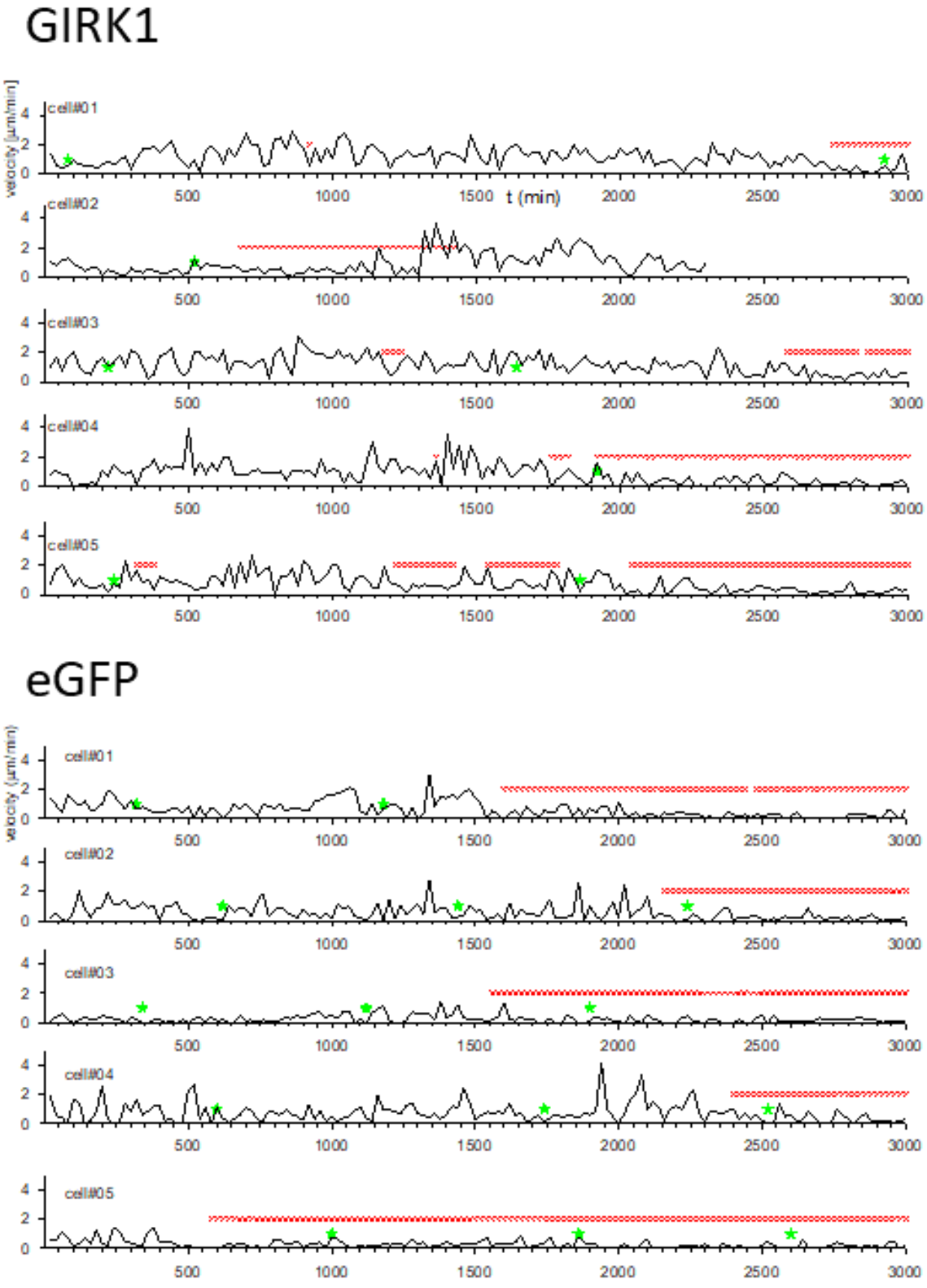

Figure 39: Effect of GIRK1 overexpression on MCF10A cell velocity. Upper: Cellular velocities for five representative MCF10A^{GIRK1} cells during the entire observation interval of 50 h. Lower: Cellular velocities for five representative MCF10A^{eGFP} cells during the entire observation interval of 50 h. Green asterisks denote cell divisions and red x denote cell aggregation. Upper: MCF10A^{GIRK1}; Lower: MCF10A^{eGFP}. Reprinted from (Schratter et al.) in press.

Figures 40-41 show graphical representation of “aggregated” and “free moving” cellular velocities for different experimental groups. The groups are: WT: MCF10A^{WT}, eGFP: MCF10A^{eGFP} and GIRK1: MCF10A^{GIRK1}. GIRK1 overexpression in MCF10A triggered the downregulation of a cluster of genes that, upon downregulation, promotes cellular migration and, in the context of cancer, metastatic spread of tumor cells. Through the observed transcriptional regulation, GIRK1 overexpression greatly enhanced migration of MCF10A as assessed via cellular motility coefficient. Accordingly, cell velocities increased significantly.

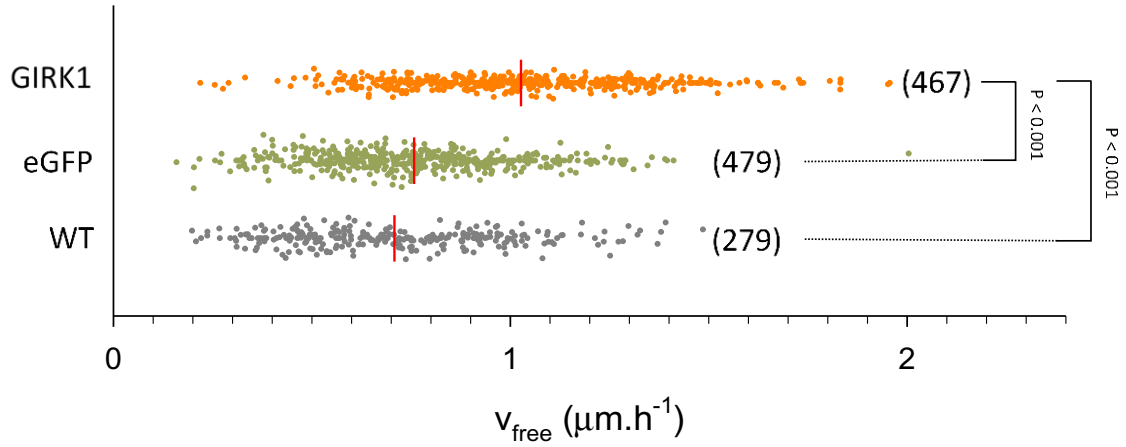

Figure 40: Effect of GIRK1 variant overexpression on cell velocity of free moving MCF10A cells. Graphical representation of velocity in µm/h. Grey: MCF10A^{WT}, green: MCF10A^{eGFP} vector control and overexpressed orange: MCF10A^{GIRK1}. The median value is represented by the black line within the box, box margins represent 75% and 25% percentiles, whiskers indicate 90% and 10% percentiles. The red line represents the mean value. Individual values are shown as colored dots. The number of individual cells is given in parenthesis besides each box. Statistical significant differences between groups are indicated by brackets. Reprinted from (Schratter et al.) in press.

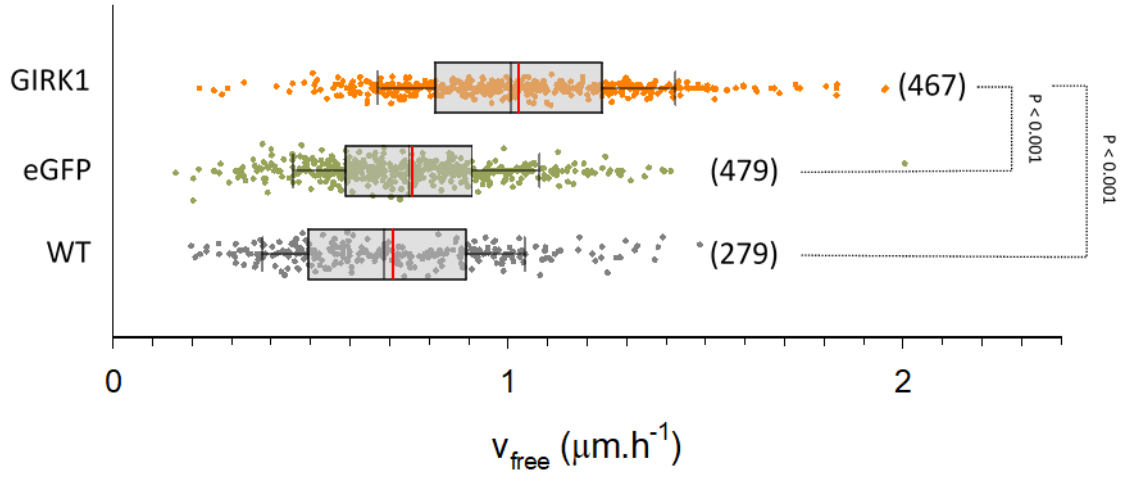

Figure 41: Effect of GIRK1 variant overexpression on cell velocity of aggregated MCF10A cells. Graphical representation of velocity in µm/h. Grey: MCF10A^{WT}, green: MCF10A^{eGFP} vector control and overexpressed orange: MCF10A^{GIRK1}. The median value is represented by the black line within the box, box margins represent 75% and 25% percentiles, whiskers indicate 90% and 10% percentiles. The red line represents the mean value. Individual values are shown as colored dots. The number of individual cells is given in parenthesis besides each box. Statistical significant differences between groups are indicated by brackets. Reprinted from (Schratter et al.) in press.

9.2.6 Effect of GIRK1 overexpression on MCF7 single cell motility and velocities

The motility and enhanced velocity of malign MCF7 cells is an important step in cancer metastasis. In this context, the effect of GIRK1 overexpression on the motility of the malign MCF7 cells was also tested. Flower plots in figure 42 show the effect of GIRK1 variant overexpression on MCF7 single cell motility (as already shown on the MCF10A cells). Time-lapse microscopy revealed that MCF7^{GIRK1} overexpressed cells exhibited elevated MCs when compared to control cell lines. This effect of GIRK1 overexpression can also see on Figure 43.

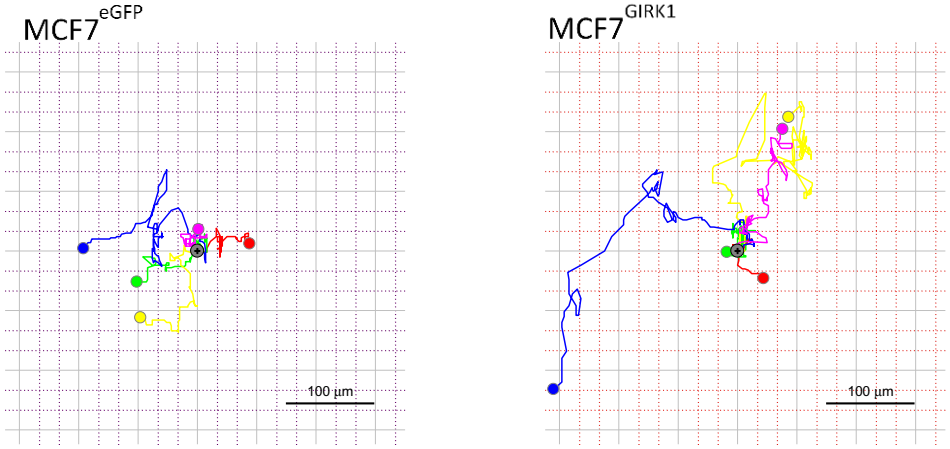

Figure 42: Effect of GIRK1 overexpression on MCF7 single cell motility. (Left) Migration of five selected MCF7^{eGFP} cells over the entire observation interval. Flower plots showing cellular trajectories for the entire observation interval of 72 h (colored line). Starting position of each individual cell was set to zero coordinates (grey circle). Colored circles indicate the positon of an individual cell after 72 h. (Right) same as left but MCF7^{GIRK1}. Reprinted from (Schratter et al.) in press.

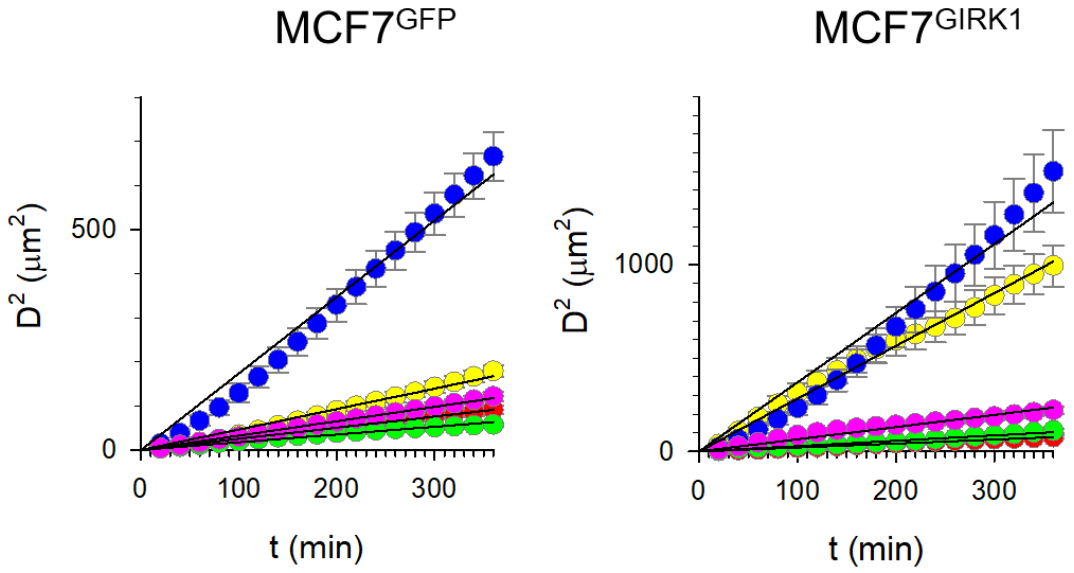

Figure 43: Effect of GIRK1 variant overexpression on MCF7 single cell motility. Squared distance as a function of time for the five cells were shown. (circles; bars indicate standard error). Lines represent a linear fits through the data. Left: MCF7^{eGFP}; Right: MCF7^{GIRK1}. Reprinted from (Schratter et al.) in press.

Reinforced migration could also be observed in overexpressed MCF7^{GIRK1} cells, but the effect was muted compared to benign MCF10A cells. In the statistical analysis, the effect of overexpression of the GIRK1 variant on MCF7 cells is not significant. But a clear trend in this direction is visible (Figure 44). The most motile third of MCF7^{GIRK1} cells displayed increased cell motility when compared to MCF7^{eGFP}. At figure 45, the data of MCs was re-evaluated. Difference in MCs ($\Delta MC=MC_{eGFP}-MC_{GIRK1}$) were calculated for 10% percentile intervals. Interestingly, the average MCs of the 70%, 80% and 90% percentile differs statistically significant between MCF7^{eGFP} and MCF7^{GIRK1}. The cell velocities of the overexpressed MCF7 cells were not increased compared to the overexpressed MCF10A cells (Figure 46).

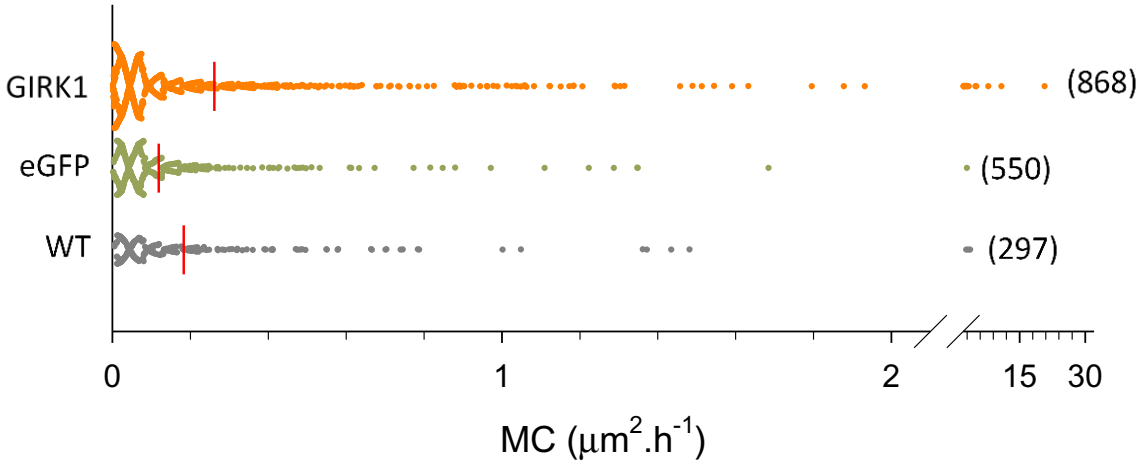

Figure 44: Effect of GIRK1 variant overexpression on MCF7 cells. Statistical analysis of motility coefficients derived from the different experimental groups. Top: WT: MCF7^{WT}, eGFP: MCF7^{eGFP} and GIRK1: MCF7^{GIRK1}. The median value is represented by the black line within the box, box margins represent 75% and 25% percentiles, whiskers indicate 90% and 10% percentiles. The red line represents the mean value. Individual values are shown as colored dots. The number of individual cells is given in parenthesis besides each box. Reprinted from (Schratter et al.) in press.

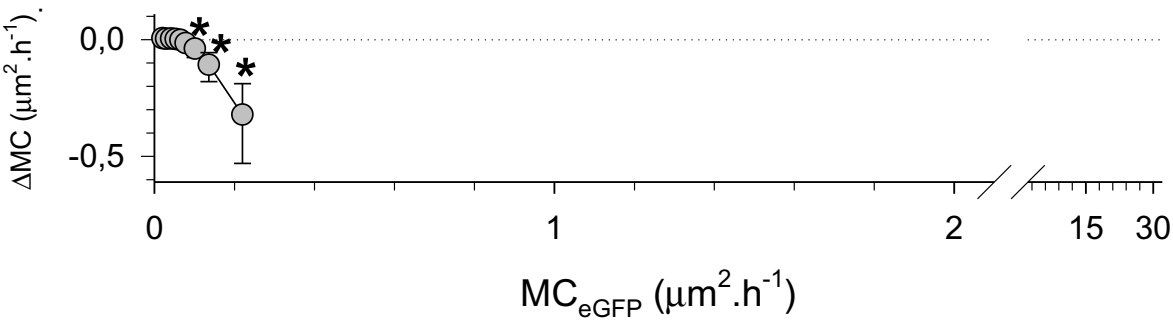

Figure 45: Statistical analysis of motility coefficients derived from the different experimental groups Difference in MCs ($\Delta MC=MC_{eGFP}-MC_{GIRK1}$) calculated for 10% percentile intervals vs. MC_{eGFP}. Whiskers represent 95% confidence intervals. *: the average MCs of the 70%, 80% and 90% percentile differs statistically significant between MCF7^{eGFP} and MCF7^{GIRK1}. Reprinted from (Schratter et al.) in press.

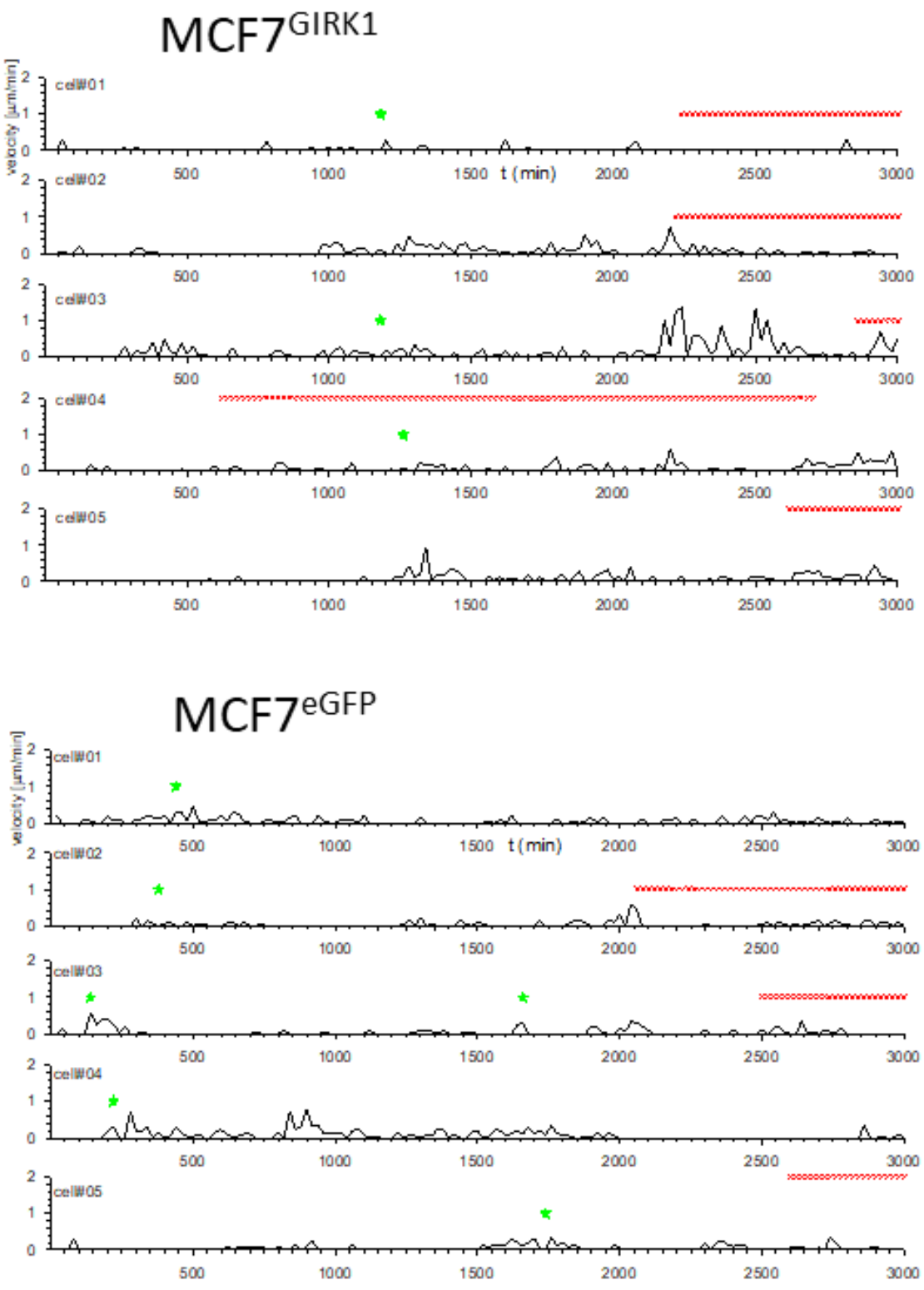

Figure 46: Effect of GIRK1 variant overexpression on MCF7 cell velocity. Upper: Cellular velocities for five representative MCFF7^{GIRK1} cells during the entire observation interval of 72 h. Lower: Cellular velocities for five representative MCFF7^{eGFP} cells during the entire observation interval of 72 h. Green asterisks denote cell divisions and red x denote cell aggregation. Reprinted from (Schratter et al.) in press.

Figures 47-48 shows graphical representation of “aggregated” and “free moving” cellular velocities for different experimental groups. The cellular velocities of MCF7^{GIRK1} cells were virtually unchanged.

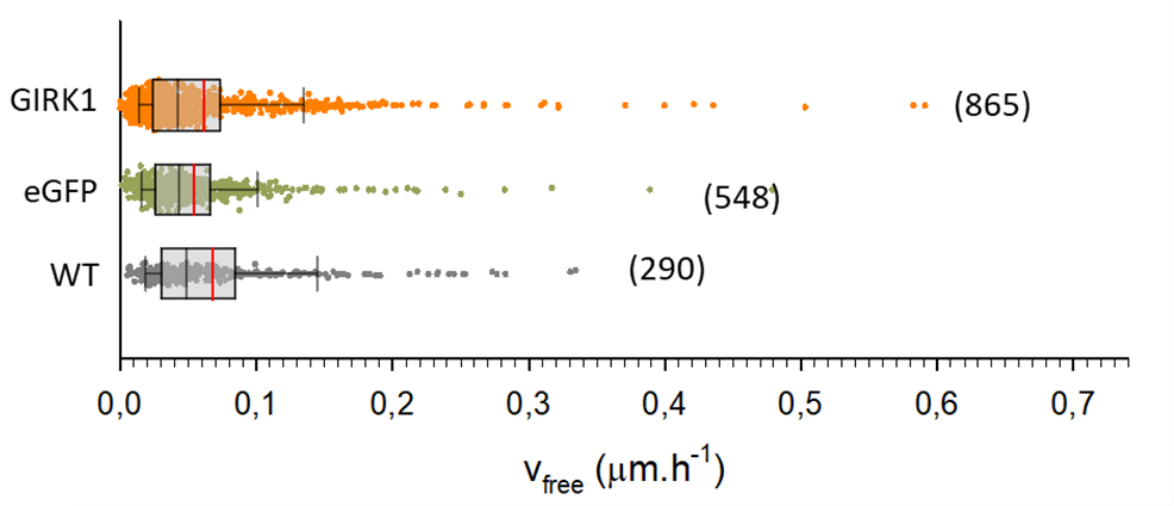

Figure 47: Effect of GIRK1 variant overexpression on cell velocity of free moving MCF7 cells. Graphical representation of velocity in µm/h. Grey: MCF7^{WT}, green: MCF7^{eGFP} vector control and overexpressed orange: MCF7^{GIRK1}. The median value is represented by the black line within the box, box margins represent 75% and 25% percentiles, whiskers indicate 90% and 10% percentiles. The red line represents the mean value. Individual values are shown as colored dots. The number of individual cells is given in parenthesis besides each box. Statistical significant differences between groups are indicated by brackets. Reprinted from (Schratter et al.) in press.

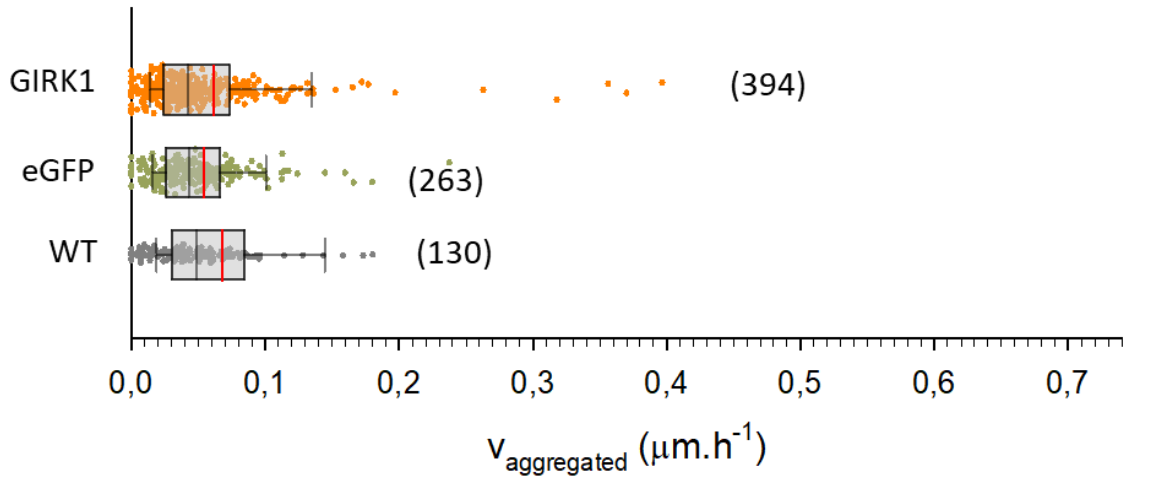

Figure 48: Effect of GIRK1 variant overexpression on cell velocity of aggregated MCF7 cells. Graphical representation of velocity in µm/h. Grey: MCF7^{WT}, green: MCF7^{eGFP} vector control and overexpressed orange: MCF7^{GIRK1}. The median value is represented by the black line within the box, box margins represent 75% and 25% percentiles, whiskers indicate 90% and 10% percentiles. The red line represents the mean value. Individual values are shown as colored dots. The number of individual cells is given in parenthesis besides each box. Statistical significant differences between groups are indicated by brackets. Reprinted from (Schratter et al.) in press.

9.2.7 Cell Adhesion Assay

The extracellular matrix (ECM) is the non-cellular component present within all tissues and provides a physical scaffolding for cellular constituents. The interactions of different cells are important determinants of tissue functions like survival, growth or differentiation. The ECM is formed out of a complex meshwork of structural molecules such as adhesive proteins to anchorage cells (Schlie-Wolter et al., 2013, Frantz et al., 2010). MCF10A^{GIRK1} differed markedly to MCF10A^{eGFP} regarding surface adherence properties as revealed by adhesion to surface coated with different extracellular matrix (ECM) molecules. Of note, the most prominently transcriptionally deregulated gene cluster in MCF10A^{GIRK1}/MCF10A^{eGFP} weakens interaction of cells with ECM molecules upon downregulation. Collagen I, collagen IV, fibronectin and tenascin-C adherence were hampered by GIRK1 overexpression. The interaction with laminin-coated surface was also weaker, but statistically not significant. Only cell adhesion to vitronectin coated surface, which was virtually undetectable in the control MCF10A^{eGFP} line, was marginally increased in MCF10A^{GIRK1}. Taken together, interactions of MCF10A^{GIRK1} to surfaces coated with seven different ECM molecules (figure 49) were heavily influenced when compared to control MCF10A^{eGFP}.

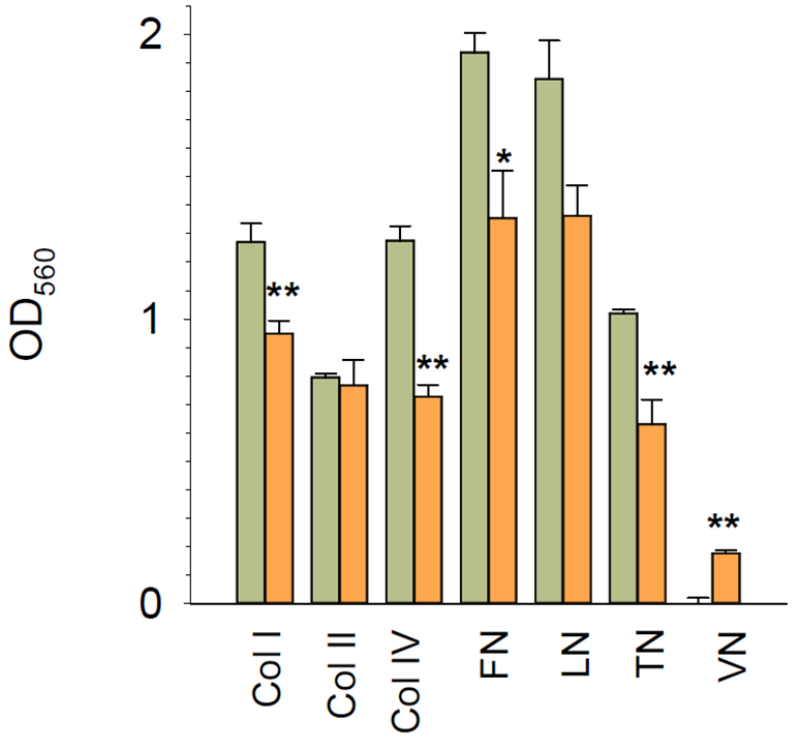

Figure 49: Effect of GIRK1 overexpression on cell adhesion of MCF10A cells. Cell adhesion (OD_{560} values) of MCF10A^{eGFP} (green) and MCF10A^{GIRK1} (orange) to surface coated with different extracellular matrix molecules: Col I: human Collagen Type I, Col II: human Collagen Type II, Col IV: human Collagen Type IV, FN: human Fibronectin, LN: human Laminin, TN: human Tenascin-C and VN: human Vitronectin. Mean values ± SEM for three or four experiments for each experimental group are shown. *(,**): The mean values differ statistically significant at the $p<0.05$ ($p<0.001$) level. Reprinted from (Schratter et al.) in press.

9.2.8 Invasion Assay

The Invasion Assay allows to test the rapid and quantitative assessment of invasiveness which alters the invasive phenotype of tumor cells (Albini et al., 1987). Invasion studies of GIRK1 overexpression were performed on MCF10A and MCF7 cell lines. Our results indicate that, GIRK1 overexpression did not affect invasiveness in MCF10A cells (Figure 50). There was no statistical difference to find between the cell lines. The ability of invasion was increased when MCF7 cells were overexpressing GIRK1 compared to MCF7 control cells (Rezania et al., 2016).

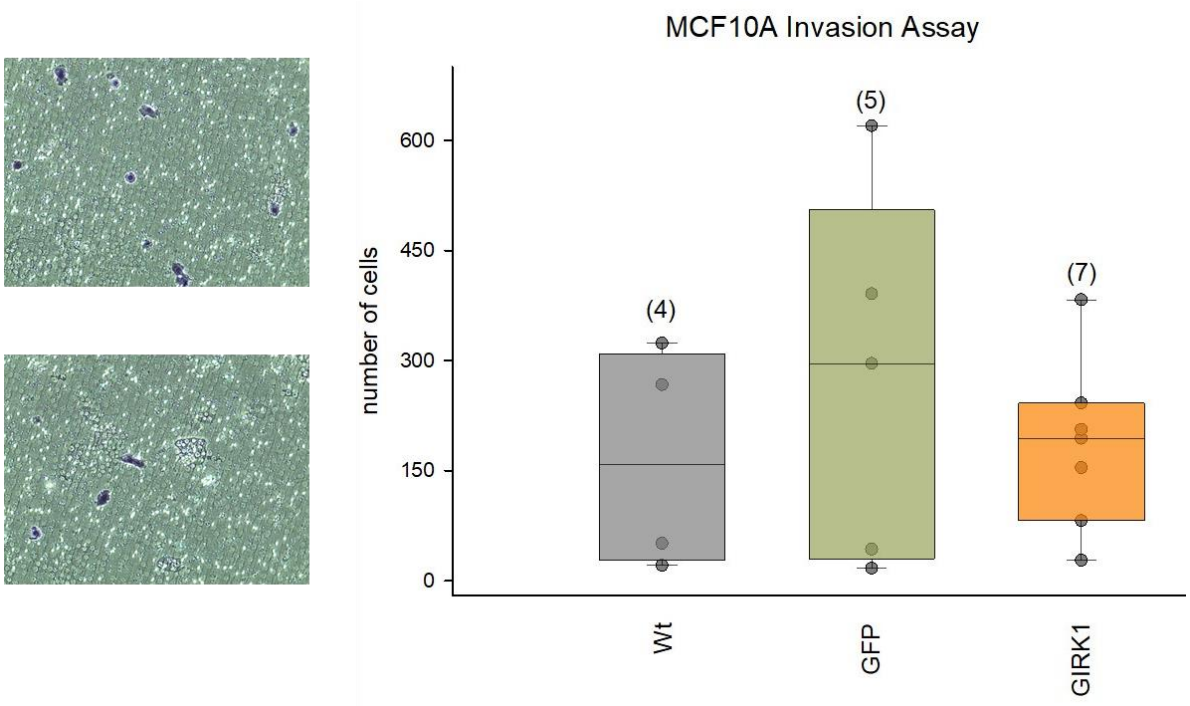

Figure 50: Effects of GIRK1 overexpression on invasion of MCF10A cells. Upper Left: Representative picture of MCF10A^{GIRK1} cells. Lower left: Representative picture of MCF10A^{eGFP} cells. Image show cells through the Matrigel, stained with crystal violet. Right: Quantification of the number of invasive cells after 24h. Number of experiments is given in parenthesis above each bar. WT: MCF10A^{WT}, eGFP: MCF10A^{eGFP} and GIRK1: MCF10A^{GIRK1}.

9.2.9 Mammosphere Forming Assay

The Mammosphere Assay is widely utilized to measure in vitro stem/progenitor cell frequency and activity in normal primary mammary epithelial cell preparations as well as in cancer stem cells (Shaw et al.). The histogram in figure (51) is displaying the differences in mammosphere forming efficiencies (MFEs) between MCF10A cell lines. There was no statistical difference to find between the cell lines MCF10A^{WT}, MCF10A^{eGFP} and MCF10A^{GIRK1}. Statistical analysis of data was performed using SPSS embedded in Sigmaplot (SPW 14.0, Systat Software Inc.).

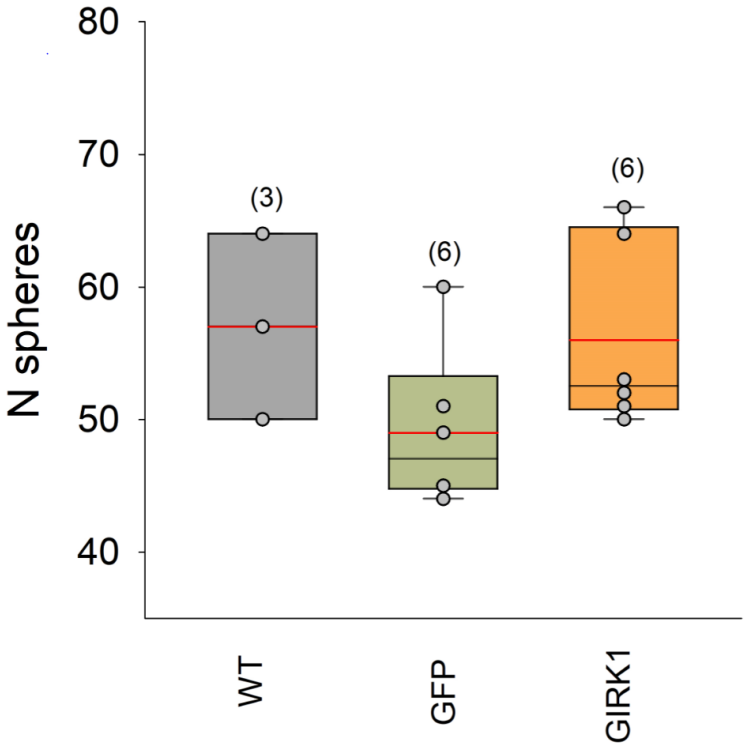

Figure 51: Mammosphere Formation Assay. Number of mammospheres formed by different MCF10A subpopulations. Number of experiments is given in parenthesis above each bar. WT: MCF10A^{WT}, eGFP: MCF10A^{eGFP} and GIRK1: MCF10A^{GIRK1}.

9.2.10 Transcriptome Analysis

In order to check the viability and possible benefit of the projected transcriptome analysis of all the generated cell lines (MCF10A^{WT}, MCF10A^{eGFP} and MCF10A^{GIRK1}) were analyzed. The number of transcriptome analysis of each clone is limited to two (N=2). In order to identify a possible cancerogenic influence of GIRK1 overexpression in benign MECs, transcriptomes of MCF10A^{eGFP} were compared to the MCF10A^{GIRK1} overexpressed cell lines. Unexpected for the overexpression of a single K^+ channel subunit, a high number of transcripts were sizably dysregulated upon GIRK1 overexpression. Of these, 829 genes were upregulated and 1073 genes were downregulated when MCF10A^{eGFP} are compared to MCF10A^{GIRK1}. (Figure 52). Analysis and classification into functionally related groups of genes using the “Database for Annotation, Visualization and Integrated Discovery” (DAVID) revealed that many of these transcripts are regulated towards specific cellular functions and pro-tumorigenic action. The gene ontology clusters were taken from DAVID functional clustering and the significance of the first nine annotated functions is ranked in figure 53. The different heat maps display the quantitative effect on selected gene clusters and underscore the amount of cellular regulation exerted by GIRK1 overexpression. Figures 54-56 are showing the top 50 genes of up- and down-regulated gene clusters. Additional cluster

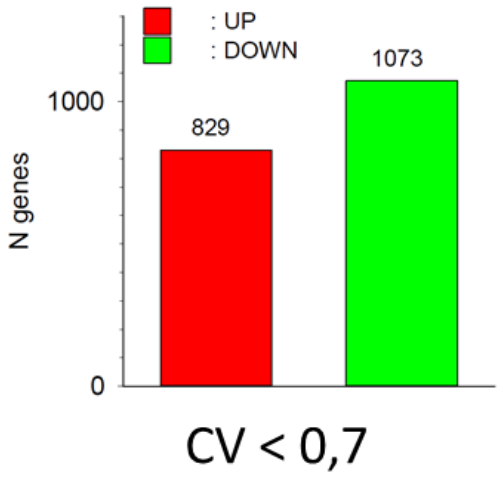

Figure 52: Transcriptional change promoted via GIRK1 overexpression in MCF10A cells. Number of significantly up- or downregulated transcripts when MCF10A^{eGFP} are compared to MCF10A^{GIRK1} overexpressor. Red: upregulated transripts, green: downregulated transcripts. For analysis coefficient of variation (CV) < 0,7 was taken. Reprinted from (Schratter et al.) in press.

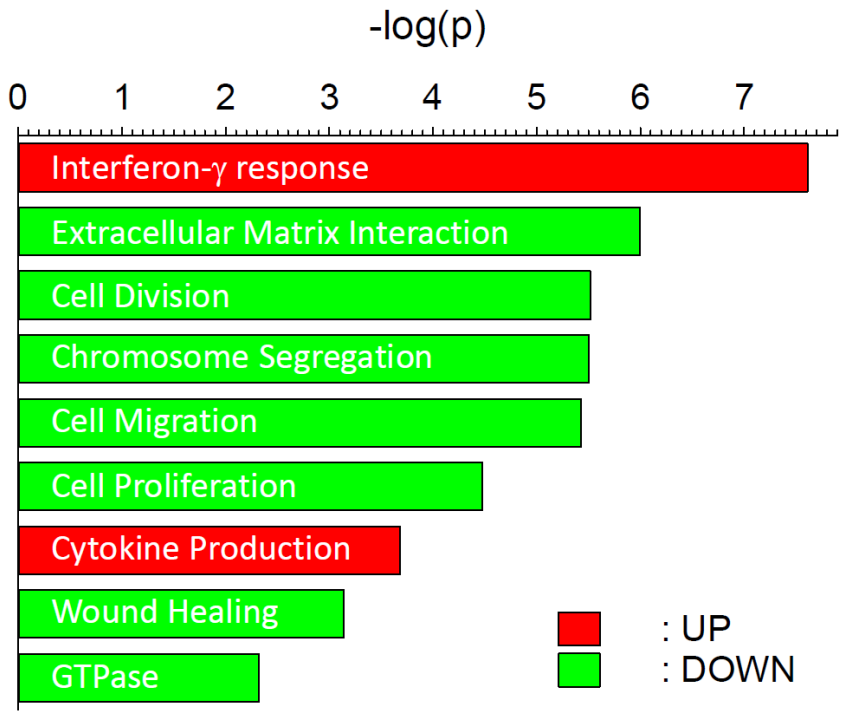

Figure 53: Differential expression of mRNA between overexpressed GIRK1 and wild type MCF10A cells. The top 9 ontological clusters of DAVID categories are reported for MCF10A datasets. Red: upregulated transcripts, green: downregulated transcripts. Reprinted from (Schratter et al.) in press.

analysis are shown in appendix 11.5. Enrichment scores (ES), p-values and False Discovery Rates (FDRs) for all significant clusters are shown in appendix 11.6 Table 8.).

Original data have been deposited in NCBI's Gene Expression Omnibus (GEO; https://www.ncbi.nlm.nih.gov/geo/) accession GSE 138155.

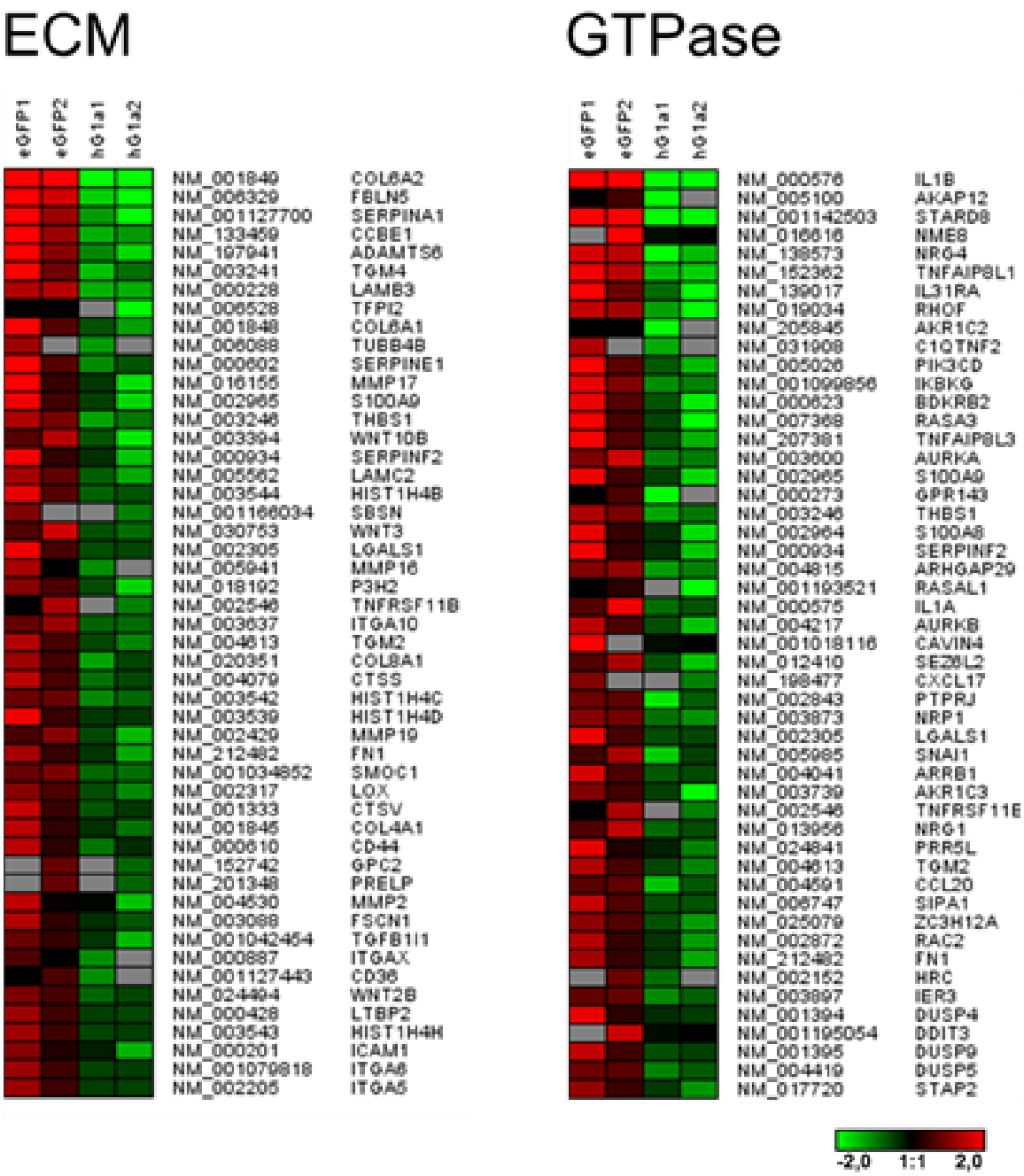

Figure 54: Effect of GIRK1 overexpression on transcriptome of MCF10A cells. Heatmaps displaying the fold changes of expression levels of each the top 50 genes of selected GO terms ECM: extracellular matrix interaction. GTPase: GTPase activating proteins. Bottom right: color coding for the log2 fold change. Red: upregulated transcripts, green: downregulated transcripts. Reprinted from (Schratter et al.) in press.

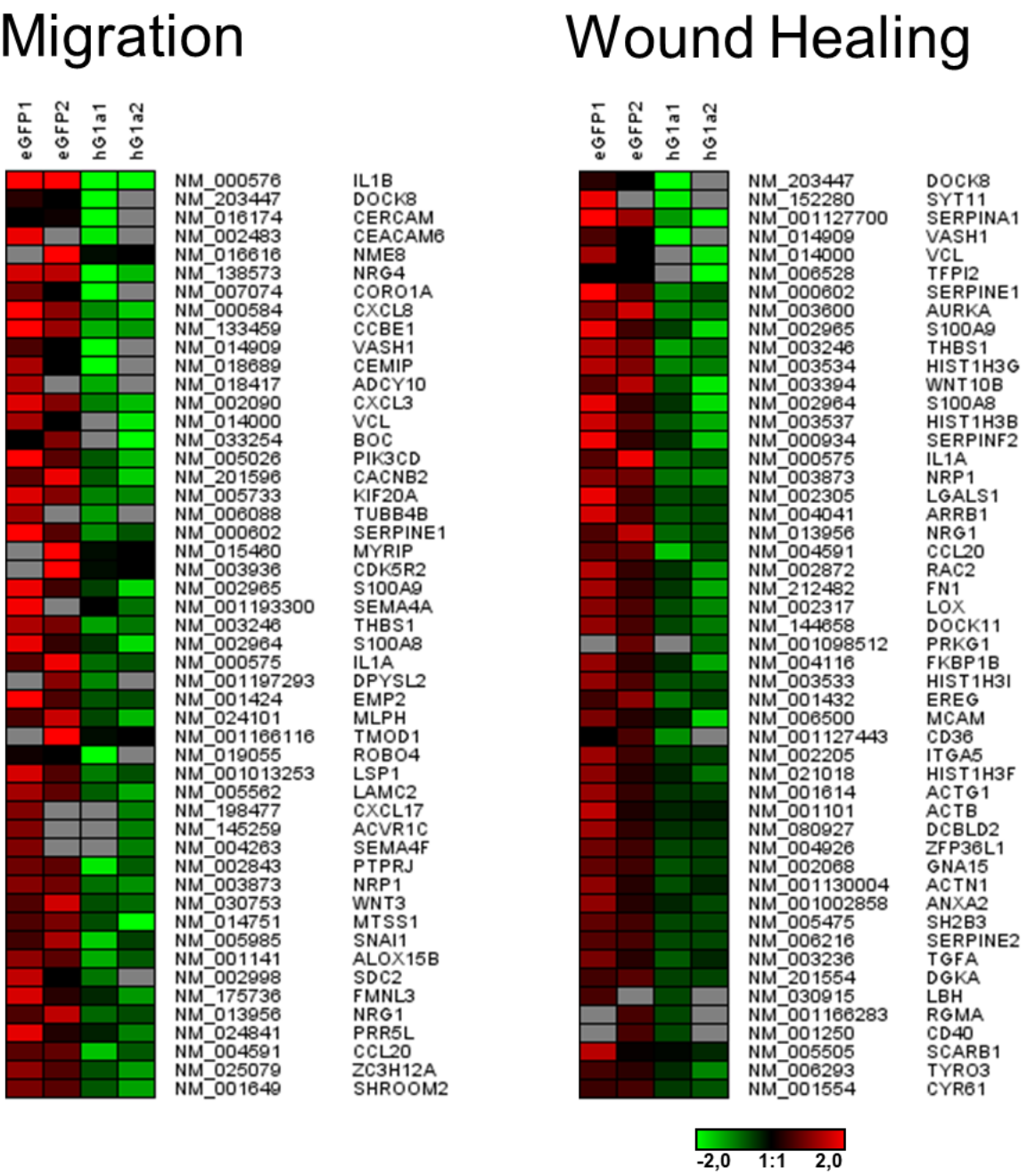

Figure 55: Effect of GIRK1 overexpression on transcriptome of MCF10A cells. Heatmaps displaying the fold changes of expression levels of each the top 50 genes of selected GO terms. Migration: cell migration and WH: wound healing. Bottom right: color coding for the log2 fold change. Red: upregulated transcripts, green: downregulated transcripts. Reprinted from (Schratter et al.) in press.

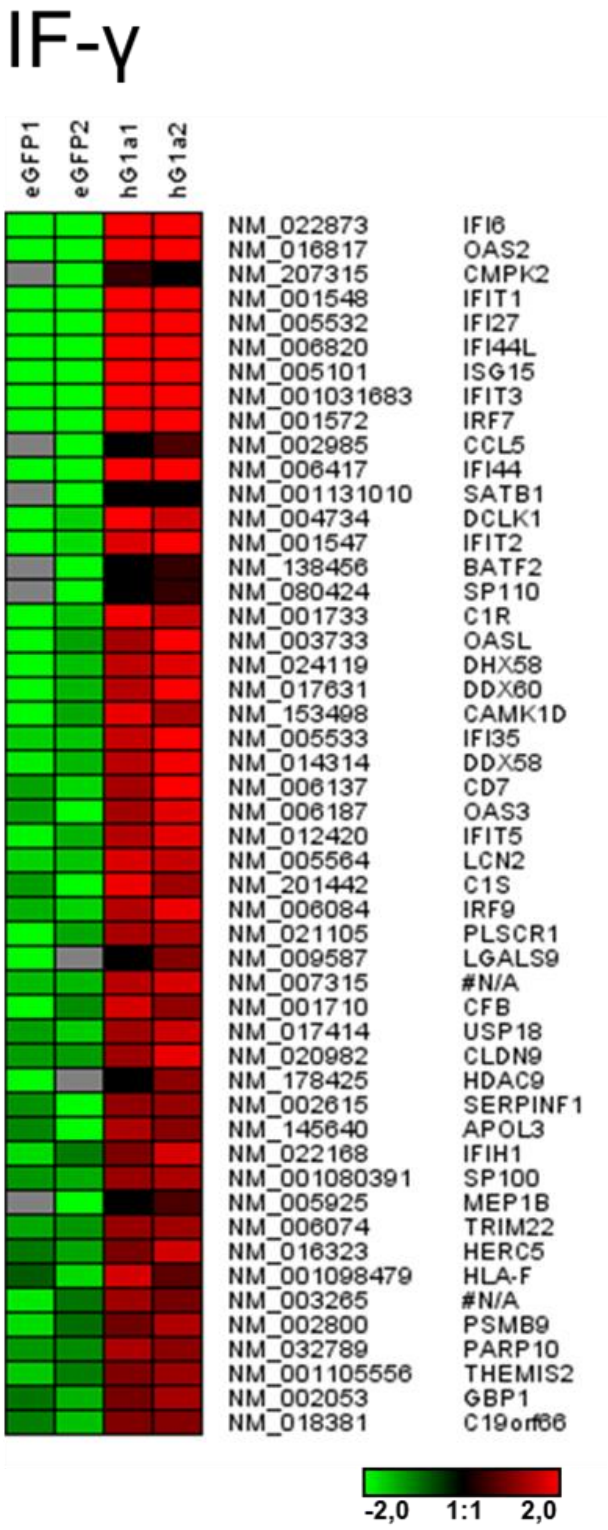

Figure 56: Effect of GIRK1 overexpression on transcriptome of MCF10A cells. Heatmaps displaying the fold changes of expression levels of each the top 50 genes of selected GO terms. IF-γ: Interferon-γ response. Bottom right: color coding for the log2 fold change. Red: upregulated transcripts, green: downregulated transcripts. Reprinted from (Schratter et al.) in press.

Heat maps of all significantly enriched clusters are shown in Figures 63A and 63B.

9.2.11 Validation of RNA-seq by qPCR

Quantification of RNA-seq expression of six genes, selected from the three most important regulated clusters as detected by DAVID were confirmed by additional and independent qPCR (YWHAZ was used as reference for qPCR). A high correlation between RNA-seq and qPCR expression levels could be detected.

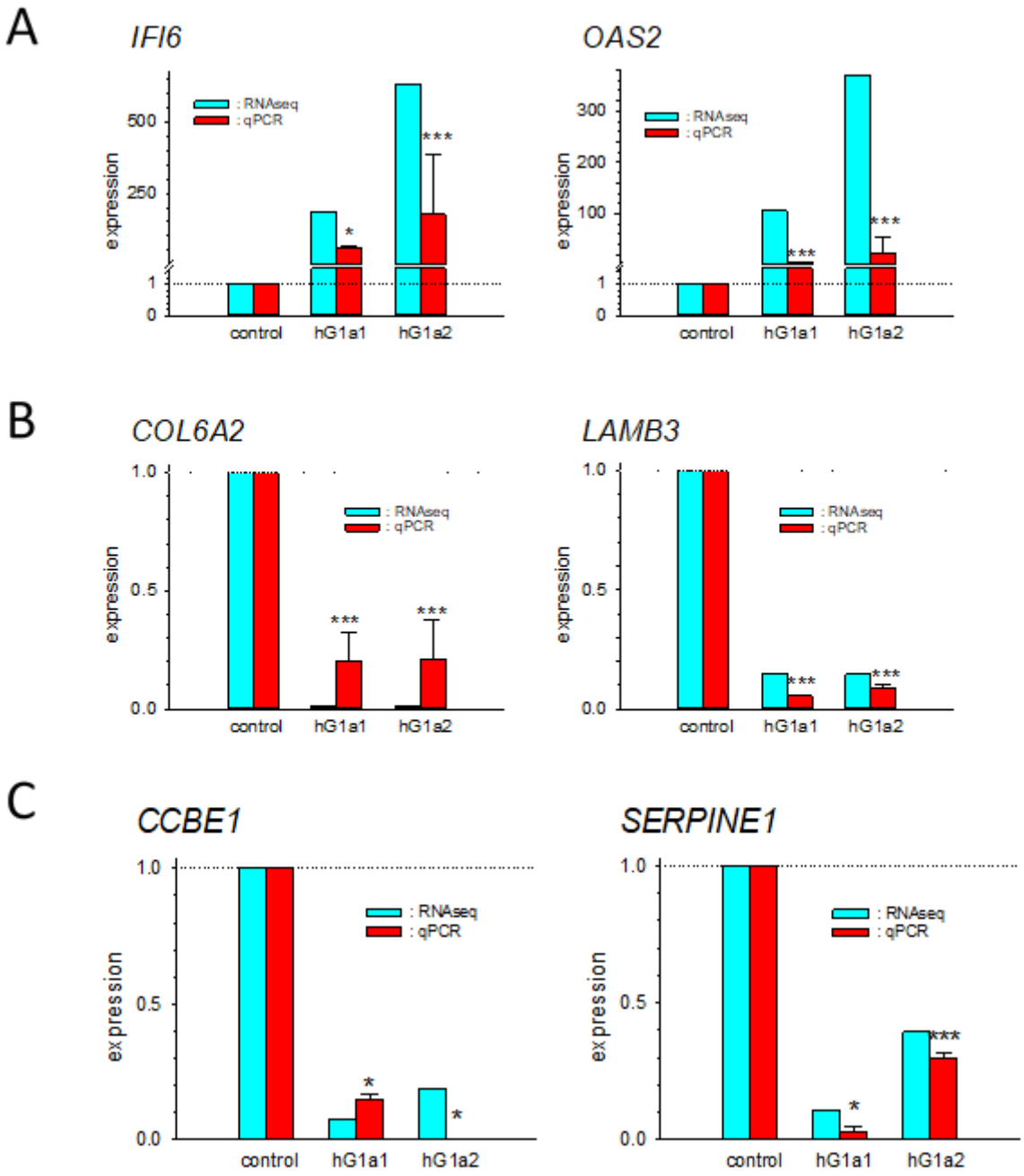

Figure 57: RNA-seq expression of six genes: Genes selected from the three most important DAVID clusters was confirmed by independent qPCR (YWHAZ was used as reference for qPCR). Expression level of the gene of interest in the libraries derived from GIRK1 overexpressors was normalized to one of the control libraries and are shown as fold change on the y-axis. eGFP#1 was used as control for hG1a1 (GIRK1#1) and eGFP#2 as control for hG1a2 (GIRK1#3), respectively. A high correlation between RNA-seq and qPCR expression levels could be detected. All genes were differentially expressed in comparison to the reference (*, (***): p-value is statistically significantly different at the <0.05, (0.001) level). (A): Gene cluster IF-γ, (B): Gene cluster ECM and (C): gene cluster migration. Reprinted from (Schratter et al.) in press.

9.2.12 Results of Kyoto Encyclopedia of Genes and Genomes (KEGG) pathway

The KEGG pathway diagram was overlaid with the computed total disorder of each gene. Red stars represent down-regulated genes. Genes in green background represent the species specific genes of *Homo sapiens*. KEGG analysis indicated that the most significantly altered category was ECM-receptor interaction. Figure 57 shows gene mapping for ECM-receptor interaction (KEGG: 04512). This map shows a high number of genes which are strongly influenced by overexpression of GIRK1.

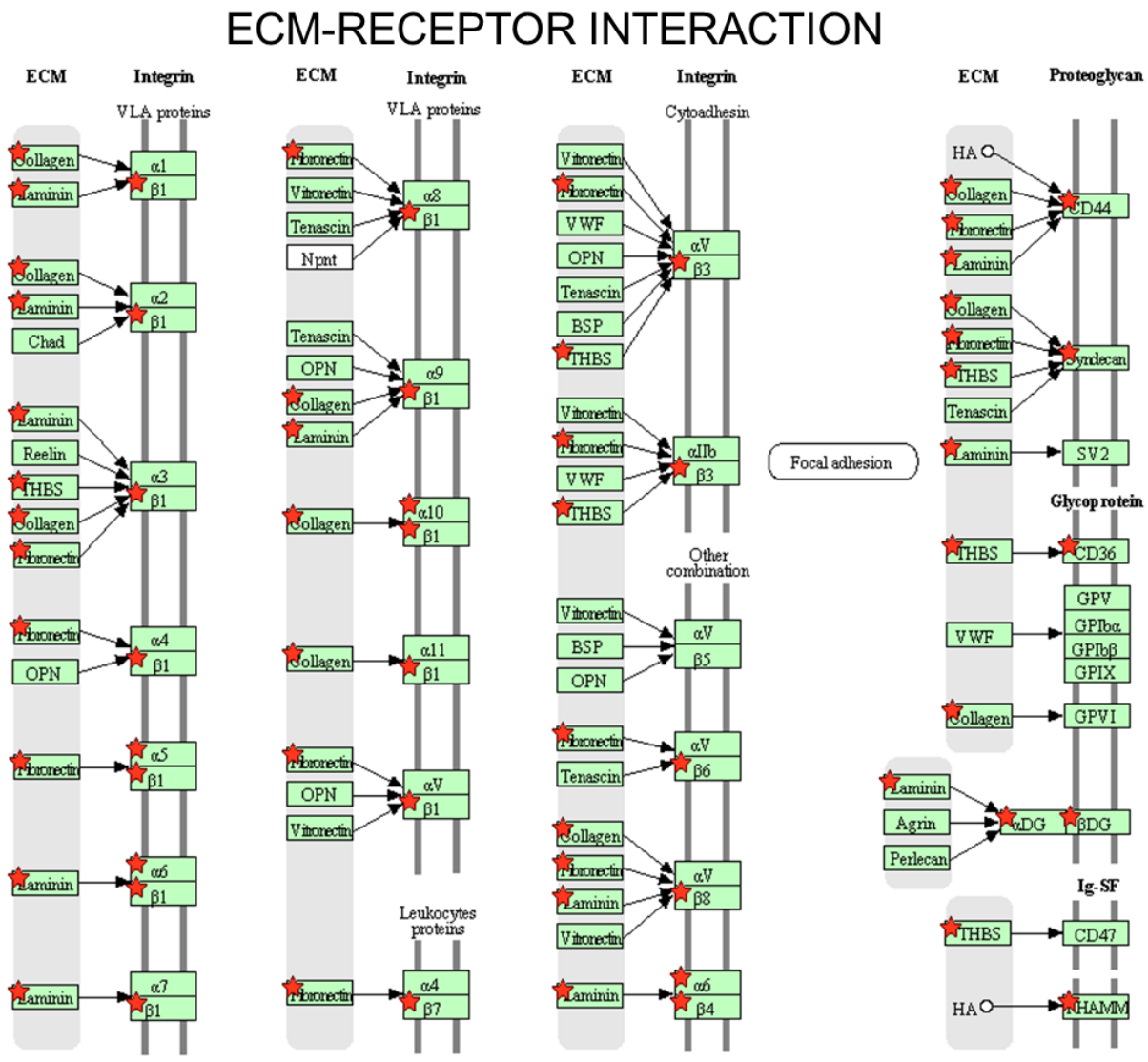

Figure 58: Enrichment of ECM-receptor interaction pathway (KEGG: 04512). Functional analysis of differentially expressed genes. Red stars indicate down-regulated genes. In this map one can see that ECM-Integrin interaction are strongly influenced by overexpression of GIRK1.

9.2.13 Colony Formation Assay (Clonogenic Assay)

Colony formation assay did not reveal a change in both MEC cell lines (MCF10A and MCF7) in the ability to form colonies, nor in the growth rate of the colonies formed. Figure 58 is showing a representative image of colonies produced by MCF10A cells (image of plating 100 cells per 6-well plate and eight days' incubation). The statistical analysis was shown in figure 59.

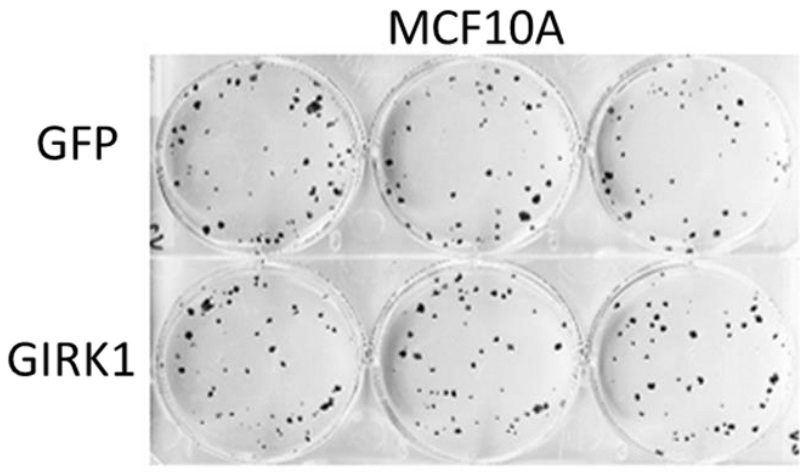

Figure 59: Colonies found by MCF10AGIRK1 and MCF10AeGFP cells. Plating of 100 cells per 6-well plate and eight days after incubation. Representative micrographs of three microplate slots per experimental group (stained colonies are visible as dark spots). Diameter of a slot is 35 mm. Upper: GPF: MCF10A^{eGFP} and Lower: GIRK1: MCF10A^{GIRK1}. Reprinted from (Schratter et al.) in press.

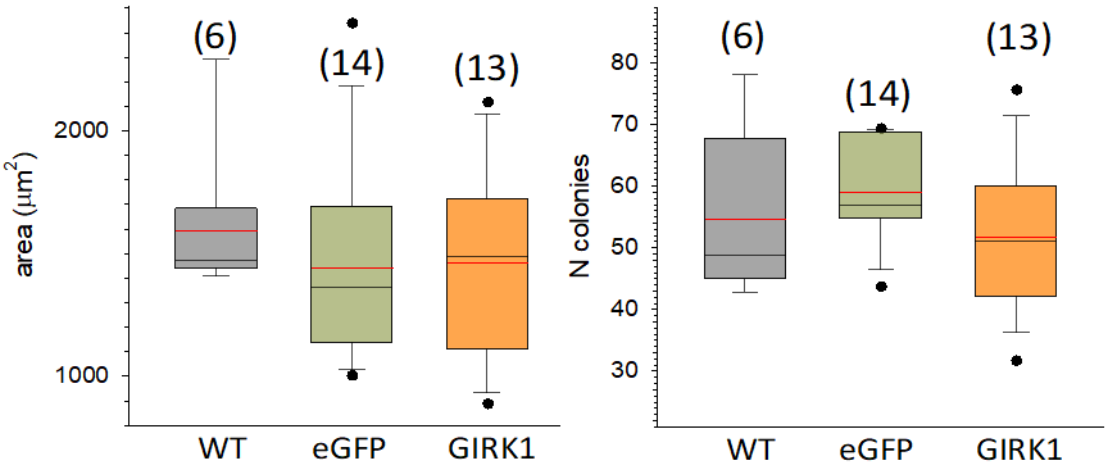

Figure 60: Quantification of the number of MCF10A cells. Statistical analysis of MCF10A lines. Left: Number of colonies formed per 100 cells/well. WT: MCF10A^{WT}, eGFP: MCF10A^{eGFP} and GIRK1: MCF10A^{GIRK1}. Right: areas of colonies at time of harvesting. WT: MCF10A^{WT}, eGFP: MCF10A^{eGFP} and GIRK1: MCF10A^{GIRK1}. The median value is represented by the black line within the box, box margins represent 75% and 25% percentiles, whiskers indicate 90% and 10% percentiles. The red line represents the mean value. Individual values outside the 10% and 90% percentiles are shown as black circles. Three independent experiments for each cell line were performed in triplicates. The differences between the experimental groups, neither for the number of colonies formed, nor for colony area, are not statistically significant different. Reprinted from (Schratter et al.) in press.

Colony formation assay did not reveal a change in GIRK1 overexpressed MCF7 compared to eGFP control cell lines in the ability to form colonies, nor in the growth rate of the colonies formed. Figure 60 is showing a representative image of colonies produced by MCF7 cells (image of plating 200 cells per 6-well plate and eight days' incubation). The statistical analysis is shown in figure 61.

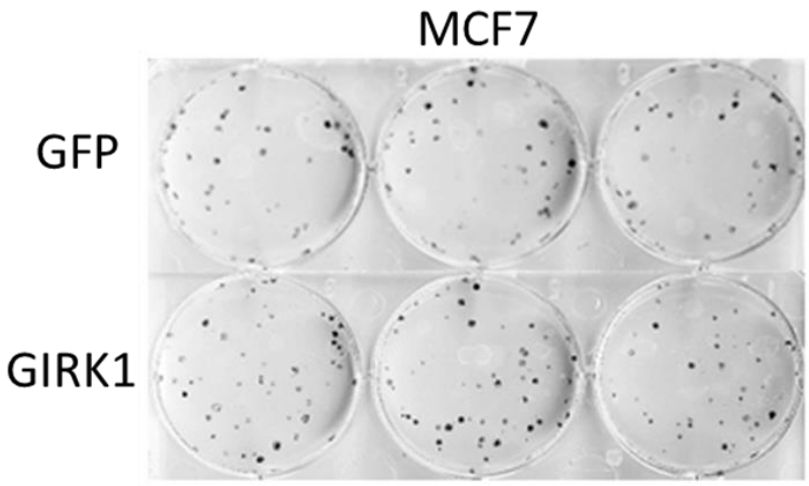

Figure 61: Effects of GIRK1 overexpression on MCF7 cells. Image showing colonies produced by MCF7 cells. Plating of 200 cells per 6-well plate and eight days after incubation. Representative micrographs of three microplate slots per experimental group (stained colonies are visible as dark spots). Diameter of a slot is 35 mm. Upper: GFP: $MCF7^{eGFP}$ and Lower: GIRK1: $MCF7^{GIRK1}$. Reprinted from (Schratter et al.) in press.

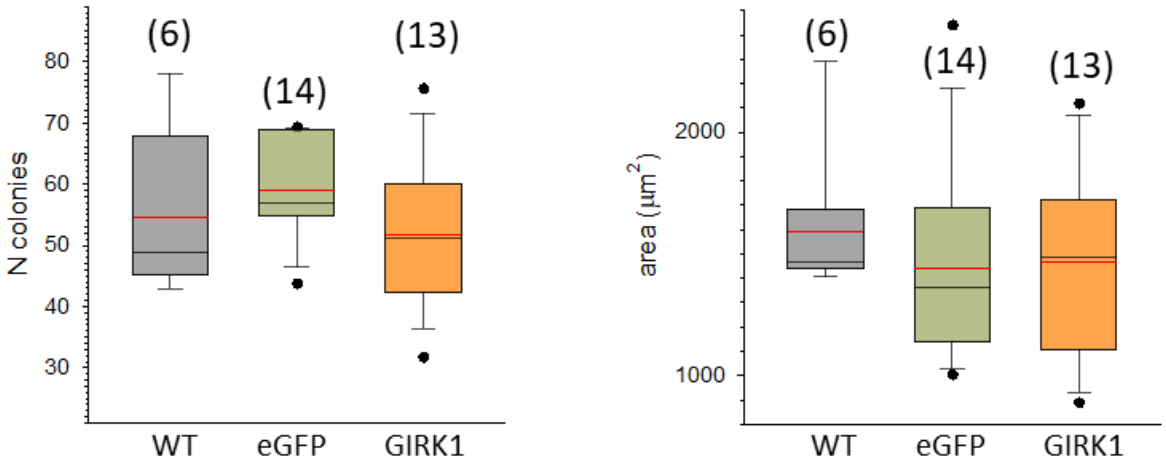

Figure 62: Quantification of the number of MCF7 cell. Statistical analysis of MCF7 lines. Left: Number of colonies formed per 200 cells/well. WT: $MCF7^{WT}$, eGFP: $MCF7^{eGFP}$ and GIRK1: $MCF7^{GIRK1}$. Right: areas of colonies at time of harvesting. WT: $MCF7^{WT}$, eGFP: $MCF7^{eGFP}$ and GIRK1: $MCF7^{GIRK1}$. The median value is represented by the black line within the box, box margins represent 75% and 25% percentiles, whiskers indicate 90% and 10% percentiles. The red line represents the mean value. Individual values outside the 10% and 90% percentiles are shown as black circles. Three independent experiments for each cell line were performed in triplicates. The differences between the experimental groups, neither for the number of colonies formed, nor for colony area, are not statistically significant different. Reprinted from (Schratter et al.) in press.

10. Discussion

In the past decades a number of studies has been devoted to cancer research. For every type of cancer new targets for therapy are constantly being identified and new forms of therapy are continuously being developed. Ion transporter are transmembrane proteins, proposed as potential targets because they are often implicated in cancer biology (Wulff et al., 2009). The study, carried out by our research department, has shown that overexpression of GIRK1 in benign MECs triggers transcriptional alterations of a great number of individual genes involved in several cellular pro-tumorigenic pathways. If one only looks at the potassium channels probably these channels have the highest variability, in term of both their biochemical structures and their role in cancer. GIRK channels are members of inwardly rectifying K^+ channels, in which the inward current is considerably greater than the outward current (Rifkin et al., 2017). Stable GIRK1 overexpression in MCF10A resulted in tertiapin-Q sensitive hyperpolarization of resting potential, indicating that functional GIRK channels are established. Four different genes exist in the human genome, encoding GIRK1, GIRK2, GIRK3 and GIRK4, which form heterotetrameric and/or homotetrameric channels in the plasma membrane (Lüscher and Slesinger, 2010). GIRK channels are involved in many cell signaling pathways and they are activated by G-protein coupled receptors (GPCRs). Since GIRK1 requires additional isoform subunits in order to assemble into functional heterotetramers (Luescher and Slesinger, 2010) one may ask whether the essential GIRK isoforms are present in the cell membrane. GIRK4 protein has been shown to preexist in benign MECs, including MCF10A (Wagner et al., 2010). Both GIRK4 and GIRK2 were identified in the malign MCF7 line (Dhar and Plummer, 2006). In the malign MCF7 line, GIRK1 overexpression resulted in hyperpolarized membrane resting potential of single cells. The effect was less pronounced when compared to benign MCF10A. Block of GIRK channels in $MCF7^{GIRK1}$ by tertiapin-Q resulted in depolarization that was even more pronounced when compared to the control $MCF7^{eYFP}$ or $MCF7^{WT}$, whose membrane potentials ranged in-between the ones of $MCF7^{GIRK1}$. We attribute the value of resting membrane potentials in control cell lines to moderate overexpression of GIRK1 that pre-existing in the malign MCF7 line yet. (Wagner et al., 2010).

For GIRK1, five splice variants were identified as well. These are referred to GIRK1a, GIRK1b, GIRK1c, GIRK1d and GIRK1e. Similar to the observed effect on membrane resting potential, silencing of preexisting GIRK complexes in MCF7 by overexpression of the dominant negative splice variant GIRK1d, had a bearing on several vital functions of MCF7 cells which were in opposition to the ones of the functional GIRK1a variant (Rezania et al., 2016). Therefore, preexisting GIRK complexes already act electrogenic and exert regulatory actions on cellular properties of the malignant MCF7 cell line. The effects induced by GIRKs

are further increased upon ectopic GIRK1 overexpression in MCF7 cell lines. Upon GIRK1 overexpression, motility and cellular velocities of the benign MCF10A control lines were substantially increased and associated with transcriptional changes of genes, which are linked to motility at the cellular level in order to find in the heat map “Cell migration” (Figure 55). Apart from their effect on cellular motility, these genes are important in mammary cancerogenesis and breast cancer progression: IL-1ß is pivotal for pathogenesis and understood to contribute to the poor prognosis of estrogen-dependent breast cancers (Giraldo, 2009). Homozygous deletions of DOCK8 exist in breast cancer and lung cancer (Takahashi et al., 2006). Reduced CCBE1 expression has shown to result in an increase of invasive capacity in breast cancer cells and to lead to poor clinical prognosis in patients (Mesci et al., 2017). In benign MECs, NOTCH-1 activation triggers downregulation of LAMC2 resulting in cellular responses towards cancer hallmarks, including cell migration (Mazzone et al., 2010). MTSS1 downregulation causes early cancerogenesis and results in increased metastatic spread as well as poor survival rates in breast cancer and lung cancer (Hicks et al., 2006, Kayser et al., 2015). In comparison to the benign MCF10A cell line, the impact of GIRK1 overexpression on motility of the malign MCF7 cell line was less pronounced. Nevertheless, these findings confirm our previous observation of increased migration of $MCF7^{GIRK1/eYFP}$ compared to control samples (Rezania et al., 2016). Upon GIRK1 overexpression, wound healing was highly impaired in the benign MCF10A line, with little influence on the malignant MCF7 MEC line. Similarly, Rezania et al. observed a small increase in wound healing rate upon overexpression of GIRK1/eYFP chimeric protein in the malignant MCF7 MEC line, but a decrease when GIRK1 function was knocked out through overexpression of the dominant negative splice variant GIRK1d (Rezania et al., 2016). Hence, marginal GIRK1 levels, as observed in $MCF7^{WT}$, have negative bearing on wound healing. Interference of wound healing is considered to be a cancer hallmark (Dvorak et al., 1986) and is co-opted as element of the developmental regulatory program, referred to as the ‘‘epithelial-mesenchymal transition’’ (EMT), by which transformed epithelial cells are able to get the abilities to invade, to resist apoptosis, and to disseminate (Hanahan and Weinberg, 2011). Transcriptional downregulation of the gene cluster “wound healing” was revealed by transcriptome analysis (see heat map “wound healing”; Figure 55). Among the genes, downregulated in $MCF10A^{GIRK1}$ and linked to impairment of wound healing, were DOCK8 and CD36 that are relevant players in breast cancer (Takahashi et al., 2006, DeFilippis et al., 2012). Breast cancer is often associated with massive alterations of ECM architecture and composition, influencing a number of biological activities such as cell proliferation, differentiation, biosynthetic ability, polarity, locomotion and mechanical stress via structurally different surface receptors (Butcher et al., 2009). GIRK1 protein possesses an extracellular integrin binding motif (Ivanina et al., 2000) and hence may contribute to

cell-ECM interactions. In the presented study, overexpression of GIRK1 in MCF10A led to reduced adherence to surfaces coated with several extracellular matrix molecules. These experimental observations were reflected by downregulation of genes comprised into a functional cluster termed “Extracellular matrix – receptor interaction” (Figure 54). Among the identified transcripts, downregulation of COL6A2, SERPINA1, CCBE1, TFPI2, THBS1 and COL8A1 have been shown to promote migration and invasion of malign breast cancer cells, aggravate metastatic spread, which result in poor prognosis of breast cancer patients (Luparello, 2013, Chan et al., 2015, Mesci et al., 2017, Roberts, 2005, Chen et al., 2014). Furthermore, SERPINA1 downregulation has been described to promote resistance towards both chemotherapy and tamoxifen treatment (Chan et al., 2015), while CCBE1 and COL8A1 are related to chemotherapy resistance (Mesci et al., 2017, Chen et al., 2014). Both, the MCF10A as well as the MCF7 cell lines, neither displayed alterations in proliferation, ability to form colonies upon seeding on petri dishes, nor in growth rates of the colonies formed. Rezania et al. (Rezania et al., 2016) obtained similar results upon overexpression of chimeric GIRK1/eYP protein in the malignant MCF7 cell line. The lack of effect of GIRK1 overexpression on cell proliferation is, to some extent, unexpected since GIRK1 overexpression in MCF10A has induced resilient changes in several gene clusters involved in cell division and proliferation. The gene clusters discussed above exert protumorigenic action upon downregulation.

The most prominently regulated functional cluster is, however, upregulated and comprises downstream elements which are triggered by the cytokine interferon-γ (IF-γ “Interferon-γ response” (Figure 56)). It is a cytokine that arrange many distinct cellular programs through transcriptional control over large numbers of genes and the biological functions are diverse. The signal resulting from the IF-γ comprises the activation of the transmembrane IF- γ receptors IFγR1 and IFγR2. This is followed by a cascade of signals, such as activation of JAK tyrosine kinase, binding and translocation of Signal Transducers and Activators of Transcription (STAT) proteins. Finally, the activation of transcription factors such as interferon response factors (IRF) follows (Schroder et al., 2004)). Under physiological settings, IF-γ signaling brings about biological functions related to antibacterial and antiviral host defense and immune regulation, cell cycle, apoptosis, inflammation and innate and acquired immunity (Schroder et al., 2004).

The flexible immunomodulatory functions implicated in IF-γ signaling prompted several clinical applications for the cure of chronic granulomatous disease, fungal infections, autoimmune diseases and cancer (Miller et al., 2009). At about the same time that IF-γ was advertised as promising antitumor agent, IF-γ had been identified to promote metastatic spread, resistance against natural killer cells, anti-apoptotic and proliferative responses of

various malignant cell types (Mojic et al., 2018, Castro et al., 2018) and, in the pathophysiological context of malignant cells and microenvironment, acts pro-tumorigenic (Zaidi, 2019). In the presented study, overexpression of GIRK1 in the benign MCF10A line triggered several downstream IF- γ signaling elements known to act pro-tumorigenic in MECs and to hamper the treatment of breast cancer. The strongest upregulated molecules include IFI6, OAS2, IFI44, ISG15, IRF7, DCLK1 and LCN2. Similar to the downregulated pathways discussed above, these genes have been shown to promote migration, invasion and metastasis formation of malignant MECs, mediate resistance towards chemotherapy and correlate with poor prognosis for patients ((Cheriyath et al., 2018, Choi et al., 2015, Ligr et al., 2011, Desai, 2015, Lan et al., 2019, Lv et al., 2017, Yang et al., 2009)). Furthermore, IFIT1, IFI27, CAMK1D, IRF9 and USP18 were displayed to correlate with two of the above-mentioned features (Danish et al., 2013, Li et al., 2015, Bergamaschi et al., 2008, Luker et al., 2001, Tan et al., 2018). In addition to the correlation with chemotherapy resistance, IFIT3 levels are associated with tamoxifen resistance of breast cancer cells (Nushtaeva et al., 2018). This is the first study to provide insight into the cellular and molecular consequences of GIRK1 overexpression in benign MCF10A cells. Our study reveals, that the overexpression of a single K^+ channel subunit shifts vital parameters of a benign MEC line towards cancer hallmarks. A profound change in the expression levels of a high number of transcripts, many involved in induction, progression and exacerbated treatment of breast cancer, accompanies the changes in cellular behavior. The observed influence on cellular behavior goes far beyond the role of overexpression of a K^+ ionophore acting on cellular motility via topical osmoregulatory K^+ levels alone and indicates that GIRK1 may represent a missing link for the complementation of pathophysiological de novo pathways, which alter cellular homeostasis towards the malign phenotype. This is in accordance to the observation of excessive GIRK1 mRNA and protein levels in breast tumors, which correlate with poor prognosis for patients with ER^+ breast cancer (Kammerer et al., 2016). Therefore, the future and detailed investigation of GIRK1 mediated pathways in MECs is likely to provide essential insight into development and progression especially in the subset of ER^+ breast cancer. Through its pronounced influence on intracellular signaling cascades, GIRK1 overexpression may open a new therapeutic window for treatment and classification of breast tumors.

11. Appendix

11.1 Construct: hG1a (GIRK1)

NCBI Reference Sequence: NM_002239.3 (from NCBI data base) https://www.ncbi.nlm.nih.gov/nuccore/386781835/

mRNA: CDS: 196.1701

01 ctccgtccca ggggagaagg agaggcgtct gcaggggga gagaccgcag ctacctgccg
61 ggtgcgcccc ccacccagga gcgctcgctt cgcccccttt cctcccccgc ccccacctcc
121 ttattggtgc tagtttgcag cgcccagctc ctgcgccttc gcttcgcgtt tgaatctggc
181 tcgccccttc gtattatgtc tgcactccga aggaaatttg gggacgatta tcaggtagtg
241 accacatcgt ccagcggctc gggcttgcag ccccaggggc caggccagga ccctcagcag
301 cagcttgtgc ccaagaagaa gcggcagcgg ttcgtggaca agaacggccg gtgcaatgta
361 cagcacggca acctgggcag cgagacaagc cgctacctct cggacctctt caccacgctg
421 gtggacctca agtggcgctg gaacctcttc atcttcattc tcacctacac cgtggcctgg
481 cttttcatgg cgtccatgtg gtgggtgatc gcctacactc ggggcgacct gaacaaagcc
541 cacgtcggta actacacgcc ttgcgtggcc aatgtctata acttcccttc tgccttcctc
601 ttcttcatcg agacggaggc caccatcggc tatggctacc gatacatcac agacaagtgc
661 cccgagggca tcatcctctt cctcttccag tccatcctgg gctccatcgt ggacgccttc
721 ctcatcggct gcatgttcat caagatgtcc cagcccaaga agcgcgccga gaccctcatg
781 ttcagcgagc acgcggtgat ctccatgagg gacggaaaac tcacgcttat gttccgggtg
841 ggcaacctgc gcaacagcca catggtctcc gcgcagattc gctgcaagct gctcaaatct
901 cggcagacac ctgagggtga gttccttccc cttgaccaac ttgaactgga tgtaggtttt
961 agtacagggg cagatcaact ttttcttgtg tccccctca caatttgcca cgtgatcgat
1021 gccaaaagcc ccttttatga cctatcccag cgaagcatgc aaactgaaca gttcgagatt
1081 gtcgtcatcc tagaaggcat tgtggaaaca actgggatga cttgtcaagc tcgaacatca
1141 tatactgaag atgaagttct ttggggtcat cgttttttc ctgtaatttc cttagaagag
1201 ggattcttta aagttgatta ctcccagttc catgcaacat ttgaagtccc caccccacct
1261 tacagtgtga aagagcagga ggaaatgctt ctcatgtcgt ccccttaat agcaccagcc
1321 ataactaaca gcaaagaaag acataattct gtggaatgct tagatggact agatgatatt
1381 actacaaaac taccatctaa gctgcagaaa attactggaa gagaagactt tcccaaaaaa
1441 ctcttgagga tgagttctac aacttcagaa aaagcctaca gcttgggaga cttgcccatg
1501 aaacttcaac gaataagttc agttccgggc aactcagaag aaaaactggt atctaaaacc
1561 accaagatgt tatctgatcc catgagccag tctgtggctg atttgccacc aaagcttcaa
1621 aagatggctg gaggagcagc taggatggaa gggaaccttc cagccaaatt aagaaaaatg
1681 aactctgatc gcttcacata acaaagcact cccttaggca ttatttaatg tttgatttag
1741 taatagtcca atatttggcg atgaggtaat tctccctaag gaatctgaaa gtatattttc
1801 ctcccagttc tacaagcata tttgagaacc cttcctttcc caagtattgc gaatgtgcag
1861 aaagcaacag ttacggaggg aggacatcat aaggaagtta ttaacgggca tgtattatca
1921 catcaagcat gcaataatgt gcaaattttg catttagttt tatggcatga tttatatatg
1981 gcatatttat attgtatatt ctggaaaaaa aatatatata tatatttaaa ggggagatac
2041 tctccctgac atttctaaca tatgtattaa gccaaacatg agtgaatagc tttcagggcg
2101 ataaaactaa atatatgtct gtgtgtgtgt gtgtatgtat acacacatat acatatatat
2161 atacacatac atacacatac atacatacat acatatatat ctgataaaat tgtgatgttt
2221 tgttcaaagt tgtagttctt gtgcatgttt actttattag agtaggaagg ctactggcat
2281 taattattaa taccaaatat tttagcctta aatttttgtc attttaaaat ctgatttaat
2341 gttttctgct gtttaaggtc ttgggaggct ttcaattgta ttttatatga gagaatcaca
2401 caagtttgtg ctatctatgg ccctgcaaaa atataaccat tacatgttta aattgtaaat
2461 tttagagcat accagtactc agtatagcat tgaacatttc ttatgatttt taaaagttgc
2521 tagtactggg gagaaataat tgttgattaa tttgagaatt attcctttcc tagactaatt
2581 aaaatctgga aatctgtttt gtatatgatc taatacaaag atgagctctg aacaaacact
2641 gaatcatgtt aatagacagt agccaagtta tattgaatat atcagaatct gtgtgaagtt
2701 acacaattaa ttgtccctgt ttcaaactga gtaaattgga aacattttct ttctttttct
2761 ggaaattttg tccattttaa aaaccaatca ttttaagaag acatgacaat gcaatgaaac
2821 agatgataaa tatttatgct taaaatatgt atgtctaatt gagtctcttt tttattctgt
2881 tttcttgttt atggcatttg ttgtaacagg atagactttt tcctcaccta ggaaacctat

2941 cccatgcctg tcacttatag ttcaggagga agtttttgca cagaccagag agaaattaaa
3001 attagatgat aaattgaaga tatcttacac acagtttttt ggtgaacact gattttattg
3061 gtgtcttaga tccctagtct acccaaataa ttttaacagt actgtttttt ctaatcctga
3121 agtctgatat ttatgactca ttagcaggaa tcaaaactag tgatcagtag aacactttca
3181 aaataaaaat ttggaatgca gacttttatg aaaatttaaa agtgctcctt aacagaatat
3241 catgggtttt cctataaaac ttctttaagt attgtaattc cagtctgccc caactttaaa
3301 aaaaattctt attaatatgt cagtcattaa ttgctagttt gggctctcat tatttcctgt
3361 tttttaacaa ttttgtgata attttattat tggcaaatta atacatcaac acttaaatca
3421 ttgactataa taataccttc tggctacctc tgtatcaacc aaattctgta ggtgcaaaca
3481 tataccaggg aattcttact ggcaaaatga tcaatctgga gtgtgcatcc actgtgaatg
3541 gagcaaattg ccctataccc attgataacc tagctttctt agtttgtaga tgtaggaaac
3601 aaaatagtga cagagagaga agggggtcca cagggcatgg tatatttatc agcagtggaa
3661 aaaaagtgca tagatcattt agtccaagaa cttaaaacta aatagagcca taatttactt
3721 tggagagtca ttttaatttg tctttggtac caaggagaag acggaaccaa aaacaaactc
3781 tccaagtata ttcacacatt caacaaaatt tttgcatgcc ttctatgtcg taggcatttt
3841 tagttcctgg ggatttggac atggctaagt cagagaaggc cattgctcac catgaacact
3901 gtataccaga aggagagtgg ggaggagaca aaaaacaaat aagaccactt cagacaatca
3961 aagtatcagt taagagaatg aaaacaggcc tgactcagtg gctcacgcct gtaatcccag
4021 tactttggga ggcggaggtt gggggatcac ctgaggtcag gagatcgaga ccagcctgga
4081 caacatggtg aaaacccgtc tctactaaaa atacaaaaat taactgggca tggtggcagg
4141 cacctgtaat cccagctact ggggaagctg aggcaggaga atcgtttgaa cctgggaggc
4201 ggaggttgca gtgagccaag attctgccac tgcactccag cctgggtgac agtgcgagac
4261 tccatctcaa catcaaaaaa aaaaaaaaaa aaaaaaaaaa aaaaaaaaaa aaaaagaata
4321 aaaacagggt aacataatgc aaagtaactg tgtggaataa aaattgatta ttttagaaaa
4381 tgtgactggc ttaggacggg gataatatgt gaacagaaat ctatctcatg agaaagtgct
4441 actgttgtca aaattacctt atctgagtga atggtatttt ttttatcttt tccacacatg
4501 cgtgggaaag gtatgatttc tgcatgtaat tgcagtttaa cccttatttc taggttgatc
4561 ataggtccca gtttacccag gaaaattcca gtttatacct gttgtacctg tgtaattatt
4621 ggtagcactc cctttcactc ttacaatgtc ttggtttgga tgatatatgg tgaagttttt
4681 gttgaaacta aattatgaag tctgatatat ttggataaaa ataaagaatt gcttttcttc

Translation: "MSALRRKFGDDYQVVTTSSSGSGLQPQGPGQDPQQQLVPKKKRQRFVDKNGRCNVQ
HGNLGSETSRYLSDLFTTLVDLKWRWNLFIFILTYTVAWLFMASMWWVIAYTRGDLNKAHVGNYTPCVA
NVYNFPSAFLFFIETEATIGYGYRYITDKCPEGIILFLFQSILGSIVDAFLIGCMFIKMSQPKKRAETLMFSEH
AVISMRDGKLTLMFRVGNLRNSHMVSAQIRCKLLKSRQTPEGEFLPLDQLELDVGFSTGADQLFLVSPL
TICHVIDAKSPFYDLSQRSMQTEQFEIVVILEGIVETTGMTCQARTSYTEDEVLWGHRFFPVISLEEGFFK
VDYSQFHATFEVPTPPYSVKEQEEMLLMSSPLIAPAITNSKERHNSVECLDGLDDITTKLPSKLQKITGRE
DFPKKLLRMSSTTSEKAYSLGDLPMKLQRISSVPGNSEEKLVSKTTKMLSDPMSQSVADLPPKLQKMAG
GAARMEGNLPAKLRKMNSDRFT"

11.2 ALGov9 macro (for wound healing)

```
// This macro is copy write of Dr Trevor DeVaney Feb 2017
//
//setBatchMode(true);
//=========================================================
//copywrite declaration
//=========================================================
	string="This macro is copyrite of Dr Trevor DeVaney Feb 2017 \n This macro is for detecting the area covered by cells in sequences of images\n Timelapse sequences for monitoring growth";
	Dialog.create("Covered area assesment macro");
	Dialog.addMessage(string);
	Dialog.show();
	string="In the composite images \n \n Red is the areas detected\n Green is the area included in the measurement\n Yellow is both detected and measured.";
	Dialog.create("Covered area assesment macro");
	Dialog.addMessage(string);
```

```
	Dialog.show();
//=====================================================
//Default parameters
//=====================================================
	inv=1;
	hole=1;
	sl=10000;
	su="Infinity";
	cl= 0.001;
	cu=0.999;
	v=30;
	m=6;
	sti=1;
	imi=1
	mni=5000
	sc=100
	fftlow=1
	ffthigh=40
//=====================================================
//Dialog import parameters
//=====================================================
Dialog.create("Choose image import selction parameters");
	Dialog.addCheckbox("Invert analysis",inv);
	Dialog.addSlider("Starting image number", 1,50000, sti);
	Dialog.addSlider("Image increment", 1, 20000000, imi);
	Dialog.addSlider("Maximum number of images to import", 5, 5000, mni);
	Dialog.addSlider("Image scale", 0, 100, sc);
	Dialog.show();

	inv = Dialog.getCheckbox();
	sti = Dialog.getNumber();
	imi = Dialog.getNumber();
	mni = Dialog.getNumber();
	sc = Dialog.getNumber();
//=====================================================
//close log window if open
//=====================================================
if (isOpen("Log")==true) {
	selectWindow("Log");
	run ("Close");
	}
//=====================================================
//open new log window for protocol
//=====================================================
print("//=========================================================\n" );
run("Set Measurements...", "area mean min median redirect=None decimal=3");
run("Input/Output...", "jpeg=100 gif=-1 file=.txt copy_column copy_row save_column save_row");
//=====================================================
//directory selection
//=====================================================
j=0;
while (j<1){
	print("sample directory selection");
		dir = getDirectory("Select a Data Directory");
		j=getBoolean("Is the sample directory correct ? \n"+dir );

	print("sample directory is =                    "+dir );
	}
//=====================================================
//results directory selection
//=====================================================
date="results";
print("results directory is =                    " +dir+"\\"+date);
		if (File.isDirectory(dir+"\\"+date)==false){
			print("directory absent, creating!");
			File.makeDirectory(dir+"\\"+date);
			}
		if (File.isDirectory(dir+"\\"+date)==true){
			print("success                                    "+dir+"\\"+date);
			}
//=====================================================
//iterative file open routine
//=====================================================
print("//=========================================================\n" );
//=====================================================
// list is an array with the file names in it
//=====================================================
	list = getFileList(dir);
//=====================================================
// recursively call the list of files
//=====================================================
```

```
	for (i=0; i<list.length; i++) {
			print("next directory i="+i);
			print("name is "+list[i]);
			print("processing "+dir+list[i]);
//=====================================================
// opening file
//=====================================================
if (File.isDirectory(dir+"\\"+date)==true){
				i=i+1;
				}
//=====================================================
// import trans image sequences
//=====================================================
	print("Importing image sequence from "+dir+list[i]);
			run("Image Sequence...", "open=["+dir+"\\"+list[i]+"\\] number="+mni+" starting="+sti+" increment="+imi+"
scale="+sc+" file=[] or=[] sort");
			//open(dir+list[i]);
run("8-bit");
//=====================================================
//repeat loop
//=====================================================
j=0;
while (j<1){
//=====================================================
//choose parameters dialog
//=====================================================
	Dialog.create("Choose selction parameters");
	Dialog.addCheckbox("Fill holes",hole);
	Dialog.addSlider("Size lower limit", 0, 5000000, sl);
	Dialog.addSlider("Size upper limit", 1, 2000000, su);
	Dialog.addSlider("Circularity lower limit", 0.0, 1.0, cl);
	Dialog.addSlider("Circularity upper limit", 0.0, 1.0, cu);
	Dialog.addSlider("Detection (Variance)", 1, 100, v);
	Dialog.addSlider("Smoothing (Median)", 1, 100, m);
	Dialog.addSlider("FFT Low Bandpass", 1, 1000, fftlow);
	Dialog.addSlider("FFT High Bandpass", 1, 1000, ffthigh);
	Dialog.show();
	hole = Dialog.getCheckbox();
	sl = Dialog.getNumber();
	su = Dialog.getNumber();
	cl = Dialog.getNumber();
	cu = Dialog.getNumber();
	v = Dialog.getNumber();
	m = Dialog.getNumber();
	fftlow = Dialog.getNumber();
	ffthigh = Dialog.getNumber();
	 if(su==2000000){
			su="Infinity";
			}
//=====================================================
//calculation
//=====================================================
//=====================================================
//duplicate image
//=====================================================
	run("Duplicate...", "title=[copy2_"+list[i]+"] duplicate range=1-500");
	run("Duplicate...", "title=[copy_"+list[i]+"] duplicate range=1-500");
//=====================================================
//FFT bandpass
//=====================================================
	run("Bandpass Filter...", "filter_large="+ffthigh+" filter_small="+fftlow+" suppress=None tolerance=5 autoscale saturate
process");
//=====================================================
//Variance analysis
//=====================================================

	run("8-bit");
	run("Variance...", "radius="+v+" stack");
//=====================================================
//threshold image
//=====================================================

	setAutoThreshold("Mean dark");
	setOption("BlackBackground", false);
	run("Convert to Mask", "stack");
//=====================================================
//median analysis
//=====================================================
	run("Median...", "radius="+m+" stack");
//=====================================================
//Measurement inversion
```

```
//=========================================================
		if (inv == true) {
		run("Invert", "stack");
		}
//=========================================================
//Hole inclusion
//=========================================================
		if (hole == true) {
		run("Analyze Particles...", "size="+sl+"-"+su+" circularity="+cl+"-"+cu+" show=Masks display clear include summarize
stack");
		} else {
//=========================================================
//Hole exclusion
//=========================================================
		run("Analyze Particles...", "size="+sl+"-"+su+" circularity="+cl+"-"+cu+" show=Masks display clear summarize stack");
		}
print("//=========================================================\n" );
//=========================================================
//image viewing
//=========================================================
		window="Mask of copy_"+list[i];
		selectWindow(window);
		run("Grays");
		run("Subtract...", "value=170 stack");
		selectWindow("copy_"+list[i]);
		run("Subtract...", "value=170 stack");
		run("Merge Channels...", "red=[copy_"+list[i]+"] green=[Mask of copy_"+list[i]+"] blue=*None* gray=[copy2_"+list[i]+"]
create keep");
//=========================================================
// repeat selection ?
//=========================================================
		waitForUser("Check the results and press OK when finished");
		j=getBoolean("Were the parameters correct ? \n Cancel cancels the macro\n No requires new parameter selection\n Yes
saves the data and continues with the next file");
		selectWindow("Composite");
			if(j==true){
					a=lengthOf(list[i]);
					name=substring(list[i],0,a-7);
					print("name= "+name);
					print("Composite saved to "+dir+date+"\\Composite_of_"+name+".tif");
					saveAs("Tiff", dir+date+"\\Composite_of_"+name);
					run("Close");
					}else{
					selectWindow("Composite");
					close();
					selectWindow("Mask of copy_"+list[i]);
					close();
					selectWindow("copy_"+list[i]);
					close();
					selectWindow("copy2_"+list[i]);
					close();
				if (isOpen("Summary of copy_"+list[i])==true) {
					selectWindow("Summary of copy_"+list[i]);
					run("Close");
					}
				if (isOpen("Results")==true) {
					selectWindow("Results");
					run("Close");
					}

		}
		}
//=========================================================
// write the parameter settings
//=========================================================
print("//=========================================================\n" );
print("Parameters for = "+list[i]);
print("Invert analysis = "+inv);
print("Fill Holes = "+hole);
print("Lower size = "+sl);
print("Upper size = "+su);
print("Lower circularity = "+cl);
print("Upper circularity = "+cu);
print("Detection = "+v);
print("Upper Smoothing = "+m);
print("Starting image number = "+sti);
print("Image increment = "+imi);
print("Maximum number of images to import = "+mni);
print("Image scale = "+sc);
print("//=========================================================\n" );
//=========================================================
```

```
// close results window
//=========================================================
if (isOpen("Results")==true) {
		selectWindow("Results");
		saveAs("Text", dir+date+"\\Results_"+name+".txt");
		run("Close");
		}
//=========================================================
// close Summary window
//=========================================================
if (isOpen("Summary of copy_"+list[i])==true) {
		selectWindow("Summary of copy_"+list[i]);
		saveAs("Text", dir+date+"\\Summary of "+name+"_.txt");
		run("Close");
		}
//=========================================================
// close image windows
//=========================================================
				while (nImages()>0) {
					selectImage(nImages());
					run("Close");
					}
//=========================================================
// close log window
//=========================================================
if (isOpen("Log")==true) {
		selectWindow("Log");
		saveAs("Text", dir+date+"\\Log"+name+".txt");
		run("Close");
		}
//=========================================================
//end directory processing
//=========================================================
i}
print("//=========================================================\n" );
print("end of processing");
print("//=========================================================\n" );
//=========================================================
// close log window
//=========================================================
if (isOpen("Log")==true)
print("//=========================================================\n" );
print("End of program");
print("//=========================================================\n" );
```

11.3 STR-Analyzis

Cell Culture Facility Cell Culture Facility Medical University of Graz

STR-Results for:	Date:
MCF-7	11.09.2015

cell culture facility

STR-Locus	your cell line	ATCC
D3S1358	16	
TH01	6	6
D21S11	30	
D18S51	14	
Penta E	7,12	
D5S818	11,12	11,12
D13S317	11	11
D7S820	8,9	8,9
D16S539	11,12	11,12
CSF1PO	10	10
Penta D	12	
Amelogenin	X	X
vWA	14,15	14,15
D8S1179	10,14	
TPOX	9,12	9,12
FGA	23,24,25	

Cell Culture Facility Cell Culture Facility Medical University of Graz

STR-Results for:	Date:
MCF-10A	11.09.2015

cell culture facility

STR-Locus	your cell line	ATCC
D3S1358	14,18	
TH01	8, 9.3	8, 9.3
D21S11	28,30	
D18S51	18,19	
Penta E	13,14	
D5S818	10,13	10,13
D13S317	8,9	8,9
D7S820	10,11	
D16S539	11,12	11,12
CSF1PO	10,12	10,12
Penta D	10,12	
Amelogenin	X	X
vWA	15,17	15,17
D8S1179	14,16	
TPOX	9,11	9,11
FGA	22,24	

Kit: Promega, PowerPlex 16HS System (Cat.No. DC2101)

durchgeführt am: 11.09.2015 von: M.T. Frisch

11.4 Heat maps of significantly DOWN-regulated gene clusters:

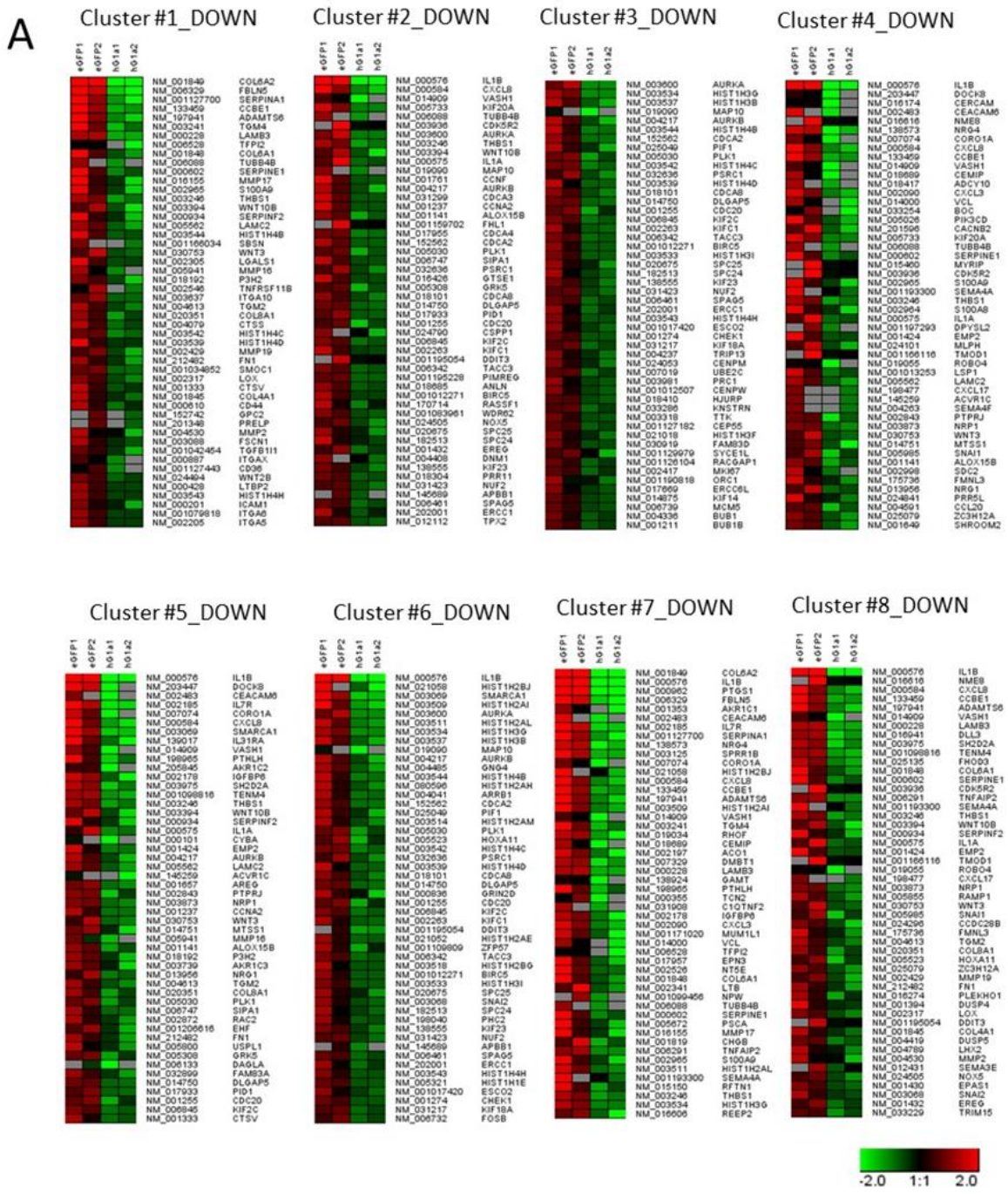

Figure 63A: Heat maps of significantly DOWN-regulated gene clusters.

B

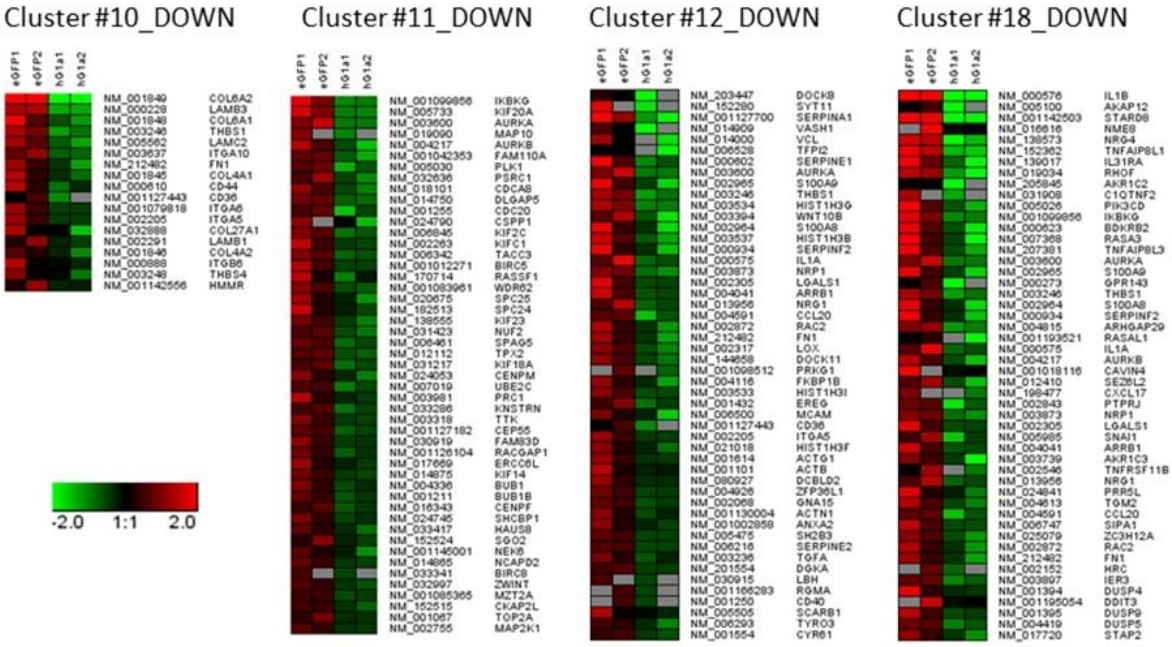

Figure 63B: Heat maps of significantly DOWN-regulated gene clusters.

11.5 Regulated clusters as detected by DAVID

Table 8: List of significantly regulated clusters as detected by DAVID. Enrichment scores, p-values and FDRs for all significant clusters are shown. Reprinted from (Schratter et al.) in press.

UP-regulated						
Cluster No.	*Enrichement Score (ES)*	*p=(10^{-ES})*	*Benjamini-Hochberg*	*FDR*	*Prototyp_Name*	*also*
1	7.611970358	2.4436E-08	2.65E-16	9.24E-17	GO:0034340~response to type I interferon	GO:0071345~cellular response to cytokine stimulus
2	3.678708775	2.0955E-04	2.63E-09	4.58E-09	GO:0045087~innate immune response	GO:0001817~regulation of cytokine production
3	3.128065629	7.4462E-04	2.83E-04	1.56E-03	hsa05168:Herpes simplex infection	hsa05160:Hepatitis C
DOWN-regulated						
Cluster No.					Prototyp_Name	also
1	5.994629397	1.0124E-06	1.25E-06	1.09E-05	GO:0031012~extracellular matrix	hsa04512:ECM-receptor interaction
2	5.518649804	3.0294E-06	1.19E-06	3.60E-07	GO:0000280~nuclear division	GO:0051301~cell division
3	5.504568335	3.1292E-06	2.00E-05	3.03E-05	GO:0000819~sister chromatid segregation	GO:0007059~chromosome segregation
4	5.428137424	3.7313E-06	1.21E-05	1.47E-05	GO:0030335~positive regulation of cell migration	GO:0006935~chemotaxis
5	4.478903449	3.3197E-05	5.09E-05	2.47E-04	GO:0008283~cell proliferation	GO:0008284~positive regulation of cell proliferation
6	4.443323983	3.6031E-05	8.18E-10	1.80E-09	GO:0044815~DNA packaging complex	GO:0000786~nucleosome
7	4.274924673	5.3098E-05	2.18E-05	3.35E-04	GO:0044421~extracellular region part	GO:0005576~extracellular region
8	4.225635365	5.9479E-05	2.69E-05	5.71E-05	GO:0001568~blood vessel development	GO:0001944~vasculature development
9	3.400777675	3.9739E-04	0.002764337	0.034363623	GO:0001704~formation of primary germ layer	GO:0001706~endoderm formation
10	3.356937953	4.3960E-04	4.63E-04	6.87E-03	hsa04512:ECM-receptor interaction	hsa04510:Focal adhesion
11	3.26593354	5.4208E-04	2.00E-05	3.03E-05	GO:0000819~sister chromatid segregation	GO:0000070~mitotic sister chromatid segregation
12	3.138542676	7.2687E-04	0.006853849	0.108241341	GO:0009611~response to wounding	GO:0042060~wound healing
13	3.061209779	8.6854E-04	0.002677864	0.032475661	GO:0007088~regulation of mitotic nuclear division	GO:0051783~regulation of nuclear division
14	2.702736206	1.9827E-03	0.061642788	2.304387456	GO:0030574~collagen catabolic process	GO:0044259~multicellular organismal macromolecule metabolic process
15	2.390350153	4.0705E-03	0.043967133	1.379243118	GO:0051781~positive regulation of cell division	GO:0045787~positive regulation of cell cycle
16	2.371547907	4.2506E-03	0.008902757	0.159649619	GO:0002687~positive regulation of leukocyte migration	GO:0097530~granulocyte migration
17	2.327843649	4.7006E-03	0.015561026	0.327171071	GO:0060707~trophoblast giant cell differentiation	GO:0009790~embryo development
18	2.316570367	4.8242E-03	0.006848572	0.110236555	GO:1902531~regulation of intracellular signal transduction	GO:0005085~guanyl-nucleotide exchange factor activity
19	2.231532319	5.8677E-03	0.02470726	0.604252092	GO:0007051~spindle organization	GO:0000022~mitotic spindle elongation
20	2.218123064	6.0517E-03	0.012299808	0.243313002	GO:0007186~G-protein coupled receptor signaling pathway	GO:0004872~receptor activity
21	2.156449856	6.9751E-03	0.038651025	1.092183278	GO:0031589~cell-substrate adhesion	GO:0010810~regulation of cell-substrate adhesion
22	2.128847423	7.4328E-03	0.033701725	2.672854827	GO:0030864~cortical actin cytoskeleton	GO:0030863~cortical cytoskeleton
23	2.069397176	8.5232E-03	0.002764337	0.034363623	GO:0001704~formation of primary germ layer	GO:0007369~gastrulation
24	2.007981647	9.8179E-03	0.006848572	0.110236555	GO:1902531~regulation of intracellular signal transduction	GO:0023051~regulation of signaling
25	1.905711994	1.2425E-02	0.081254757	0.977197772	GO:0008092~cytoskeletal protein binding	GO:0030029~actin filament-based process
26	1.854749417	1.3972E-02	0.0478295	1.531717555	GO:0048608~reproductive structure development	GO:0061458~reproductive system development
27	1.851650373	1.4072E-02	1.39E-04	1.01E-03	GO:0051290~protein heterotetramerization	GO:0034723~DNA replication-dependent nucleosome organization
28	1.835203732	1.4615E-02	0.015773628	0.346064714	GO:0007346~regulation of mitotic cell cycle	GO:1902749~regulation of cell cycle G2/M phase transition
29	1.794551181	1.6049E-02	0.294675707	8.884232497	GO:0005539~glycosaminoglycan binding	GO:0008201~heparin binding
30	1.765752957	1.7149E-02	0.008298175	0.141211424	GO:0007350~blastoderm segmentation	GO:0048846~axon extension involved in axon guidance

12. References

ALBINI, A., IWAMOTO, Y., KLEINMAN, H. K., MARTIN, G. R., AARONSON, S. A., KOZLOWSKI, J. M. & MCEWAN, R. N. 1987. A rapid in vitro assay for quantitating the invasive potential of tumor cells. *Cancer Res,* 47**,** 3239-45.

BERGAMASCHI, A., KIM, Y. H., KWEI, K. A., LA CHOI, Y., BOCANEGRA, M., LANGERØD, A., HAN, W., NOH, D.-Y., HUNTSMAN, D. G., JEFFREY, S. S., BØRRESEN-DALE, A.-L. & POLLACK, J. R. 2008. CAMK1D amplification implicated in epithelial–mesenchymal transition in basal-like breast cancer. *Molecular Oncology,* 2**,** 327-339.

BRADFORD, M. M. 1976. A rapid and sensitive method for the quantitation of microgram quantities of protein utilizing the principle of protein-dye binding. *Anal Biochem,* 72**,** 248-54.

BREVET, M., AHIDOUCH, A., SEVESTRE, H., MERVIEL, P., EL HIANI, Y., ROBBE, M. & OUADID-AHIDOUCH, H. 2008. Expression of K+ channels in normal and cancerous human breast. *Histol Histopathol,* 23**,** 965-72.

BUCK, S. B., BRADFORD, J., GEE, K. R., AGNEW, B. J., CLARKE, S. T. & SALIC, A. 2008. Detection of S-phase cell cycle progression using 5-ethynyl-2'-deoxyuridine incorporation with click chemistry, an alternative to using 5-bromo-2'-deoxyuridine antibodies. *Biotechniques,* 44**,** 927-9.

BUTCHER, D. T., ALLISTON, T. & WEAVER, V. M. 2009. A tense situation: forcing tumour progression. *Nature Reviews Cancer,* 9**,** 108-122.

CASTRO, F., CARDOSO, A. P., GONCALVES, R. M., SERRE, K. & OLIVEIRA, M. J. 2018. Interferon-Gamma at the Crossroads of Tumor Immune Surveillance or Evasion. *Frontiers in Immunology,* 9.

CHAN, H. J., LI, H. Q., LIU, Z., YUAN, Y. C., MORTIMER, J. & CHEN, S. A. 2015. SERPINA1 is a direct estrogen receptor target gene and a predictor of survival in breast cancer patients. *Oncotarget,* 6**,** 25815-25827.

CHEN, A., BEETHAM, H., BLACK, M. A., PRIYA, R., TELFORD, B. J., GUEST, J., WIGGINS, G. A. R., GODWIN, T. D., YAP, A. S. & GUILFORD, P. J. 2014. E-cadherin loss alters cytoskeletal organization and adhesion in non-malignant breast cells but is insufficient to induce an epithelial-mesenchymal transition. *Bmc Cancer,* 14.

CHERIYATH, V., KAUR, J., DAVENPORT, A., KHALEL, A., CHOWDHURY, N. & GADDIPATI, L. 2018. G1P3 (IFI6), a mitochondrial localised antiapoptotic protein, promotes metastatic potential of breast cancer cells through mtROS. *British Journal of Cancer,* 119**,** 52-64.

CHOI, U. Y., KANG, J.-S., HWANG, Y. S. & KIM, Y.-J. 2015. Oligoadenylate synthase-like (OASL) proteins: dual functions and associations with diseases. *Experimental &Amp; Molecular Medicine,* 47**,** e144.

DANISH, H. H., GOYAL, S., TAUNK, N. K., WU, H., MORAN, M. S. & HAFFTY, B. G. 2013. Interferon-Induced Protein with Tetratricopeptide Repeats 1 (IFIT1) as a Prognostic Marker for Local Control in T1-2 N0 Breast Cancer Treated with Breast-Conserving Surgery and Radiation Therapy (BCS+RT). *Breast Journal,* 19**,** 231-239.

DASCAL, N. 1997. Signalling via the G protein-activated K+ channels. *Cellular Signalling,* 9**,** 551-573.

DASCAL, N. 2001. Ion-channel regulation by G proteins. *Trends in Endocrinology and Metabolism,* 12**,** 391-398.

DEFILIPPIS, R. A., CHANG, H., DUMONT, N., RABBAN, J. T., CHEN, Y. Y., FONTENAY, G. V., BERMAN, H. K., GAUTHIER, M. L., ZHAO, J. X., HU, D. L., MARX, J. J., TJOE, J. A., ZIV, E., FEBBRAIO, M., KERLIKOWSKE, K., PARVIN, B. & TLSTY, T. D. 2012. CD36 Repression Activates a Multicellular Stromal Program Shared by High Mammographic Density and Tumor Tissues. *Cancer Discovery,* 2**,** 826-839.

DESAI, S. D. 2015. ISG15: A double edged sword in cancer. *OncoImmunology,* 4**,** e1052935.
DHAR, M. S. & PLUMMER, H. K. 2006. Protein expression of G-protein inwardly rectifying potassium channels (GIRK) in breast cancer cells. *BMC Physiol,* 6**,** 8.
DRICI, M. D., DIOCHOT, S., TERRENOIRE, C., ROMEY, G. & LAZDUNSKI, M. 2000. The bee venom peptide tertiapin underlines the role of I-KACh in acetylcholine-induced atrioventricular blocks. *British Journal of Pharmacology,* 131**,** 569-577.
DVORAK, H. F., FLIER, J. & FRANK, H. 1986. Tumors - Wounds That Do Not Heal - Similarities between Tumor Stroma Generation and Wound-Healing. *New England Journal of Medicine,* 315**,** 1650-1659.
FRANKEN, N. A., RODERMOND, H. M., STAP, J., HAVEMAN, J. & VAN BREE, C. 2006. Clonogenic assay of cells in vitro. *Nat Protoc,* 1**,** 2315-9.
FRANTZ, C., STEWART, K. M. & WEAVER, V. M. 2010. The extracellular matrix at a glance. *J Cell Sci,* 123**,** 4195-200.
GIRALDO, S. S., J; FELTY, Q; ROY, D 2009. IL1B (interleukin 1, beta). *Atlas of Genetics and Cytogenetics in Oncology and Haematology,* 13.
HANAHAN, D. & WEINBERG, R. A. 2011. Hallmarks of cancer: the next generation. *Cell,* 144**,** 646-74.
HELLEWELL, A. L., ROSINI, S. & ADAMS, J. C. 2017. A Rapid, Scalable Method for the Isolation, Functional Study, and Analysis of Cell-derived Extracellular Matrix. *J Vis Exp*.
HIBINO, H., INANOBE, A., FURUTANI, K., MURAKAMI, S., FINDLAY, I. & KURACHI, Y. 2010. Inwardly rectifying potassium channels: their structure, function, and physiological roles. *Physiol Rev,* 90**,** 291-366.
HICKS, D. G., YODER, B. J., SHORT, S., TARR, S., PRESCOTT, N., CROWE, J. P., DAWSON, A. E., BUDD, G. T., SIZEMORE, S., CICEK, M., CHOUEIRI, T. K., TUBBS, R. R., GAILE, D., NOWAK, N., ACCAVITTI-LOPER, M., FROST, A. R., WELCH, D. R. & CASEY, G. 2006. Loss of breast cancer metastasis suppressor 1 protein expression predicts reduced disease-free survival in subsets of breast cancer patients. *Clinical Cancer Research,* 12**,** 6702-6708.
HUANG DA, W., SHERMAN, B. T. & LEMPICKI, R. A. 2009. Systematic and integrative analysis of large gene lists using DAVID bioinformatics resources. *Nat Protoc,* 4**,** 44-57.
ILINA, O. & FRIEDL, P. 2009. Mechanisms of collective cell migration at a glance. *J Cell Sci,* 122**,** 3203-8.
IVANINA, T., NEUSCH, C., LI, Y. X., TONG, Y. H., LABARCA, C., MOSHER, D. F. & LESTER, H. A. 2000. Expression of GIRK (Kir3.1/Kir3.4) channels in mouse fibroblast cells with and without beta 1 integrins. *Febs Letters,* 466**,** 327-332.
IWANIR, S. & REUVENY, E. 2008. Adrenaline-induced hyperpolarization of mouse pancreatic islet cells is mediated by G protein-gated inwardly rectifying potassium (GIRK) channels. *Pflugers Archiv-European Journal of Physiology,* 456**,** 1097-1108.
JAVED, A. & LTEIF, A. 2013. Development of the human breast. *Semin Plast Surg,* 27**,** 5-12.
JEMAL, A., SIEGEL, R., XU, J. & WARD, E. 2010. Cancer statistics, 2010. *CA Cancer J Clin,* 60**,** 277-300.
JONATHAN, D., JOSH, H., FUKUSHIRO-LOPES, D. F., LACZYNSKI, D. & GENTILE, S. 2017. *Ion Channels in Breast Cancer: From Signaling to Therapy, Breast Cancer - From Biology to Medicine*, IntechOpen.
JUSTUS, C. R., LEFFLER, N., RUIZ-ECHEVARRIA, M. & YANG, L. V. 2014. In vitro cell migration and invasion assays. *J Vis Exp*.
KAINZ, P., MAYRHOFER-REINHARTSHUBER, M. & AHAMMER, H. 2015. IQM: an extensible and portable open source application for image and signal analysis in Java. *PLoS One,* 10**,** e0116329.
KAMMERER, S., SOKOLOWSKI, A., HACKL, H., PLATZER, D., JAHN, S. W., EL-HELIEBI, A., SCHWARZENBACHER, D., STIEGELBAUER, V., PICHLER, M., REZANIA, S.,

FIEGL, H., PEINTINGER, F., REGITNIG, P., HOEFLER, G., SCHREIBMAYER, W. & BAUERNHOFER, T. 2016. KCNJ3 is a new independent prognostic marker for estrogen receptor positive breast cancer patients. *Oncotarget,* 7**,** 84705-84717.

KAYSER, G., CSANADI, A., KAKANOU, S., PRASSE, A., KASSEM, A., STICKELER, E., PASSLICK, B. & ZUR HAUSEN, A. 2015. Downregulation of MTSS1 expression is an independent prognosticator in squamous cell carcinoma of the lung. *British Journal of Cancer,* 112**,** 866-873.

KITAMURA, H., YOKOYAMA, M., AKITA, H., MATSUSHITA, K., KURACHI, Y. & YAMADA, M. 2000. Tertiapin potently and selectively blocks muscarinic K+ channels in rabbit cardiac myocytes. *Journal of Pharmacology and Experimental Therapeutics,* 293**,** 196-205.

KRAMER, N., WALZL, A., UNGER, C., ROSNER, M., KRUPITZA, G., HENGSTSCHLAGER, M. & DOLZNIG, H. 2013. In vitro cell migration and invasion assays. *Mutat Res,* 752**,** 10-24.

LAEMMLI, U. K. 1970. Cleavage of structural proteins during the assembly of the head of bacteriophage T4. *Nature,* 227**,** 680-5.

LAN, Q., PEYVANDI, S., DUFFEY, N., HUANG, Y.-T., BARRAS, D., HELD, W., RICHARD, F., DELORENZI, M., SOTIRIOU, C., DESMEDT, C., LORUSSO, G. & RÜEGG, C. 2019. Type I interferon/IRF7 axis instigates chemotherapy-induced immunological dormancy in breast cancer. *Oncogene,* 38**,** 2814-2829.

LI, S. Q., XIE, Y., ZHANG, W., GAO, J. F., WANG, M., ZHENG, G. X., YIN, X., XIA, H. P. & TAO, X. 2015. Interferon alpha-inducible protein 27 promotes epithelial-mesenchymal transition and induces ovarian tumorigenicity and stemness. *Journal of Surgical Research,* 193**,** 255-264.

LIANG, C. C., PARK, A. Y. & GUAN, J. L. 2007. In vitro scratch assay: a convenient and inexpensive method for analysis of cell migration in vitro. *Nat Protoc,* 2**,** 329-33.

LIGR, M., PATWA, R. R., DANIELS, G., PAN, L., WU, X. Y., LI, Y. R., TIAN, L. T., WANG, Z. X., XU, R. L., WU, J. J., CHEN, F., LIU, J. S., WEI, J. J. & LEE, P. 2011. Expression and Function of Androgen Receptor Coactivator p44/Mep50/WDR77 in Ovarian Cancer. *Plos One,* 6.

LIVAK, K. J. & SCHMITTGEN, T. D. 2001. Analysis of relative gene expression data using real-time quantitative PCR and the 2(-Delta Delta C(T)) Method. *Methods,* 25**,** 402-8.

LUESCHER, C. & SLESINGER, P. A. 2010. Emerging roles for G protein-gated inwardly rectifying potassium (GIRK) channels in health and disease. *Nature Reviews Neuroscience,* 11**,** 301-315.

LUKER, K. E., PICA, C. M., SCHREIBER, R. D. & PIWNICA-WORMS, D. 2001. Overexpression of IRF9 confers resistance to antimicrotubule agents in breast cancer cells. *Cancer Research,* 61**,** 6540-6547.

LUPARELLO, C. 2013. Aspects of Collagen Changes in Breast Cancer. *Journal of Carcinogenesis and Mutagenesis,* **,** 007.

LUSCHER, C. & SLESINGER, P. A. 2010. Emerging roles for G protein-gated inwardly rectifying potassium (GIRK) channels in health and disease. *Nat Rev Neurosci,* 11**,** 301-15.

LÜSCHER, C. & SLESINGER, P. A. 2010. Emerging roles for G protein-gated inwardly rectifying potassium (GIRK) channels in health and disease. *Nat Rev Neurosci,* 11**,** 301-315.

LV, Y., SONG, G., WANG, R., DI, L. & WANG, J. 2017. Doublecortin-like kinase 1 is a novel biomarker for prognosis and regulates growth and metastasis in basal-like breast cancer. *Biomedicine & Pharmacotherapy,* 88**,** 1198-1205.

MANUEL IGLESIAS, J., BELOQUI, I., GARCIA-GARCIA, F., LEIS, O., VAZQUEZ-MARTIN, A., EGUIARA, A., CUFI, S., PAVON, A., MENENDEZ, J. A., DOPAZO, J. & MARTIN, A. G. 2013. Mammosphere formation in breast carcinoma cell lines depends upon expression of E-cadherin. *PLoS One,* 8**,** e77281.

MAZZONE, M., SELFORS, L. M., ALBECK, J., OVERHOLTZER, M., SALE, S., CARROLL, D. L., PANDYA, D., LU, Y. L., MILLS, G. B., ASTER, J. C., ARTAVANIS-TSAKONAS, S. & BRUGGE, J. S. 2010. Dose-dependent induction of distinct phenotypic responses to Notch pathway activation in mammary epithelial cells. *Proceedings of the National Academy of Sciences of the United States of America,* 107**,** 5012-5017.

MESCI, A., HUANG, X. Y., TAEB, S., JAHANGIRI, S., KIM, Y. H., FOKAS, E., BRUCE, J., LEONG, H. S. & LIU, S. K. 2017. Targeting of CCBE1 by miR-330-3p in human breast cancer promotes metastasis. *British Journal of Cancer,* 116**,** 1350-1357.

MILLER, C. H. T., MAHER, S. G. & YOUNG, H. A. 2009. Clinical Use of Interferon-gamma. *Cytokine Therapies: Novel Approaches for Clinical Indications,* 1182**,** 69-79.

MOJIC, M., TAKEDA, K. & HAYAKAWA, Y. 2018. The Dark Side of IFN-: Its Role in Promoting Cancer Immunoevasion. *International Journal of Molecular Sciences,* 19.

MULATERO, P., MONTICONE, S., RAINEY, W. E., VEGLIO, F. & WILLIAMS, T. A. 2013. Role of KCNJ5 in familial and sporadic primary aldosteronism. *Nature Reviews Endocrinology,* 9**,** 104-112.

MULLER, P. A. & VOUSDEN, K. H. 2014. Mutant p53 in cancer: new functions and therapeutic opportunities. *Cancer Cell,* 25**,** 304-17.

MULLNER, C., VOROBIOV, D., BERA, A. K., UEZONO, Y., YAKUBOVICH, D., FROHNWIESER-STEINECKER, B., DASCAL, N. & SCHREIBMAYER, W. 2000. Heterologous facilitation of G protein-activated K+ channels by beta-adrenergic stimulation via cAMP-dependent protein kinase. *Journal of General Physiology,* 115**,** 547-557.

NOLTE, I. M., MUNOZ, M. L., TRAGANTE, V., AMARE, A. T., JANSEN, R., VAEZ, A., VON DER HEYDE, B., AVERY, C. L., BIS, J. C., DIERCKX, B., VAN DONGEN, J., GOGARTEN, S. M., GOYETTE, P., HERNESNIEMI, J., HUIKARI, V., HWANG, S. J., JAJU, D., KERR, K. F., KLUTTIG, A., KRIJTHE, B. P., KUMAR, J., VAN DER LAAN, S. W., LYYTIKAINEN, L. P., MAIHOFER, A. X., MINASSIAN, A., VAN DER MOST, P. J., MULLER-NURASYID, M., NIVARD, M., SALVI, E., STEWART, J. D., THAYER, J. F., VERWEIJ, N., WONG, A., ZABANEH, D., ZAFARMAND, M. H., ABDELLAOUI, A., ALBARWANI, S., ALBERT, C., ALONSO, A., ASHAR, F., AUVINEN, J., AXELSSON, T., BAKER, D. G., DE BAKKER, P. I. W., BARCELLA, M., BAYOUMI, R., BIERINGA, R. J., BOOMSMA, D., BOUCHER, G., BRITTON, A. R., CHRISTOPHERSEN, I. E., DIETRICH, A., EHRET, G. B., ELLINOR, P. T., ESKOLA, M., FELIX, J. F., FLORAS, J. S., FRANCO, O. H., FRIBERG, P., GADEMAN, M. G. J., GEYER, M. A., GIEDRAITIS, V., HARTMAN, C. A., HEMERICH, D., HOFMAN, A., HOTTENGA, J. J., HUIKURI, H., HUTRI-KAHONEN, N., ASHAR, F., ASHAR, F., JUONALA, M., KIVINIEMI, A. M., KORS, J. A., KUMARI, M., KUZNETSOVA, T., LAURIE, C. C., LEFRANDT, J. D., LI, Y., LI, Y., LIAO, D. P., LIMACHER, M. C., LIN, H. J., LINDGREN, C. M., LUBITZ, S. A., MAHAJAN, A., MCKNIGHT, B., ZU SCHWABEDISSEN, H. M., MILANESCHI, Y., MONONEN, N., MORRIS, A. P., NALLS, M. A., NAVIS, G., NEIJTS, M., NIKUS, K., NORTH, K. E., O'CONNOR, D. T., ORMEL, J., PERZ, S., PETERS, A., PSATY, B. M., et al. 2017. Genetic loci associated with heart rate variability and their effects on cardiac disease risk. *Nature Communications,* 8.

NUSHTAEVA, A. A., STEPANOV, G. A., SEMENOV, D. V., JURAVLEV, E. S., BALAHONOVA, E. A., GERASIMOV, A. V., SIDOROV, S. V., SAVELYEV, E. I., KULIGINA, E. V., RICHTER, V. A. & KOVAL, O. A. 2018. Characterization of primary normal and malignant breast cancer cell and their response to chemotherapy and immunostimulatory agents. *BMC Cancer,* 18**,** 728.

PARDO, L. A. & STUHMER, W. 2014. The roles of K(+) channels in cancer. *Nat Rev Cancer,* 14**,** 39-48.

PERRY, C. A., PRAVETONI, M., TESKE, J. A., AGUADO, C., ERICKSON, D. J., MEDRANO, J. F., LUJAN, R., KOTZ, C. M. & WICKMAN, K. 2008. Predisposition

to late-onset obesity in GIRK4 knockout mice. *Proceedings of the National Academy of Sciences of the United States of America,* 105**,** 8148-8153.
PFAFFL, M. W., HORGAN, G. W. & DEMPFLE, L. 2002. Relative expression software tool (REST) for group-wise comparison and statistical analysis of relative expression results in real-time PCR. *Nucleic Acids Res,* 30**,** e36.
PLUMMER, H. K., YU, Q., CAKIR, Y. & SCHULLER, H. M. 2004. Expression of inwardly rectifying potassium channels (GIRKs) and beta-adrenergic regulation of breast cancer cell lines. *Bmc Cancer,* 4.
PREVARSKAYA, N., SKRYMA, R. & SHUBA, Y. 2018. Ion Channels in Cancer: Are Cancer Hallmarks Oncochannelopathies? *Physiol Rev,* 98**,** 559-621.
REZANIA, S., KAMMERER, S., LI, C., STEINECKER-FROHNWIESER, B., GORISCHEK, A., DEVANEY, T. T., VERHEYEN, S., PASSEGGER, C. A., TABRIZI-WIZSY, N. G., HACKL, H., PLATZER, D., ZARNANI, A. H., MALLE, E., JAHN, S. W., BAUERNHOFER, T. & SCHREIBMAYER, W. 2016. Overexpression of KCNJ3 gene splice variants affects vital parameters of the malignant breast cancer cell line MCF-7 in an opposing manner. *BMC Cancer,* 16**,** 628.
RIBATTI, D., NICO, B., VACCA, A. & PRESTA, M. 2006a. *The gelatin sponge-chorioallantoic membrane assay*.
RIBATTI, D., NICO, B., VACCA, A. & PRESTA, M. 2006b. The gelatin sponge-chorioallantoic membrane assay. *Nat Protoc,* 1**,** 85-91.
RIFKIN, R. A., MOSS, S. J. & SLESINGER, P. A. 2017. G Protein-Gated Potassium Channels: A Link to Drug Addiction. *Trends Pharmacol Sci,* 38**,** 378-392.
ROBERTS, D. D. 2005. RTHBS1 (thrombospondin-1). *Atlas Genet Cytogenet Oncol Haematol,* 9**,** 231-233.
SALIC, A. & MITCHISON, T. J. 2008. A chemical method for fast and sensitive detection of DNA synthesis in vivo. *Proc Natl Acad Sci U S A,* 105**,** 2415-20.
SCHLIE-WOLTER, S., NGEZAHAYO, A. & CHICHKOV, B. N. 2013. The selective role of ECM components on cell adhesion, morphology, proliferation and communication in vitro. *Exp Cell Res,* 319**,** 1553-61.
SCHNEIDER, C. A., RASBAND, W. S. & ELICEIRI, K. W. 2012. NIH Image to ImageJ: 25 years of image analysis. *Nat Methods,* 9**,** 671-5.
SCHRATTER, G., SCHERÜBEL, S., LANGTHALER, S., ESTER, K., PELZMANN, B., GHAFFARI-TABRIZI-WIZSY, N., REZANIA, S., GORISCHEK, A., PLATZER, D., ZORN-PAULY, K., AHAMMER, H., PROKESCH, A., STANZER, S., DEVANEY, T. T. J., SCHMIDT, K., JAHN, S. W., PRASSL, R., BAUERNHOFER, T. & SCHREIBMAYER, W. in press. GIRK1 triggers multiple cancer-related pathways in the benign mammary epithelial cell line MCF10A. *Scientific Reports*.
SCHRODER, K., HERTZOG, P. J., RAVASI, T. & HUME, D. A. 2004. Interferon-gamma: an overview of signals, mechanisms and functions. *Journal of Leukocyte Biology,* 75**,** 163-189.
SCHWARZENBACHER, D., KLEC, C., PASCULLI, B., CERK, S., RINNER, B., KARBIENER, M., IVAN, C., BARBANO, R., LING, H., WULF-GOLDENBERG, A., STANZER, S., RINNERTHALER, G., STOEGER, H., BAUERNHOFER, T., HAYBAECK, J., HOEFLER, G., JAHN, S. W., PARRELLA, P., CALIN, G. A. & PICHLER, M. 2019. MiR-1287-5p inhibits triple negative breast cancer growth by interaction with phosphoinositide 3-kinase CB, thereby sensitizing cells for PI3Kinase inhibitors. *Breast Cancer Res,* 21**,** 20.
SHANKAR, H., KAHNER, B. N., PRABHAKAR, J., LAKHANI, P., KIM, S. & KUNAPULI, S. P. 2006. G-protein-gated inwardly rectifying potassium channels regulate ADP-induced cPLA(2) activity in platelets through Src family kinases. *Blood,* 108**,** 3027-3034.
SHANKAR, H., MURUGAPPAN, S., KIM, S., JIN, J. G., DING, Z. R., WICKMAN, K. & KUNAPULI, S. P. 2004. Role of G protein-gated inwardly rectifying potassium channels in P2Y(12) receptor-mediated platelet functional responses. *Blood,* 104**,** 1335-1343.

SHAW, F. L., HARRISON, H., SPENCE, K., ABLETT, M. P., SIMOES, B. M., FARNIE, G. & CLARKE, R. B. 2012. A detailed mammosphere assay protocol for the quantification of breast stem cell activity. *J Mammary Gland Biol Neoplasia,* 17**,** 111-7.

SMITH, P. A., SELLERS, L. A. & HUMPHREY, P. P. A. 2001. Somatostatin activates two types of inwardly rectifying K+ channels in MIN-6 cells. *Journal of Physiology-London,* 532**,** 127-142.

STRINGER, B. K., COOPER, A. G. & SHEPARD, S. B. 2001. Overexpression of the G-protein inwardly rectifying potassium channel 1 (GIRK1) in primary breast carcinomas correlates with axillary lymph node metastasis. *Cancer Res,* 61**,** 582-8.

TAKAHASHI, K., KOHNO, T., AJIMA, R., SASAKI, H., MINNA, J. D., FUJIWARA, T., TANAKA, N. & YOKOTA, J. 2006. Homozygous deletion and reduced expression of the DOCK8 gene in human lung cancer. *International Journal of Oncology,* 28**,** 321-328.

TAN, Y. W., ZHOU, G. L., WANG, X. M., CHEN, W. C. & GAO, H. D. 2018. USP18 promotes breast cancer growth by upregulating EGFR and activating the AKT/Skp2 pathway. *International Journal of Oncology,* 53**,** 371-383.

TANG, F., LAO, K. & SURANI, M. A. 2011. Development and applications of single-cell transcriptome analysis. *Nat Methods,* 8**,** S6-11.

TINOCO, G., WARSCH, S., GLUCK, S., AVANCHA, K. & MONTERO, A. J. 2013. Treating breast cancer in the 21st century: emerging biological therapies. *J Cancer,* 4**,** 117-32.

TURNBULL, L. & WHITCHURCH, C. B. 2014. Motility assay: twitching motility. *Methods Mol Biol,* 1149**,** 73-86.

WAGNER, V., STADELMEYER, E., RIEDERER, M., REGITNIG, P., GORISCHEK, A., DEVANEY, T., SCHMIDT, K., TRITTHART, H. A., HIRSCHBERG, K., BAUERNHOFER, T. & SCHREIBMAYER, W. 2010. Cloning and characterisation of GIRK1 variants resulting from alternative RNA editing of the KCNJ3 gene transcript in a human breast cancer cell line. *J Cell Biochem,* 110**,** 598-608.

WALSH, K. B. 2011. Targeting GIRK Channels for the Development of New Therapeutic Agents. *Front Pharmacol,* 2**,** 64.

WILCOX, R. 2017. *Modern Statistics for the Social and Behavioural Sciences. A practical Introduction,* Boca Raton, FL, Chapman and Hall /CRC.

WOOLSTON, C. 2015. Breast cancer. *Nature,* 527**,** S101-S101.

WULFF, H., CASTLE, N. A. & PARDO, L. A. 2009. Voltage-gated potassium channels as therapeutic targets. *Nat Rev Drug Discov,* 8**,** 982-1001.

YANG, J., BIELENBERG, D. R., RODIG, S. J., DOIRON, R., CLIFTON, M. C., KUNG, A. L., STRONG, R. K., ZURAKOWSKI, D. & MOSES, M. A. 2009. Lipocalin 2 promotes breast cancer progression. *Proceedings of the National Academy of Sciences,* 106**,** 3913-3918.

ZAIDI, M. R. 2019. The Interferon-Gamma Paradox in Cancer. *Journal of Interferon and Cytokine Research,* 39**,** 30-38.

ZIEBERT, F. & ARANSON, I. S. 2016. Computational approaches to substrate-based cell motility. *Npj Computational Materials,* 2**,** 16019.